UNIVERSITY OF CALIFORNIA, SAN DIEGO

The Role the Saharan Heat Low Plays in the Variability of Dust Emission and Transport in North Africa from Synoptic to Decadal Scales

A dissertation submitted in partial satisfaction of the requirements for the degree

Doctor of Philosophy

in

Earth Sciences

by

Weijie Wang

Committee in charge:

Amato T. Evan, Chair
Katherine A. Barbeau
Arthur J. Miller
Mark Thiemens
Shang-Ping Xie

2017

The dissertation of Weijie Wang is approved, and it is acceptable in quality and form for publication on microfilm and electronically:

Chair

University of California, San Diego

2017

DEDICATION

To my parents.

EPIGRAPH

The Earth is the only world known so far to harbor life. There is nowhere else, at least in the near future, to which our species could migrate. Visit, yes. Settle, not yet. Like it or not, for the moment the Earth is where we make our stand.

Carl Sagan, *Pale Blue Dot,* 1994

TABLE OF CONTENTS

LIST OF FIGURES

LIST OF TABLES

ACKNOWLEDGEMENTS

I would like to acknowledge Professor Amato Evan for his support as the chair of my committee. Through years of graduate school, his guidance and support have been invaluable. His scientific insights and passion have driven me to explore the unknown. I would also like to thank the other members of my PhD committee for their suggestions – Professor Art Miller, Kathy Barbeau, Mark Thiemens, and Shang-Ping Xie.

Chapter 2, in part, is a reprint of the material as it appears in On the Decadal Scale Correlation between African Dust and Sahel Rainfall: The Role of Saharan Heat Low–forced Winds. Wang, Weijie; Evan, Amato; Flamant, Cyrille; Lavaysse, Christophe, Science Advances, 2015. The dissertation author was the primary investigator and author of this paper.

Chapter 3, in part, has been submitted for publication of the material as it may appear in The Role the Saharan Heat Low Plays in Dust Emission and Transport during Summertime in North Africa. Wang, Weijie; Evan, Amato; Flamant, Cyrille; Lavaysse, Christophe, Aeolian Research, 2017. The dissertation author was the primary investigator and author of this paper.

Chapter 4, in part, is currently being prepared for submission for publication of the material. Wang, Weijie; Evan, Amato; Zhao, Chun. The dissertation author was the primary investigator and author of this paper.

VITA

2010 B. S. in Environmental Sciences, Fudan University, Shanghai, China

2010-2012 Research Assistant, University of Virginia, Charlottesville, VA

2012 M. S. in Environmental Sciences, University of Virginia, Charlottesville, VA

2012-2013 Research Scientist, Science Systems and Applications, Inc, Hampton, VA

2013-2017 Research Assistant, University of California, San Diego, San Diego, CA

2016 Teaching Assistant, University of California, San Diego, San Diego, CA

2017 Ph. D. in Earth Sciences, University of California, San Diego, San Diego, CA

PUBLICATIONS

Wang, W., A. Evan, C. Lavaysse, and C. Flamant, The role the Saharan Heat Low plays in dust emission and transport during summertime in North Africa, *Aeolian Res*., 28, 1-12 (2017).

Wang, W., A. Evan, C. Flamant, and C. Lavaysse, On the Decadal Scale Correlation Between African Dust and Sahel Rainfall: the Role of Saharan Heat Low-Forced Winds, *Sci. Advances*, 1(9), e1500646 (2015).

Loeb, N. G., D. A. Rutan, S. Kato, and W. Wang, Observing Interannual Variations in Hadley Circulation Atmospheric Diabatic Heating and Circulation Strength. *J. Climate*, 27, 4139–4158 (2014).

Wang, W., T. Cheng, R. Zhang, X. Jia, Z. Han, X. Zhang, X. Xu, and D. Li, Insights into an Asian dust event sweeping Beijing during April 2006: Particle chemical composition, boundary layer structure, and radiative forcing, *J. Geophys. Res.*, 115, D18208, doi:10.1029/2009JD013391 (2010).

Li, H., Z. Han, T. Cheng, H. Du, L. Kong, J. Chen, R, Zhang, and W. Wang, Agricultural fire impacts on the air quality of Shanghai during summer harvest time, *Aerosol and Air Quality Res.,* 10: 95–101 (2010).

ABSTRACT OF THE DISSERTATION

The Role the Saharan Heat Low Plays in the Variability of Dust Emission and Transport in North Africa from Synoptic to Decadal Scales

by

Weijie Wang

Doctor of Philosophy in Earth Sciences

University of California, San Diego, 2017

Professor Amato T. Evan, Chair

Dust over the Atlantic undergoes decadal variability. Over the past three decades, satellite and in-situ measurements show a downward trend in dust concentration over the Atlantic, indicating there is less dust emission in the Sahara. Meanwhile, observations show an upward trend in the Sahel precipitation. However, it is unknown what affects dust emission in the Sahara and precipitation in the Sahel simultaneously. Dust emission in North Africa also undergoes synoptic variability and high concentration of dust is often observed in the western Sahara, but it is unclear whether dust over the western Sahara is due to local emission or dust transport from the east.

The aim of this thesis is twofold, first, to examine the role the Saharan heat low (SHL) plays in dust emission and precipitation from synoptic to decadal timescales. and second, to identify bias of dust in the model. To do so I use reanalysis and satellite products to construct the time series of dust, precipitation and the SHL and perform regression analysis to examine the effect of the SHL on precipitation and winds, which are associated with dust emission. Then I study the lead and lag relationship between the SHL and dust concentration in North African on the synoptic scale to identify source regions. Lastly, I identify the biases in a dust source function using dust output from a climate model.

The results from this thesis suggest that the warming of the SHL results in the increase of precipitation in the Sahel and the reduction in dust emission by changing low-level winds on the decadal timescale. On the synoptic scale, cool phases of the SHL is associated with more dust emission and 10% of the dust over western Africa is from source regions to the east. Lastly, the dust source function may overestimate dust emission in the Sahel and western Africa.

Chapter 1

Introduction

1.1 Thesis Outline

This thesis explores the role of the SHL in African monsoon rainfall and dust emission using a combination of satellite products, reanalyses, ground-based observations and climate models. This work is organized as follows. Chapter 1.2 briefly describes the effect of dust on the climate system. Chapter 1.3 offers an overview of aerosol observations and products. Chapter 1.4 gives a literature review of research into the factors that cause droughts in the Sahara and the Sahel as well as dust sources, emission and transport in North Africa. Chapter 1.5 gives a review of field campaigns conducted in North Africa.

Chapter 2 focuses on the decadal scale correlation between African dust and Sahel rainfall within the context of the Saharan Heat Low (SHL)-forced winds. More specifically, Chapter 2.1 gives an introduction on the existing theories of the correlation between dust emission and precipitation. Chapter 2.2 describes the datasets used in this chapter. Chapter 2.3 presents time series of dust over the Atlantic, Sahel precipitation and the strength of the SHL. Chapter 2.4 defines the SHL and explains the mechanism that governs the interannual variability of dust emission in North Africa and intraseasonal variability of Sahel precipitation. Chapter 2.5 compares winds from different reanalyses. Chapter 2.6 examines visibility from several synoptic stations in North Africa. Lastly, chapter 2.7 summarizes the work in this chapter.

Chapter 3 exams what governs dust emission and transport on the synoptic scale in the summertime and the major dust source regions in North Africa. More specifically, Chapter 3.1 gives an introduction on what affects dust variability on the synoptic scale. Chapter 3.2 describes the satellite and reanalysis products used in this chapter. Chapter 3.3 examines how the variability in the SHL is related to dust emission and transport over North Africa and the tropical Atlantic in the summertime, and a brief conclusion is provided in Chapter 3.4.

Chapter 4, Chapter 4.1 gives an introduction an existing dust source function. Chapter 4.2 describes the satellite products and a model used in this chapter. Chapter 4.3 compares the seasonal dust climatology from two satellite products. Chapter 4.4 examines a dust source function from satellite and identifies biases in the source function. Chapter 4.5 summarizes the work in this chapter.

Chapter 5 gives a summary of the work presented in this dissertation and discusses the implications of my findings in understanding the climate in North Africa. Future works are also suggested.

1.2 Dust

Dust is the most pervasive aerosol in the atmosphere (*Kaufman et al.,* 2005) and it has various impacts on the Earth system. It directly affects the atmospheric radiation budget via the reflection and absorption of incoming shortwave and outgoing longwave radiation (*Tegen et al*., 1996; *Miller and Tegen*, 1998; *Ramanathan et al*., 2001; *Kaufman et al.,* 2002), and the magnitude of radiative forcing varies with dust aerosol properties, such as the single scattering albedo, the asymmetry parameter and

size distribution (*Sokolik and Toon*, 1996; *Tegen et al*., 1996; *Liao and Seinfeld*, 1998), and it also depends on the vertical profile of the dust (*Liao and Seinfeld*, 1998; *Meloni et al*., 2005). Dust can act as cloud condensation nuclei and indirectly changes the atmospheric radiation budget through affecting the cloud cover (*Wurzler et al*., 2000; *DeMott et al*., 2003), and changes in cloud properties further modify the hydrological cycle through affecting precipitation and evaporation (*Miller et al*., 2004; *Andreae and Rosenfeld*, 2008; *Rosenfeld et al*., 2008; *Creamean et al.,* 2013). In addition, dust plays a non-negligible role in the biogeochemical processes by transporting nutrients into the oceanic ecosystem (*Savoie and Prospero*, 1980; *Swap et al*., 1996; *Okin et al*. 2011) and the terrestrial ecosystem (*Swap et al*., 1992; *Formenti et al*., 2001). Aside from those impacts on the Earth system, dust also generates health concerns as it carries pollutants that cause respiratory and cardiovascular diseases (*Onishi et al*., 2012; *Longueville et al*., 2013).

Although it is important to determine the radiative properties of dust, to quantify the amount of dust being emitted and transported globally and to understand the mechanisms that govern dust emission in the source regions, the impacts of dust on the climate system are not well quantified due to the spatial and temporal heterogeneity of dust and the lack of observations in the remote areas. For example, the Intergovernmental Panel on Climate Change (IPCC) Fifth Assessment Report estimates that radiative forcing due to mineral dust is -0.1 ± 0.2 W m^{-2}. The determination of sign remains a problem. Estimates of global dust emission have large uncertainties. Simulations from various models differ by more than a factor of 2 due to

different parameterizations (*Zender et al*., 2004) and the lack of understanding of dust sources. Furthermore, anthropogenic dust emission due to land use change is estimated to account for 25% of global dust emission (*Ginoux et al*., 2012). However, how natural and anthropogenic dust emission will be affected by climate change is highly uncertain (*Tegen et al*., 2004).

1.3 Aerosol Observations and Products

Since 1979, the launch of multiple satellites has greatly contributed to the continuous measurements of aerosols with global coverage. Satellites such as the Advanced Very High Resolution Radiometer (AVHRR), the Total Ozone Mapping Spectrometer (TOMS), the Ozone Monitoring Instrument (OMI), the Spinning Enhanced Visible and Infrared Imager (SEVIRI), the Moderate Resolution Imaging Spectroradiometer (MODIS), the Multi-angle Imaging Spectroradiometer (MISR), and the Cloud-Aerosol Lidar and Infrared Pathfinder Satellite Observations (CALIPSO) provide near-daily observations with retrieved information on aerosol properties. In addition, ground-based observations, such as the Aerosol Robotic Network (AERONET), provide long-term and continuous database for aerosol research and validation of satellite retrievals. Recently, reanalysis products, such as the Modern-Era Retrospective Analysis for Research and Applications Aerosol Reanalysis (MERRAero) and the Monitoring Atmospheric Composition and Climate (MACC), have also included aerosol products.

1.3.1 AVHRR

The AVHRR is one of the earliest satellite instruments used to study aerosols. It is a broadband scanner sensing in visible, near-infrared, and thermal infrared bands. The first AVHRR instrument aboard Television Infrared Observation Satellite has 4 channels and was launched in October 1978. The second instrument aboard National Oceanic and Atmospheric Administration (NOAA) 7 has 5 channels and was launched in June 1981. The third instrument aboard NOAA-15 has 6 channels and was launched in 1998.

Aerosol optical depth (AOD) retrievals were made over oceans using radiance in channel 1 (630 nm) of AVHRR (*Stowe et al*., 1997). Due to the requirement for low surface reflectivity, AOD retrievals were not made over land, and thus AVHRR cannot be used to obtain source regions. *Evan et al*., (2006) pointed out that AOD over oceans is underestimated as the cloud detection algorithms tend to misclassify optically thick dust storms as clouds, and they implemented a dust detection algorithm within the Pathfinder Atmospheres Extended project and showed improved accuracy of monthly mean AOD when compared to data from the AERONET.

1.3.2 TOMS

The TOMS instruments were on board the Nimbus-9 satellite from November 1978 through April 1993 and Earth Prove satellite from August 1996 through March 2005. TOMS measures backscattered ultraviolate (UV) radiance in six wavelengths (313, 318, 331, 340, 360 and 380 nm). The TOMS aerosol index (AI) is a nonquantitative measure of aerosol concentration calculated using the spectral contrast

between 340 nm and 380 nm channels (*Herman et al*., 1997), and is sensitive to a number of aerosol properties, such as the aerosol layer height and the optical properties of aerosols. The strong molecular scattering in the near UV allows the separation of absorbing aerosols from non-absorbing aerosols (*Torres et al*., 1998). UV-absorbing aerosols such as dust have smaller spectral contrast while non-absorbing aerosols such as sulfate have greater contrast. The TOMS can detect aerosols over land as well as oceans.

One of the shortcomings of the retrieval algorithm is that aerosol detection can be obscured by clouds within a kilometer of the surface (*Herman et al*., 1997; *Torres et al*., 1998). Nevertheless, the TOMS AI is widely used to study global dust aerosol distribution, transport and seasonal cycle in the past two decades (e.g. *Chiapello et al*., 1999, 2002; *Cakmur et al*., 2001; *Prospero et al.*, 2002; *Torres et al*., 2002; *Washington et al*., 2003; *Ginoux et al*., 2012).

1.3.3 OMI

The OMI instrument is aboard the Earth Observing System Aura satellite, which circulates in a sun-synchronize polar orbit with an equator crossing time at 13:45 (*Levelt et al*., 2006). The OMI launched in July 2004 continues the TOMS record for atmospheric parameters and provides near global coverage in one day with a spatial resolution of 13 km × 24 km (*Levelt et al*., 2006). It observes solar backscatter radiation in the visible and UV bands (270-550 nm) and can distinguish between aerosol types, such as smoke, dust and sulfates.

Two algorithms are used to retrieve aerosol characteristics over the ocean and land (*Torres et al*., 2007). The near UV algorithm makes use of the 350–390 nm spectral band to retrieve the absorption capacity of aerosols and provides absorption optical depth at 388 nm. The other algorithm makes use of the full UV-to-visible spectral bands to derive aerosol extinction optical depth (*Torres et al*., 2007).

1.3.4 SEVIRI

The SEVIRI on board the geostationary Meteosat Second Generation satellite is an imaging radiometer with 12 channels ranging from the visible to infrared spectral bands (*Schmetz et al*., 2002). The brightness temperature (BT) in the infrared band measured by the SEVIRI instrument is used to identify dust source areas in the Sahara and Sahel region (*Schepanski et al.*, 2007). Compared with clear sky conditions, the difference in the BT between the 10.8 μm and 12.0 μm band (BT(12, 10.8)) as well as between the 8.7 μm and 10.8 μm band (BT(10.8, 8.7)) decreases if there is dust in the atmosphere. Therefore, the differences in BT(12, 10.8) and BT(10.8, 8.7) are used for dust detection. The SEVIRI has a spatial resolution of 3 km a temporal resolution of 15 minutes, and such a high spatiotemporal resolution is useful in identifying activated dust sources.

1.3.5 MODIS

The MODIS instrument has two spaceflight units, one aboard the Terra satellite launched in December 1999 and the other aboard the Aqua satellite launched in May 2002. Terra passes the earth from north to south and crosses the equator in the morning. Aqua passes the earth from south to north and crosses the equator in the

afternoon. The MODIS instrument has 36 bands from 0.4 to 14.4 μm, among which bands 1 to 7 and 20 are used to retrieve AOD globally and aerosol size distribution over the oceans. Such retrieval is made possible by the blue channel on the MODIS. The MODIS Deep Blue aerosol product has AOD at 550 nm over bright land surfaces such as deserts (*Hsu et al*., 2004). The dark surface and Deep Blue combined AOD provides global observations of AOD on a daily basis. The Level 2 aerosol products of MODIS have a spatial resolution of 10 km × 10 km (0.1° × 0.1°) and the Level 3 products 1° × 1°.

The MODIS aerosol products have been validated by comparison with the AERONET (*Chu et al*., 2002; *Remer et al*., 2002; *Remer et al*., 2005) and are widely used in aerosol research (e.g. *Kaufman et al*., 2005; *Liang et al*., 2006; *Remer et al*., 2008; *Ginoux et al*., 2012).

1.3.6 MISR

The MISR instrument aboard the Terra satellite was launched in 1998. MISR views the sunlit side of the Earth with cameras in 9 difference directions in four wavelengths, blue, green, red, and near-infrared (*Diner et al*., 1989, 1991). Large viewing angles provide enhanced sensitivity to aerosols. MISR obtains a swath of imagery 360 km wide by 20,000 km long, and such swath width allows MISR viewing the Earth's surface in 9 days. MISR provides aerosol properties, such as AOD, size and composition, at 0.275 km and 1.1 km resolution on a global basis. MISR level 2 products provide the fine, medium and large fraction of AOD as well as the spherical and nonspherical fraction of AOD (*Martonchik et al*., 2002)

1.3.7 CALIPSO

CALIPSO was launched in April 2006 as part of NASA's A-Train constellation. It is an along-track, nadir-viewing satellite that crosses the equator at around 1:30 pm and 1:30 am local solar time. The main instrument carried by CALIPSO is the Cloud-Aerosol Lidar with Orthogonal Polarization (CALIOP), an along-track, nadir-pointing two-wavelength lidar that measures attenuated backscatter extinction coefficients at visible (532 nm) and infrared (1064 nm) wavelengths.

CALIPSO Level 2 products include the aerosol layer product and the aerosol profile product. The aerosol layer product contains a vertical feature mask (VFM) that has a mechanism to distinguish aerosol from clouds based on particulate backscatter color ratio. This product can also distinguish dust from other types of aerosol, namely marine, continental, polluted continental and biomass burning based on aerosol lidar ratio (*Vaughan et al.*, 2004). This product provides aerosol optical depth (AOD) of up to 8 layers from surface to 40 km based on the output of the VFM. The aerosol profile product contains extinction coefficients at 60 m vertical resolution.

CALIPSO Level 3 products are aggregated of Level 2 aerosol profiles and provide monthly mean AOD in all sky and clear sky conditions at 5° longitude by 2° latitude resolution.

CALIPSO is the only satellite that measures the vertical profile of aerosols and thus is helpful for understanding aerosol transport (e.g. *Liu et al*., 2008; *Liu et al*., 2008a, b; *Ben-Ami et al*., 2009) and the impact of aerosols on climate change (e.g. *Huang et al*., 2010).

1.3.8 AERONET

The AERONET is a ground-based remote sensing aerosol network initiated by the National Aeronautic and Space Administration and expanded by federation with many other institutions (*Holben et al*., 1998). The AERONET offers standardization for regional to global scale aerosol monitoring by using automatic Sun and sky scanning spectral radiometer. The radiometer makes two measurements, direct sun or sky. The direct Sun measurements are made in eight bands (anywhere between 340 and 1020 nm, 440, 670, 870, 940 and 1020 nm) and the sky measurements are made at four bands (440, 670, 870 and 1020 nm) (*Holben et al*., 1998). These measurements are used to retrieve the size distribution, the phase function and AOD.

1.3.9 MERRAero

MERRAero developed by the Global Modeling Assimilation Office is based on the Goddard Earth Observing System Data Assimilation version 5 (GEOS-5) model (*Rienecker et al*., 2008), which includes aerosol processes based on the Goddard Chemistry, Aerosol, Radiation, and Transport (GOCART) aerosol module. In addition, MERRAero includes AOD assimilations from the MODIS Aqua and Terra satellites (*Buchard et al*., 2016). MERRAero provides AI, AOD, extinction, backscatter, and other aerosol parameters for fine aerosols (PM2.5) and all aerosols from 2002 to present at 1° by 1° resolution. *Buchard et al*. (2015) found a good correlation between the MERRAero and OMI AI over the Sahara and the North Atlantic dust region in summer 2007, and a comparison between MERRAero and AERONET AOD at eight Sahara stations also indicates that these two products are well correlated.

1.3.10 MACC

MACC built on the Global and Regional Earth-System Monitoring using satellite and in-situ data (*Hollingsworth et al*., 2008). The data assimilation system used in MACC was based on the European Centre for Medium-Range Weather Forecasts' (ECMWF) Integrated Forecast System (*Inness et al*., 2013). MACC assimilated chemically reactive gases as well as dust parameters from 2003 through 2012. *Cuevas et al*. (2015) evaluated dust from MACC-II over North Africa using MODIS and AERONET data and concluded overall, the seasonal variation of dust optical depth is well simulated by MACC-II.

1.4 The Saharan and Sahel Regions

1.4.1 The Sahara

The Sahara Desert in North Africa is the largest desert in the world with its surface area of 9,400,000 square kilometers, comparable to the land area of the contiguous United States (Fig. 1.1). In Arabic, the Saharan desert is الصحراء الكبرى, which means the Greatest Desert. However, paleoclimatological records show that during the early to middle Holocene period, about 12000 to 5000 years ago, the Sahara and Sahel regions were wetter than today (*Sarntheim*, 1978; *Dupont*, 1993; *Yu and Harrison*, 1996). The now hyper-arid region was then nearly completely vegetated with grasses and shrubs (*COHMAP Members*, 1988). The transition from a "green Sahara" to the desert is attributed to changes in the tilt of the Earth's axis and the eccentricity of the Earth's orbit (*Kutzbach et al*., 1986). Stronger tilt of the Earth's axis and larger eccentricity of the Earth's orbit led to amplified seasonal cycle of solar

radiation, enhanced land-sea temperature contrast and thus strengthened African summer monsoon (*Kutzbach and Otto-Bliesner*, 1982; *Kutzbach et al*., 1986; *Prell and Kutzbach*, 1987; *Joussaume et al*., 1999). In addition, changes in vegetation and soil increased the climate response to orbital forcing as wet soil and grassland further enhanced summer rainfall (*Kutzbach et al*., 1996).

This African humid period abruptly shifted toward more arid conditions between 5000 and 6000 years before the present (*deMenocal et al*., 2000). Geological record downwind from the Sahara showed a sudden increase in dust deposition 5500 years before the present (*deMenocal et al*., 2000). Such abrupt shift is associated with the gradual decline in summer solar radiation (*Petit-Maire and Guo*, 1996). The African monsoonal precipitation is highly sensitive to orbital insolation forcing and 1% increase in summer radiation forcing could result in approximately 5% increase in North African rainfall (*Prell and Kutzbach*, 1987). Furthermore, the variations in monsoonal rainfall affect the surface circulation of adjacent regions that are dynamically linked to the monsoonal surface winds (*McIntyre et al*., 1989; *Kutzbach and Liu*, 1997). The decline in rainfall and vegetation cover allowed dust mobilization from 4300 years ago and present day desert was established about 2700 years ago (*Kröpelin et al*., 2008).

The vast majority of North Africa is uninhabited and surface observations in this area are sparse, thus making it difficult to trace dust origins and to estimate dust fluxes in the source regions. Early studies used element ratios, such as Si/Al and Fe/Al, and back trajectories to identify source regions in North Africa (e.g. *Bergametti et al.*,

1989; *Chiapello et al*., 1997). Recent studies using reanalysis, satellite observations, models as well as chemical analysis suggest several major dust source regions. For example, *Scheuvens et al*. (2013) found topographic lows along the Algeria – Morocco Western Sahara border, northern Algeria – Tunisia, Southern Algeria and Bodélé are large source of dust based on chemical analysis, such as calcite abundance, palygorskite occurrence and abundance, illite/kaolinite ratio, etc. *Formenti et al*. (2011) suggested six major dust sources in North Africa based on previous works, including zone of chottts in Tunisia and Northern Algeria, foothills of Atlas Mountains and western coastal region, Mali-Algerian border region, Central Libya, the Bodélé depression, and Southern Egypt, Northern Sudan (*Brooks and Legrand*, 2000; *Caquineau et al*., 2002; *Prospero et al*., 2002; *Israelevich et al*., 2002, *Goudie*, 2003; *Schepanski et al*., 2009; *Formenti et al*., 2011; *Scheuvens et al*., 2013; *Formenti et al*., 2014). *Washington et al*. (2003, 2006), *Schepanski et al*. (2013) and *Evan et al*. (2015) found that the Bodélé is the region of the highest dust emission, accounting for 64% (±16%) of the total North Africa dust emission (*Evan et al*., 2015). Such high emission is the result of two key prerequisites: strong surface winds and a large source of suitable sediment (*Washington et al*., 2006). *Prospero et al*. (2002) indicated the most intense dust activity occurs in an area centered at 33.5°N and 7.5°E in northeastern Algeria using the TOMS AI. *Ginoux et al*. (2012) listed 24 dust sources including both natural and anthropogenic emissions using MODIS. *Ashpole and Washington* (2013a, b) found two major source regions in the central and western Sahara, one in southwest Algeria and northwest Mali and the other in southern Algeria, northwest Niger, and

northeast Mali using data from SEVIRI. The disagreement on dust source regions is due to the difference in dust detection algorithm of each satellite product and the methodology used to identify dust source regions.

1.4.2 The Decadal Variability of African Dust

Dust concentration of the tropical north Atlantic undergoes decadal variability (*Prospero and Lamb*, 2003; *Evan and Mukhopadhyay*, 2010, *Evan et al*., 2016). Over the past century, high concentrations of dust occurred from the 1910s to the 1940s and the 1970s to the 1980s, and anomalously low dust concentrations occurred in the 1950s and 2000s (*Evan et al*., 2016). Previous studies have found that the decadal variability in African dust is associated with various atmospheric phenomena. *DeFlorio et al*. (2016) found El Niño/Southern Oscillation exerts a control on North African dust transport during boreal summer. Using in situ observation from Barbados and satellite observation from the AVHRR and a century-length fully coupled Community Earth System Model, they found a statistically significant increase in North African dust transport over the Atlantic during strong La Niña summers due to increased easterly winds. *Moulin et al*. (1997) found the interannual variations in dust transport over the Atlantic are well correlated with the North Atlantic Oscillation (NAO). The NAO is defined as the difference in normalized sea level pressures between Lisbon, Portugal and Stykkisholmur, Iceland in winter (*Hurrell*, 1995). When the NAO index is low, there is a northward shift of the North Atlantic westerlies which provide much of the moisture to North Africa. When the NAO index is high, there is more moisture and thus more precipitation in North Africa, limiting dust mobilization

and transport. *Doherty et al*. (2012, 2014) found the meridional position of the intertropical convergence zone (ITCZ) is correlated with the dust load in Barbados in winter and summer. A southward movement of the ITCZ is associated with an increase in dust load at Barbados by changing near-surface northeasterly winds in North Africa. *Rodríguez et al*. (2015) the North African dipole is associated with dust export. High North African dipole summers are associated with major dust export in the subtropics and minor dust loads in the tropics due to the variability in winds. *Evan et al*. (2016) pointed out the surface winds are responsible for most of the variability in North African dust emission. Using 10 m winds from the European Centre for Medium-Range Weather Forecasts Interim reanalysis product (ERA-I) and dust from AVHRR, they showed ERA-I winds can explain 58% of the variance in the AVHRR dust data.

1.4.3 The Sahel

The Sahel is the semiarid transition zone that lies between the Sahara Desert to the north and the tropical climate to the south (Fig. 1.1). It receives most of its rainfall during the summer monsoon season. In the past 100 years, Sahel rainfall undergoes interannual and decadal variability with above average rainfall from the 1950s to the 1960s followed by drought from the late 1960s to the 1980s (*Nicholson*, 1989; *Folland et al*., 1986). Numerous studies including field campaigns and modeling have attempted to understand what drives such variability (e.g. *Held et al*., 2005; *Redelsperger et al*., 2006). Early works proposed that the positive albedo-precipitation hypothesis could explain the prolonged Sahel drought (*Charney et al*., 1975). Since

desert surface has higher surface albedo and is hotter compared with vegetated surface, consequently, desert emits more radiation to the space. When air loses heat radiatively, it has to descend in order to maintain thermal equilibrium, thus bringing dry air to the surface and further reducing rainfall. Recent works suggested that oceanic forcing drives the variability of rainfall in the Sahel as warmer-than average low-latitude waters around Africa weaken continental convergence by favoring the formation of deep convection over the ocean (*Giannini et al*., 2003; *Lu et al*., 2005), and land and atmosphere feedback amplifies drought through changing the vegetation cover (*Otterman*, 1974; *Giannini et al*., 2003). In other words, changes in the sea surface temperature (SST) weaken the African monsoon circulation, leading to low vegetation cover, increased albedo and less evaporation, thus further reducing moisture transport and rainfall over land, creating a vicious cycle (Fig. 1.2). It is also pointed out that extratropical North Atlantic cooling is tied to the droughts over the Sahel (*Mulitza et al*., 2008; *Liu and Chiang*, 2012; *Liu et al*., 2014). A slowdown of the Atlantic meridional overturning circulation (AMOC) reduces heat transport into the North Atlantic, particularly cooling the extratropical North Atlantic (*Broecker et al*., 1985; Alley, 2007), and causes the droughts in Sahel via an atmospheric teleconnection (*Liu et al*., 2014). Another theory that tries to explain the Sahel droughts is the southward shift of the Intertropical Convergence Zone (ITCZ) (e.g. *Dahl et al*., 2005). However, *Mulitza et al*. (2008) noted that such theory is problematic and it is the strengthening and the southward shift of the African easterly jet (AEJ) that causes the widespread drought (*Newell and Kidson*, 1984; *Skinner et al*., 2012) as the AEJ affects moisture

divergence over West Africa by transporting moisture away from the continent to the Atlantic (*Cook*, 1999).

In the late 20th century, there has been a recovery of the Sahel drought and a greening of the Sahel (*Nicholson*, 2005; *Olsson et al*., 2005) that cannot be explained by the theories stated above. *Evan et al*. (2015) suggested this recovery coincides with an upward trend in the SHL temperature. The rise in temperature is a result of greenhouse gas warming by water vapor, and changes in water vapor strongly depend on the temperature of the SHL. Rising temperature increases water vapor, which further increases temperature, thus creating a positive feedback.

1.4.4 Meteorology in North Africa

A couple of atmospheric circulations affect the climate in North Africa. For example, the AEJ plays a crucial role in the west African monsoon system (*Thorncroft and Blackburn*, 1999). The AEJ is a midtropospheric jet located over North African in boreal summer and is maintained by the thermal contrast between high surface temperatures near the Sahara and the cool sea surface temperatures of the coast of Guinea (*Fontaine et al*., 1995). African easterly waves (AEW), a fundamental synoptic feature over western African in summer, are known to modulate dust variability in North African (*Jones et al.*, 2003). AEW form west of 20°E and are maintained by barotropic and baroclinic energy conversions from the AEJ at the 600-hPa level (*Norquist et al*. 1977). The West African heat low (WAHL), a region of high surface temperature and low surface pressure, migrates with solar insolation and occurs where insolation is high. In the summertime, the WAHL is positioned over the Sahara and is

often referred to as the SHL, which is generally within 20°-30°N, 7°W-5°E (*Lavaysse et al*., 2009). The SHL is associated with a low-level cyclonic circulation and a midlevel anticyclonic circulation, and the intensity of the SHL impacts the intraseasonal variability of West Africa monsoon together with the AEJ (e.g., *Lavaysse et al*., 2009; *Chauvin et al*., 2010). Strong (warm) phases of the SHL are associated with intensified low-level cyclonic circulation and increased precipitation in the eastern and central Sahel as the anomalous southerlies bring moisture from the Gulf of Guinea in land (*Lavaysse et al*., 2010).

Prospero and Lamb (2003) found Sahelian precipitation is anticorrelated with dust concentration at Barbados (13°10'N, 59°30'W), and precipitation is thought to affect dust emission and transport (*Moulin et al*., 1997). However, most precipitation occurs in the Sahel region whereas most dust emission occurs in the Sahara where there is not much precipitation. It seems rainfall is insufficient in explaining the variability in dust and it is unclear why there is a robust correlation between the two.

1.5 Field Campaigns

Field campaigns help improve our knowledge and understanding of the climate in North Africa as well as validate existing satellite products and models. In the 21st century there has been several field campaigns conducted in North Africa to observe the monsoon season, dust properties, and thermodynamics. For example, African Monsoon Multidisciplinary Analysis in 2006 aimed to understand the West African monsoon on daily-to-interannual time scale (*Redelsperger et al*., 2006). Dust Outflow and Deposition in 2006 sought to characterize the physical and chemical properties of

dust in winter and summer and quantified dust deposition into the ocean (*McConnell et al*., 2008). The Saharan Mineral Dust Experiment in 2006 and 2008 measured chemical composition, size distribution and optical properties of dust (*Heintzenberg*, 2009; *Ansmann et al*., 2011). Geostationary Earth Radiation Budget Experiment Intercomparison of Longwave and Shortwave Radiation in 2007 sought to characterize the geographic distribution and the physical and optical properties of dust and to assess the atmospheric radiative impact of dust (*Haywood et al*., 2001). The most recent campaign Fennec conducted in June 2011 and 2012 aimed to observe dust and thermodynamics over the SHL region, namely northern Mali, southern Algeria and eastern Mauritania, in summer using aircrafts as well as ground stations in Algeria and Mauritania (*Washington et al*., 2012).

1.6 Figures

Figure 1.1 A satellite image of the Sahara and the Sahel. The Sahara is a hyper-arid region with high albedo that comprises much of the land in North Africa. The Sahel is the semiarid transition zone (blue) between the Sahara Desert and the tropical climate.

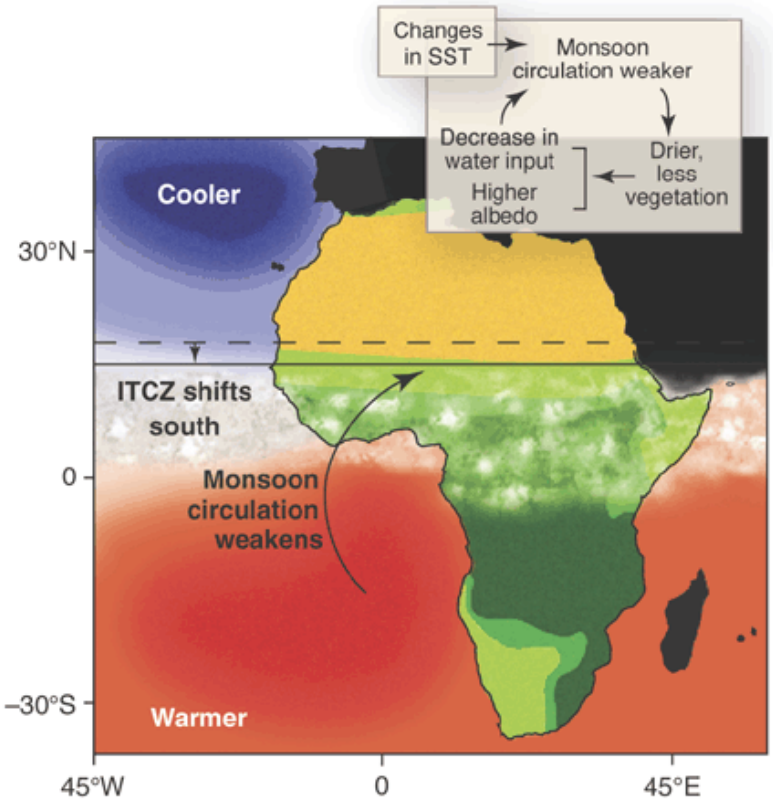

Figure 1.2 Schematics of how changes in SST affect monsoon circulation, vegetation, albedo and water cycle (from *Zeng*, 2003).

Chapter 2

On the Decadal Scale Correlation Between African Dust and Sahel Rainfall: the Role of Saharan Heat Low-Forced Winds

Abstract

A large body of work has shown that year-to-year variations in North African dust emission are inversely proportional to previous year monsoon rainfall in the Sahel, implying that African dust emission is highly sensitive to vegetation changes in this narrow transitional zone. However, such a theory is not supported by field observations or modeling studies, as both suggest that interannual variability in dust is due to changes in winds over the major emitting regions, which lie to the north of the Sahelian vegetated zone. Here I reconcile this contradiction showing that interannual variability in Sahelian rainfall, and surface winds over the Sahara, are the result of changes in lower tropospheric air temperatures over the SHL. As the SHL warms an anomalous tropospheric circulation develops that weakens the climatological northeastlies over the Sahara and displaces the monsoonal rainfall northward, thus simultaneously increasing Sahelian rainfall and reducing dust emission from the major dust "hot-spots" in the Sahara. These results shed light on why climate models are, to-date, unable to reproduce observed historical variability in dust emission and transport from this region.

2.1 Introduction

By mass, aeolian dust is the most pervasive aerosol in the atmosphere (*Kaufman et al.,* 2005). The presence of suspended dust affects the local energy balance through direct (*Evan et al.,* 2009) and indirect effects (*DeMott et al.,* 2003), modifies the hydrological cycle via radiative forcing (*Yoshioka,* 2007) and modification of cloud microphysical properties (*Creamean et al.,* 2013), and is a vehicle for the long-range transport of nutrients to global oceans (*Okin et al.,* 2011) and terrestrial land surfaces (*Das et al.,* 2013). However, despite the importance of dust to Earth system, coupled climate models are not able to reproduce historical variability in dust emission and transport (*Evan et al.,* 2014) and thus there is little confidence in projections of how atmospheric dust concentrations will change in the future. As such, there is a need to understand the controls on historical changes in dust using observational data.

North Africa is the world's largest dust source; accounting for more than 55% of the global dust emissions (*Engelstaedter et al.,* 2006; *Ginoux et al.,* 2012), and nearly 60% of the dust transported off the continent is deposited in the Atlantic Ocean (*Kaufman et al.,* 2005). Long-term in-situ observations at Barbados (*Prospero and Lamb,* 2003) and coral reef proxy and satellite data (*Evan and Mukhopadhyay*, 2010; *Foltz and McPhaden,* 2008) have shown that dust emission from North Africa peaked during the mid-1980s and has followed a downward trend through at least the late 2000s. Studies have found dust cover over the Atlantic is anticorrelated with precious-year Sahelian precipitation (*Prospero and Lamb,* 2003), and a causal relationship

between the decline in dust emission and increase in Sahelian rainfall is plausible since increasing soil moisture would strengthen soil cohesion forces (*Fecan et al.,* 1999), and more dense vegetation cover would increase surface roughness (*Cowie et al.,* 2013), both acting to limit erosion and the mobilization of particles from the surface into the atmosphere. However, there are several aspects of such a theory that are not consistent. For example, satellite imagery suggests that the vast majority of dust-emitting regions lie to the north of the vegetated region of the Sahel (*Ginoux et al.*, 2012; *Schepanski et al.,* 2009), and in-situ observations have shown that a more northward propagation of the monsoon, which results in greater Sahelian rainfall, should increase the occurrence of dust emission from sources in the Sahel via haboobs (*Knippertz and Todd,* 2012). Additionally, a recent study demonstrated that the downward trend in dust that started in the mid-1980s could be reproduced in an aerosol emission and transport model when forced only by historical wind fields from reanalysis, and when holding Sahelian vegetation density constant (*Ridley et al.,* 2014).

Therefore, on the one hand it would appear as though changes in surface winds over the hyper-arid Sahara Desert should be sufficient to describe year-to-year changes in summertime dust emission, yet on the other hand there is clear evidence showing that dust transported across the Atlantic is inversely proportional to rainfall, and vegetation density, in the Sahel. Here I reconcile this contradiction by showing that both Saharan surface wind fields over the major regional dust emitting regions, and the northward propagation of the monsoon flow and thus Sahel rainfall, are forced by the thermodynamic state of a meteorological feature termed the Saharan Heat Low (SHL).

2.2 Data and Method

2.2.1 Dust

Monthly mean dust optical depth (τ_d), retrieved from satellite radiance measurements from the Advanced Very High Resolution Radiometer (AVHRR), is used to construct the time series of τ_d over the Northern tropical Atlantic for the summer months (June-August) from 1982 through 2009 (*Evan and Mukhopadhyay*, 2010). AVHRR τ_d retrievals compare well against measurements from AERONET (*Evan et al*., 2006).

Dust mass flux in the Sahara is derived using the output of five models, namely TEGEN (*Tegen et al*., 2002), WRF-GOCART (*Zhao et al*., 2013), WRF-Kok (*Kok et al*., 2014), CESM (*Mahowald et al*., 2006), and CHIMERE (*Menut et al*., 2013), that simulate dust based on the relationship between mass flux and dust storm frequency (*Evan et al*., 2015). Dust storm frequency is identified using Fifteen-minute Meteosat SEVIRI infrared dust index images from March 2006 to February 2008 (*Schepanski et al.,* 2009).

2.2.2 Precipitation

I use monthly mean precipitation data from the version 2 Global Precipitation Climatology Project (GPCP) to construct the time series of Sahel precipitation (*Lavaysse et al.,* 2009). GPCP merges data from rain gauge stations, satellites, and sounding observations to estimate monthly precipitation on a 2.5° by 2.5° grid (*Adler et al*., 2003) and has been validated over West Africa (Nicholson et al., 2003). The

precipitation series is averaged over 5° W to 20° E, 10° to 20° N in the summer months (June–August) from 1979 through 2012.

2.2.3 The SHL

The SHL is estimated using the mean of low-level atmospheric thickness (LLAT) between the 700 and 925 hPa pressure levels over West Africa following *Lavaysse et al*. (2009).

$$LLAT = \frac{R}{g}\int_{p2}^{p1} Td(\ln(p)) \quad (1)$$

where R is the gas constant for air, g is gravitational acceleration, T is the mean low-level temperature, and p is pressure at 925 and 700 hPa. The LLAT is used as a proxy for the daily SHL index (Z_{hl}), and it increases as the low-level temperature warms.

I construct daily time series of the SHL in summer from 1979 through 2012 using 0600 UTC pressure and temperature at 700 hPa and 925 hPa from the European Centre for Medium-Range Weather Forecasts Interim Reanalysis (ERA Interim; *Dee et al*., 2011). Daily Z_{hl} is used to calculate monthly mean Z_{hl}.

I apply a high-pass filter and a low-pass filter to the Z_{hl} time series to study the mode of variability of Z_{hl} on various time scales. For the daily Z_{hl} I apply a high-pass filter with a cutoff frequency of 30 days to study the effect of the Z_{hl} on winds on the synoptic scale, and a low-pass filter with a cutoff frequency of 300 days to study the seasonal and multi-year evolution of these components. For the monthly Z_{hl} I apply a high-pass filter with a cutoff frequency of 3 months to study the effect of the Z_{hl} on precipitation and tropical North Atlantic τ_d on intraseasonal scale and a low-pass filter

with a cutoff frequency of 12 months to study the seasonal and multi-year evolution of these components. These filters are applied to winds and precipitation as well.

2.2.4 Winds

925 hPa meridional and zonal winds at 0600 UTC are from ERA-Interim daily product from 1979 through 2012, and 10m meridional and zonal winds at 0000, 0600, 1200 and 1800 UTC from ERA-Interim are used for the same period of time. Although wind speeds in the data sparse Sahara are subject to errors, a recent comparison of reanalysis and observed surface winds within the Sahel demonstrated that ERA-Interim is best suited for analysis of dust emission processes there (*Largeron et al.,* 2015).

In addition to ERA-Interim, I also analyze winds from another three reanalysis products, namely Modern Era Retrospective Analysis for Research (MERRA) (*Rienecker et al.,* 2011), National Centers for Environmental Prediction-Department of Energy Reanalysis 2 (NCEP2) (*Kanamitsu et al.,* 2002), and NCEP-National Center for Atmospheric Research Reanalysis Product (NNRP) (*Kalnay et al.,* 1996), to examine how results from these three reanalyses compared to those from ERA-Interim.

MERRA is available from 1979 through present. It uses the state-of-the-art GOES 5 data assimilation system to integrate observations with numerical models to produce spatially and temporally consistent variables. MERRA daily mean product has a spatial resolution of 0.67° longitude by 0.67° latitude for surface parameters and a reduced resolution of 1.25° longitude by 1.25° latitude on pressure levels.

NNRP contains gridded atmospheric parameters dated back to 1948. The

completeness and consistency of the database are ensured by incorporating in-situ measurements and satellite observations and by using a frozen global data assimilation system (*Kalnay et al.,* 1996). NNRP daily mean product has a spatial resolution of 2.5° longitude by 2.5° latitude. NCEP2 is an improvement upon the NNRP and has the same spatial resolution.

2.2.5 Synoptic Stations

I use visibility from five synoptic stations in North Africa, four in Algeria (DAAJ, DAAT, DATM, DAOF), and one in Niger (DRZA) as they have observations for more than five years. The location, altitude and data availability of each station are listed in Table 2.1 (Fig. 2.1). Visibility is measured every 30 minutes at each of these stations.

2.3 Dust and Precipitation

The Sahelian region of North Africa is an arid to semi-arid region lying between the Sahara and the more tropical regions near the Guinea coast that is characterized by average summertime precipitation rates from 4 to 8 mm day^{-1}. Numerous studies have suggested that Atlantic dust cover is sensitive to rainfall in the Sahel, given the negative correlations between dust and monsoon season precipitation (*Prospero and Lamb*, 2003; *Knippertz and Todd,* 2012). Indeed, time series of summertime, June-August, the season when dust production peaks (*Engelstaedter et al.,* 2007), tropical North Atlantic τ_d estimated from satellites (*Evan and Mukhopadhyay*, 2010), shows that τ_d has been decreasing since the mid-1980s, while Sahelian rainfall, from the Global Precipitation Climatology Project (*Adler et al.,*

2003), has been increasing over the same time period (Fig. 2.2). The time series of monsoon season Sahelian rainfall and satellite-retrieved τ_d, over the period 1982–2010, are statistically significantly correlated at an r-value of -0.53 (p-value 0.01) (Table 2.2). Using dust concentration measurements from Barbados (*Prospero and Lamb*, 2003) and the same rainfall data, but over the period 1965–2009, the correlation between dust and precipitation is -0.52.

The basis for the theory that Sahelian rainfall affects dust emission is that while the correlation between concurrent year rainfall and dust is statistically significant and negative, the magnitude of the correlation between previous year rainfall and dust is larger in magnitude (*Prospero and Lamb*, 2003) (-0.68 using satellite data and -0.66 using the Barbados data). However, based on the results from a Fisher-z test to determine the significance of the difference in correlation coefficients, I cannot rule out the null hypothesis that the lagged correlations are statistically indistinguishable from the non-lagged correlations. In other words, the fact that the correlation magnitude peaks when Sahelian rainfall leads dust by one year may simply be a statistical artifact.

2.4 The SHL

I next examine the concurrent roles of the SHL in dust emission and rainfall in the summer from 1979 through 2012. The SHL is a region of a local surface and lower tropospheric temperature maximum and surface pressure minimum that is present in the western Sahara Desert during the summer (June-August) months, and is characterized by a broad low-level cyclonic circulation, and mid-level anticyclonic

circulation, about the SHL center (*Lavaysse et al.,* 2009) (Fig. 2.3a). The magnitude and extent of these two circulation features can be described by the atmospheric thickness between the 700 hPa and 925 hPa levels, averaged spatially over the SHL center. Larger values of Z_{hl} indicate a strengthening of the characteristic SHL circulation features (*Lavaysse et al.,* 2009). The SHL center is detected in a manner identical to the Lagrangian SHL tracking method described in (*Lavaysse et al.,* 2009). The temperature and thickness of the SHL change on time scales ranging from synoptic (*Lavaysse et al.,* 2010) to interannual (*Evan et al.,* 2015a), and over the last three decades Z_{hl} has increased (Fig. 2.2), a trend that is corroborated by in-situ observations (*Evan et al.,* 2015a).

As the SHL warms, and Z_{hl} increases, there is an intensification of the low-level cyclonic circulation that has its center of action about the SHL (*Lavaysse et al.,* 2009), and this strengthened low-level circulation increases Sahelian rainfall during the monsoon season via a northward displacement of the monsoon flow (*Evan et al.,* 2015a). Co-variability of Z_{hl} and precipitation on the decadal scale is evidenced by a statistically significant correlation of their seasonal time series (r-value of 0.54, p-value of 0.01) (Fig. 2.2). The decadal-scale co-variability is also seen in Figure 2.3b, which shows coefficients of the regression of monthly precipitation anomalies onto monthly mean Z_{hl} anomalies, for the summer months (June-August) and from 1979 through 2012. Here, given an anomalously warm SHL there is an increase in Sahelian precipitation and a reduction in rainfall along the Gulf of Guinea (Fig. 2.3b), indicating an anomalously northward position of monsoon rain band, consistent with

other studies (*Evan et al.,* 2015a). Model projection suggests that there is tendency towards more rainfall over the central-eastern Sahel in the mid 21st century (*Monerie et al*., 2012, 2013). The dependency of Sahelian rainfall on the intensity of the SHL is also evident in the regression of 925hPa winds onto Z_{hl}, also for the months of the monsoon season, which show an anomalous low-level southwesterly flow between the Gulf of Guinea and the Sahel (Fig. 2.3b) that intensifies the climatological southerly monsoon flow (Fig. 2.3a) and thus increases the northward transport of moisture to the Sahel (*Evan et al.,* 2015a).

Simultaneous with the increase in Sahel rainfall that is associated with an anomalously warm SHL, there is an anomalous low-level southwesterly flow over the three most important dust-emitting regions of the Sahara, the Bodélé depression, a depression in the lee of the Aïr and Adrar Mountains, and western Mauritania and Western Sahara (Fig. 2.3b; *Schepanski et al.,* 2009; *Evan et al.,* 2015a*,* 2015b; *Ginoux et al.,* 2012). I note that while the dust emission map from (*Evan et al.,* 2015b) does not show high (relative) emission rates over western Mauritania and Western Sahara, another independent estimate of North African dust emission (*Ginoux et al.,* 2012) suggests that this region has the highest emission rates for the entire region.

All three major dust source regions are located on the Intertropical Discontinuity (ITD), the interface between the cool moist southwesterly monsoon flow and the warm and dry northeasterly flow. On the north edge of the ITD, the climatological low-level winds are northerly to northeasterly (Fig. 2.3a), but the anomalous wind fields associated with an increase in Z_{hl} are southwesterly over the

Bodélé depression and a depression in the lee of the Aïr and Adrar Mountains (Fig. 2.3b), a result of the anomalous cyclonic rotation about the SHL center of action. Consequently, as Z_{hl} increases and the SHL circulation strengthens there is a net reduction in the scalar 925 mb wind speeds to the northeast of these important source regions, as evidenced by the statistically significant coefficients of the regression of wind speed onto Z_{hl} (shading, Fig. 2.3b). Thus, the regressions of monsoon rainfall and winds onto Z_{hl} (Fig. 2.3b) demonstrate that changes in the low-level circulation associated with the SHL can simultaneously increase Sahelian rainfall and reduce North African dust emission on various time scales, via the well-established relationship between surface wind speeds and emission (*e.g. Fecan et al.,* 1999).

2.5 Other Reanalyses

I also examine the concurrent roles of the SHL in dust emission and rainfall in the summer using three other reanalysis products, namely, MERRA, NCEP2, and NNRP.

2.5.1 MERRA

MERRA shows that associated with an anomalously warm SHL there is an anomalous low-level southwesterly flow over the major dust-emitting regions (Fig. 2.4), consistent with the results from ERA-Interim (Fig. 2.3b). MERRA also shows strengthened cyclonic circulation about the SHL center and a reduction in wind speeds to the northeast of the three dust hot spots when the Z_{hl} warms (Fig. 2.4), whereas the reduction in wind speeds on the northeast edge over the dust hot spots associated with warm Z_{hl} is not observed in ERA-Interim (Fig. 2.3b). The regression coefficients are

larger in MERRA compared with ERA-Interim, especially in the lee of the Aïr and Adrar Mountains and to the northeast of the western Mauritania dust hot spot (Fig. 2.4).

2.5.2 NCEP2

NCEP2 exhibit an anomalous low-level southwesterly flow between the Gulf of Guinea and the Sahel associated with an anomalously warm SHL (Fig. 2.5). The strengthened cyclonic circulation about the SHL center associated warm SHL is also observed using NECP2 (Fig. 2.5). A reduction in 925 mb wind speeds is observed over the Bodélé depression (Fig. 2.5), identical to MERRA (Fig. 2.4), and to the northeast of the lee of the Aïr and Adrar Mountains (Fig. 2.5), identical to ERA-Interim (Fig. 2.3b). However, NCEP2 does not show a reduction in wind speeds to the northeast of the Bodélé depression as shown in ERA-Interim and MERRA (Fig2.3b, Fig2.4).

2.5.3 NNRP

NNRP has the same spatial resolution as NCEP2, and results from NNRP are the same as NCEP2 (Fig.2.5, Fig.2.6).

2.6 Synoptic Stations

Visibility is used as an indication of dust storms as the visibility drops significantly when a dust storm occurs. I examine the monthly mean visibility at each station. DATM and DAAJ have a relatively short period of data availability of less than 10 years. Among these five station, DATM has the lowest mean visibility of 5.6 km, indicating dust loading is persistently high in southern Algeria in summer (Table

2.3). DAOD in eastern Algeria and DAAJ in western Algeria have mean visibility above 9 km, indicating dust loading is low in these two regions in summer (Table 2.3). A downward trend is observed at each station; however, none of these trends are statistically significant. The visibility trend and uncertainties for each station are summarized in Table 2.3.

2.7 Conclusions

My results suggest that the long-noted negative correlation between dust and rainfall is by association, and that both features are simultaneously responding to large-scale forcing by the SHL. Such an interpretation of the data is consistent with previous work regarding the influence of the SHL on the physical characteristics of the West African Monsoon (*Lavaysse et al.*, 2009; *Lavaysse et al., 2010*; *Evan et al.,* 2015a), and with model (*Ridley et al.,* 2014) and observational (*Ginoux et al.*, 2012; *Schepanski et al.,* 2009; *Evan et al., 2015b*) studies of North African dust sources. I cannot exclude the possibility that dust emission in Sahel is causally correlated to rainfall via changes in vegetation cover and soil moisture (*e.g.*, *Cowie et al.,* 2013), rather I suggest that such effects are to first-order negligible when compared to the coincident changes in dust emission over the vastly larger Sahara.

Finally, when forced with observed sea surface temperatures climate models are unable to reproduce the observed year-to-year variability of dust over the North Atlantic (*Evan et al.,* 2014). In light of this work it is plausible that an underlying cause of this deficiency is an inaccurate representation of the location of the major dust emitting regions (*Evan et al.,* 2014). Additionally, initial work (*Yoshioka,* 2007)

suggests that climate models may not sufficiently represent the SHL and its influence on the regional climate, which I have shown is requisite to represent the dust-cycle in this part of the world, although more work is needed to comprehensively evaluate the representation of the SHL in climate models.

Acknowledgements

Chapter 2, in part, is a reprint of the material as it appears in On the Decadal Scale Correlation between African Dust and Sahel Rainfall: The Role of Saharan Heat Low–forced Winds. Wang, Weijie; Evan, Amato; Flamant, Cyrille; Lavaysse, Christophe, Science Advances, 2015. The dissertation author was the primary investigator and author of this paper.

2.8 Figures

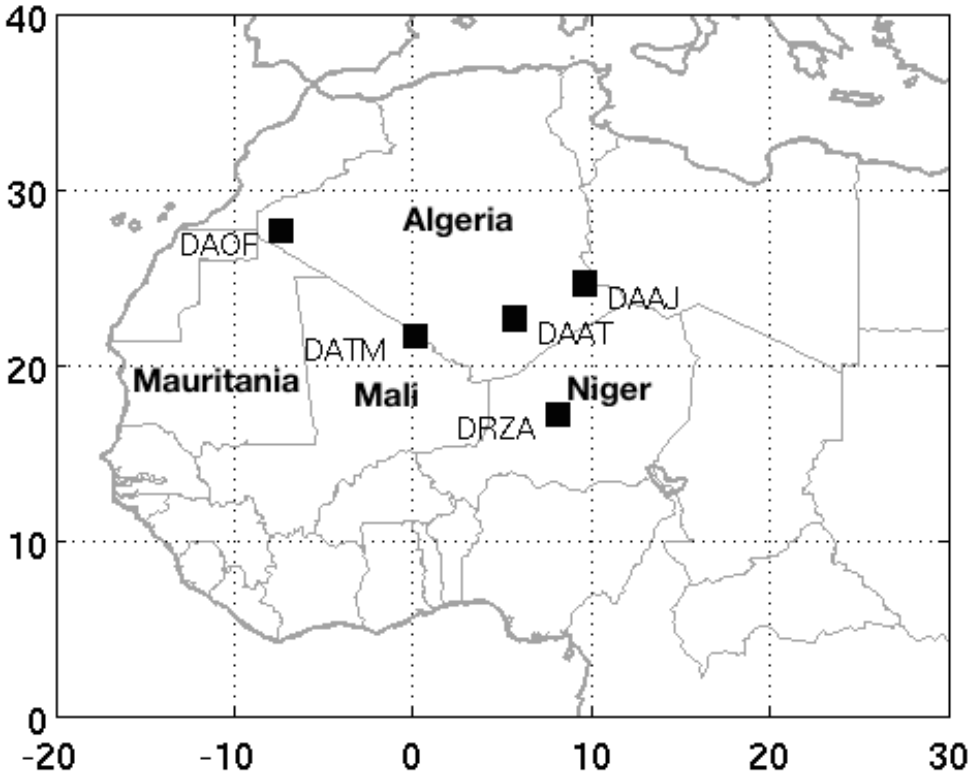

Figure 2.1 Locations of synoptic stations in North Africa.

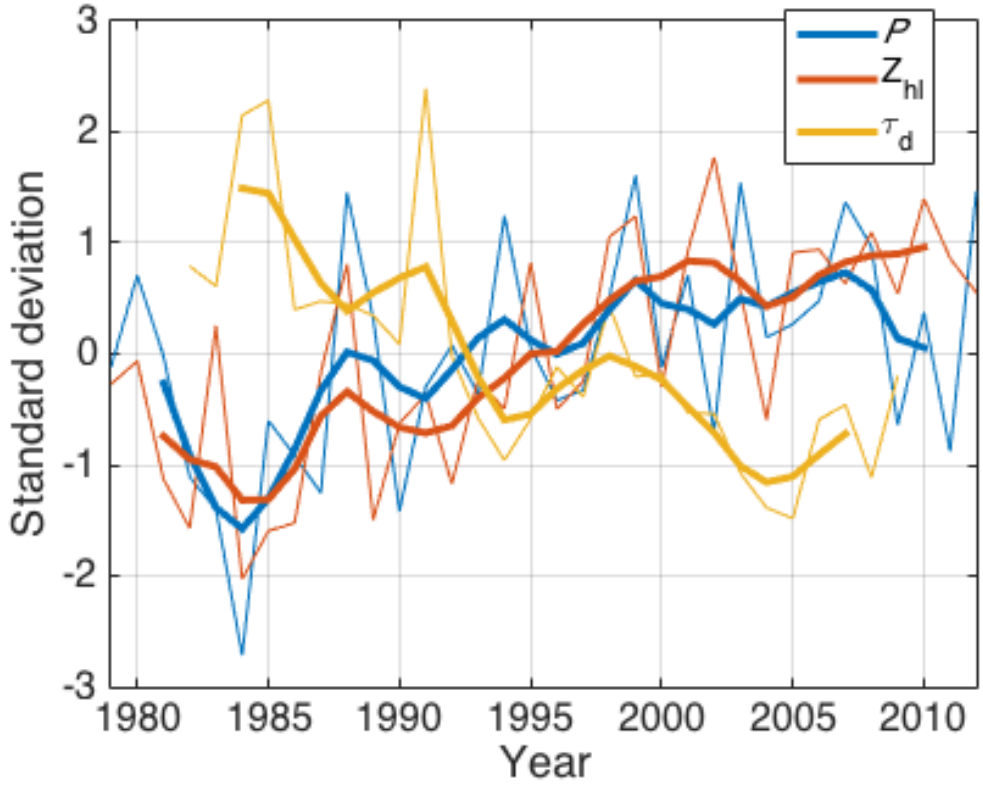

Figure 2.2 Seasonal (June-August) time series of Z_{hl} (red), precipitation (P, blue) and τ_d (yellow). The monthly mean precipitation series is averaged over 5° W to 20° E, 10° to 20° N, and τ_d is averaged over 10° to 65° W and 0° to 30°N. The thin lines are the seasonal means and the thick lines are the 5-season smoothed time series (via a 1-4-7-4-1 filter).

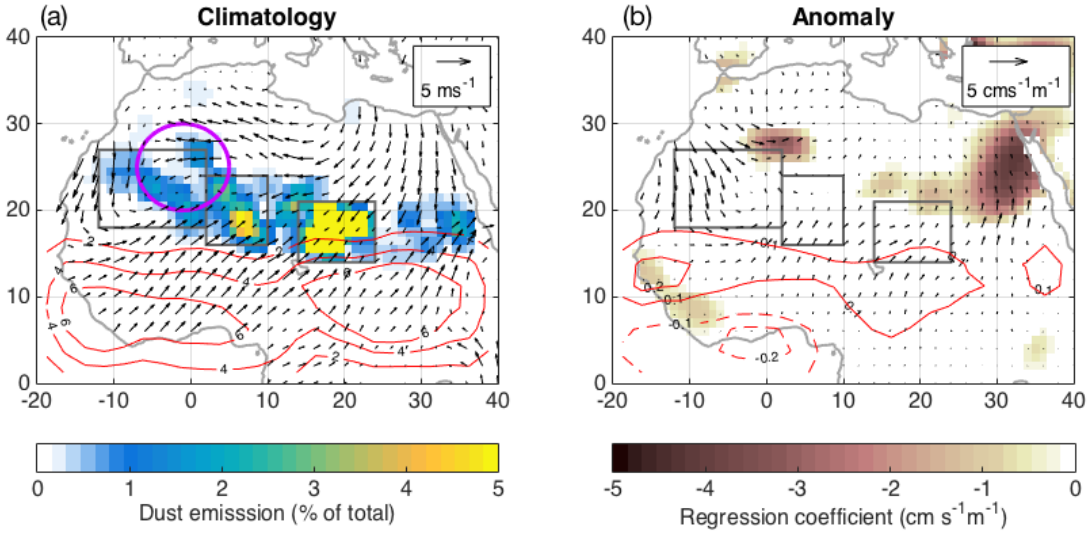

Figure 2.3 Climatology (a) and regressed (b) precipitation and winds. (a) Shown is a map of long-term mean dust emission (shading), seasonal mean precipitation (magenta contour lines, mm day^{-1}) and seasonal mean 925 hPa climatological wind vectors (both June–August). Dust emission rates are in non-dimensional units of % of total annual mean North Africa dust emission rates. The red circle indicates the location of the mean seasonal (June–August) position of the SHL. The gray boxes are the major dust hotspots of the Bodélé Depression (14° to 24° E, 14° to 21° N), the depression in the lee of Aïr and Adrar Mountains (2° to 10° E, 16° to 24° N), and the Mauritania and Western Sahara source region (12°W to 2° W, 18° to 27° N, dashed lines). (b) Map of the coefficients of the regression of 925 hPa meridional and zonal winds (vectors and shading) and precipitation onto Z_{hl}, for June–August and 1979 through 2012. Vectors indicate anomalous wind direction, and the shaded regions are the wind speed coefficients, where only coefficients statistically significant at the 90% level are shown.

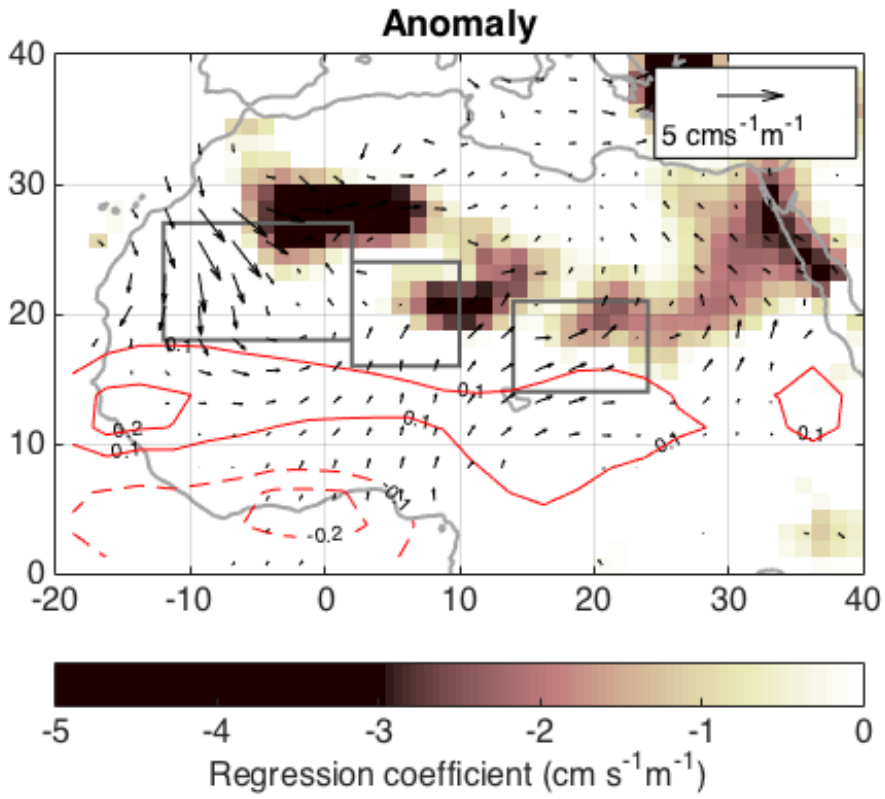

Figure 2.4 Same as Figure 2.3b but using MERRA.

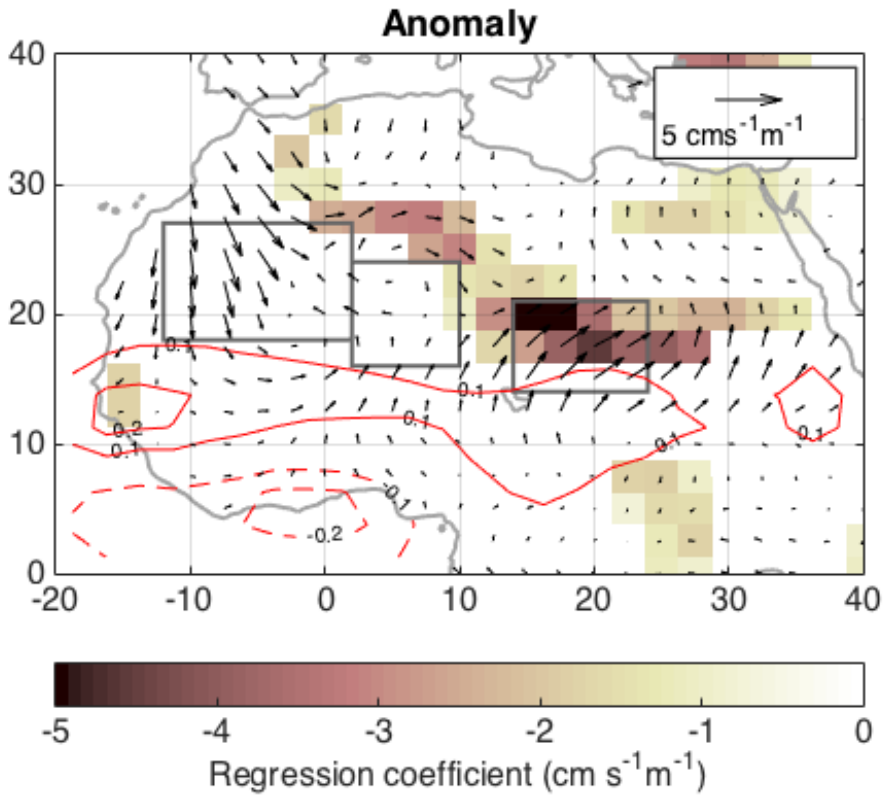

Figure 2.5 Same as Figure 2.3b but using NCEP2.

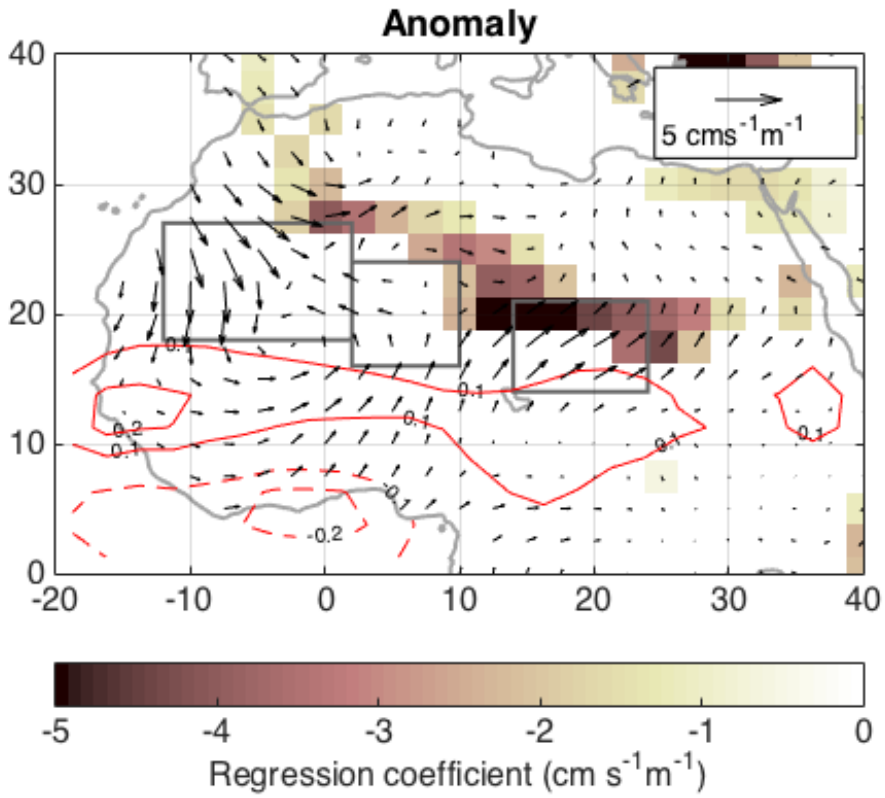

Figure 2.6 Same as Figure 2.3b but using NNRP.

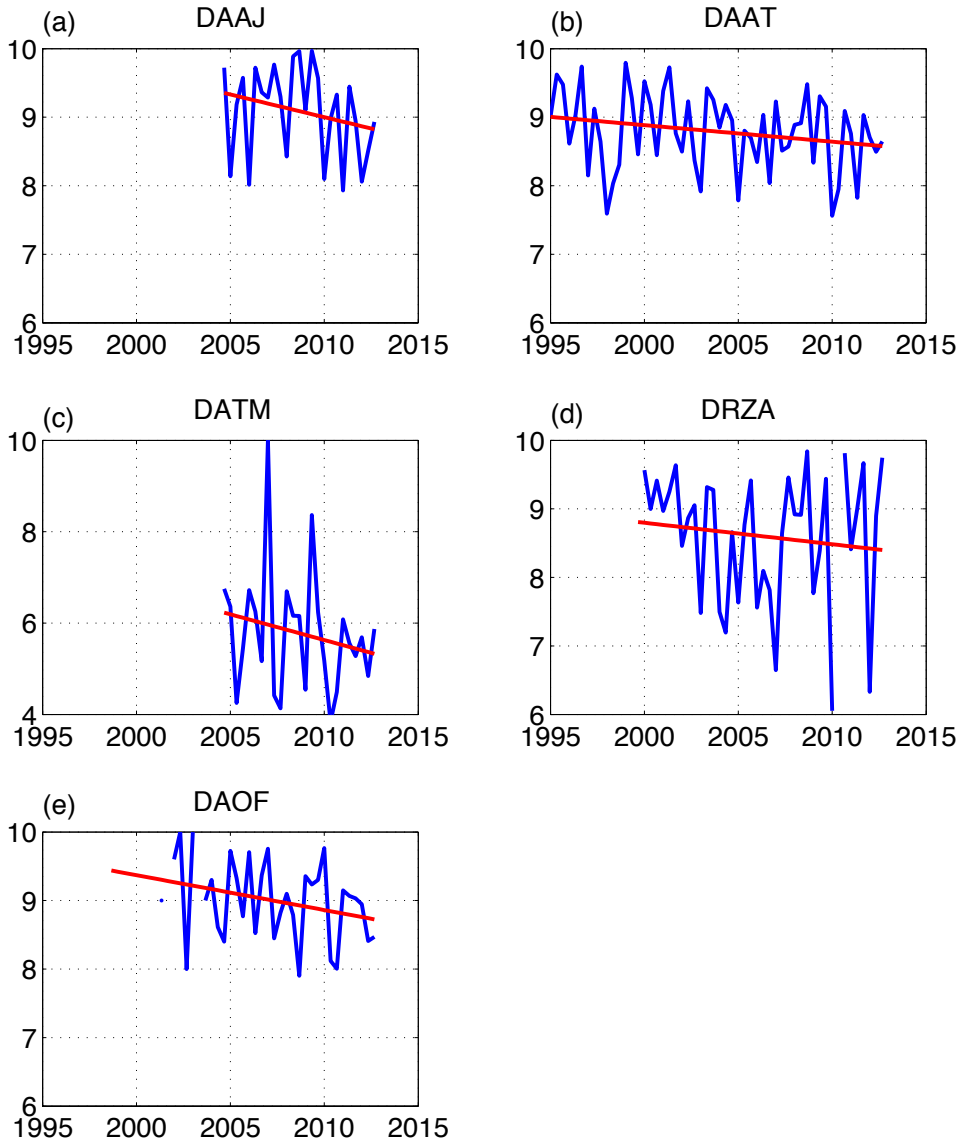

Figure 2.7 Time series (blue) of visibility at five synoptic stations in North Africa. Red line indicates the trend of visibility.

2.9 Tables

Table 2.1 Location, elevation and data availability of each synoptic station in North Africa.

Station	Longitude (°E)	Latitude (°N)	Elevation (m)	Data availability	Mean visibility (km)
DAAJ	9.47	24.55	1054	2004-2012	9.1
DAAT	5.47	22.82	1377	1995-2012	8.8
DATM	0.92	21.38	396	2004-2012	5.8
DRZA	7.98	16.97	502	2000-2012	8.6
DAOF	-8.13	27.67	431	2001-2012	9.0

Table 2.2 R values and p values for time series of Z_{hl}, P, and τ_d. r and p values significant at the 90% confidence level are in bold.

	Z_{hl} , τ_d	Z_{hl}, P	P, τ_d
r	**-0.54**	**0.54**	**-0.53**
p	**0.003**	**0.01**	**0.01**

Table 2.3 Visibility trend and uncertainties of each synoptic station in North Africa.

Station	Mean visibility (km)	Trend (uncertainty)
DAAJ	9.1	-0.066 (±0.11)
DAAT	8.8	-0.024 (±0.03)
DATM	5.8	-0.112 (±0.23)
DRZA	8.6	-0.031 (±0.09)
DAOF	9.0	-0.051 (±0.06)

Chapter 3

The Role the Saharan Heat Low Plays in Dust Emission and Transport in North Africa during Summertime

Abstract

The Saharan Heat Low (SHL) is an important element in the meteorological system in North Africa in summer. However, it is unclear how the SHL affects North African dust emission and transport. Here I investigate the impact of the SHL on dust emission and transport on synoptic time scales in North Africa during the summer over the period 2003-2015 using satellite retrievals of dust optical depth (DOD) and vertical profiles. During the cool phases of the SHL, dust is preferentially emitted from the Bodélé depression. Then, as the SHL warms, the dust emitted from the Bodélé depression is advected westward due to the intensified African Easterly Jet, resulting in anomalously high DOD values over Mali and Mauritania, where persistent lower troposphere convergence within the SHL sustains the high concentrations of dust. Thus, the persistently high dust DOD from satellite retrievals over Mali and Mauritania in conditions of warm SHL are a combination of dust advection from the east and local emission.

3.1 Introduction

Aeolian dust is the most pervasive aerosol in the atmosphere (*Kaufman et al*., 2005) and it has various impacts on the Earth system. Dust can absorb and scatter visible and infrared radiation and thus affect the atmospheric radiation budget (*Golitsyn and Gillette*, 1993; *Kaufman et al*., 2002). Dust can act as a cloud condensation nuclei, indirectly changing the atmospheric radiation budget and the hydrological cycle by modifying cloud cover (*Wurzler et al*., 2000; *DeMott et al*., 2003) and cloud properties (*Miller et al*., 2004; *Andreae and Rosenfeld*, 2008; *Rosenfeld et al*., 2008; *Creamean et al*., 2013). In addition, dust plays a non-negligible role in biogeochemical processes by transporting nutrients to oceanic (*Savoie and Prospero*, 1980; *Swap et al*., 1996; *Okin et al*. 2011) and terrestrial ecosystems (*Swap et al*., 1992; *Formenti et al*., 2001; *Das et al*., 2013).

The Sahara is the world's largest source of aeolian dust (*D'Almeida*, 1987), and it is estimated that each year several hundred teragrams (Tg) of African dust is transported over the Atlantic to the United States, the Caribbean and South America (*Prospero*, 1996; *Chin et al*., 2007). There are a number of major dust source regions in North Africa, including Tunisia and Northern Algeria, the foothills of the Atlas, the Ahaggar and the Aïr Mountains, the coastal region in Western Sahara and western Mauritania, the Mali-Algerian border region, Central Libya, the Bodélé depression, and Southern Egypt and Northern Sudan (*Brooks and Legrand*, 2000; *Caquineau et al*., 2002; *Prospero et al*., 2002; *Israelevich et al*., 2002, *Goudie*, 2003; *Schepanski et al*., 2009; *Formenti et al*., 2011; *Scheuvens et al*., 2013). Among those dust source regions

the Bodélé is found to be the largest contributor to the atmospheric dust load, accounting for 64% (±16%) of the total North Africa dust emission (*Evan et al*. 2015).

Meteorological processes prompting dust emissions and transport are different at the north and at the south of the Intertropical Discontinuity (ITD), the interface between the cool moist southwesterly monsoon flow and the warm and dry northeasterly flown, which location exhibits a significant variability at diurnal to seasonal scales. North of the ITD, the northeasterly Harmattan flow drives dust emissions and transport in summer (*Rodriguez et al*., 2015) whereas dust mobilization south of the ITD is influenced by the monsoon front (*Bou Karam et al*., 2008) and African easterly waves (AEW, *Jones et al*., 2003).

The Saharan Heat Low (SHL) plays an important role in the dynamics of the West African monsoon system. The SHL is an area of high surface temperature and low surface pressure within the summertime Sahara Desert, and is characterized by a low-level cyclonic circulation and mid-level anticyclonic circulation about the SHL center (*Lavaysse et al*., 2009). The warm phases of the SHL indicate a dilatation of the lower atmosphere in response to an increase in low-level temperature and are associated with a strengthened low-level cyclonic circulation that opposes the northeasterlies along the southeastern branch of the SHL and enhances them along the northwestern branch. *Lavaysse et al*. (2010b) and *Chauvin et al*. (2010) showed that AEWs, Rossby waves (and other mid-latitude circulations) and low level advection of moisture from the south (monsoon intrusions) or the north (Mediterranean surges) influence the structure and intensity of the SHL at synoptic scales.

During the summer, the warm phases of the SHL are associated with an intensification of the African easterly jet (AEJ, *Lavaysse et al*., 2010a), and barotropic and baroclinic energy conversions from the AEJ are the main maintenance mechanisms for AEWs (*Norquist et al*., 1977). AEWs dominate synoptic-scale variability over West Africa (*Kiladis et al*., 2006) and modify dustiness over the Atlantic (*Jones et al*., 2003) and West Africa (*Knippertz and Todd*, 2010).

In this chapter, I describe how the intensity of the SHL affects dust emission and transport on the synoptic scale in North Africa in the summertime (July and August) via analysis of 13 years of reanalysis and satellite data. I aim to provide a comprehensive description of the relationship between the phase and strength of the SHL and the North African dust cycle. The remainder of this chapter is organized as follows: In Chapter 3.2, I describe the datasets used in this study. In Chapter 3.3, I examine the periodicity of the intensity of the SHL, how the variability in the SHL is related to dust emission and transport over North Africa. and the tropical Atlantic, and how the vertical distribution of dust varies with the intensity of the SHL. A brief conclusion is provided in Chapter 3.4.

3.2 Data and Methods

Here I describe the reanalysis product, satellite data, and surface observations used in this study to understand how dust transport is associated with the strength of the SHL.

3.2.1 Winds

ERA Interim has modeled variables on 23 pressure levels from 1000 to 1 hPa. I use 600 hPa, 925 hPa and 10 m winds with a horizontal resolution of 1° × 1° at 0600 UTC from ERA Interim reanalysis daily product in July and August from 2003 through 2015 to examine the variability of winds with the strength of the SHL. Winds from ERA Interim have been proven to be well suited for analysis of dust emission and transport in North Africa among all the reanalysis products (*Evan et al*, 2016; *Largeron et al*., 2015).

3.2.2 Satellite Data

Satellite products are useful to study dust transport as they represent the only observational method to characterize the large-scale variability of aerosols. Observations from the Moderate Resolution Imaging Spectroradiometer (MODIS), aboard the Terra and Aqua satellites, have been widely used to study dust over the ocean and the land (e.g. *Kaufman et al*., 2005; *Ginoux et al*., 2012). MODIS level 3 aerosol products provide global coverage of aerosol properties using the Dark Target and Deep Blue algorithms at a 1° by 1° spatial resolution on a daily basis (*Levy et al*., 2015). The Dark Target algorithm retrieves aerosol optical depth (AOD) at 550 nm over ocean and dark land, while the Deep Blue algorithm covers both dark and bright land surface (*Hsu et al*., 2013). Following the methodology of *Ginoux et al*. (2012) I classify a scene as dust over land based on the follow criteria. The first criterion is that Angstrom exponent is less than 0.6 (*Schepanski et al*., 2007) as fine aerosols have larger Angstrom exponent. The second criterion is that the single scattering albedo (ω)

at 412 nm is less than 0.95 as sea salt ω is near 1 (*Ginoux et al*. 2012). The third criterion requires ω at 660 nm to be larger than ω at 412 nm as dust absorption increases sharply from red to deep blue spectrum (*Ginoux et al*., 2012). I also eliminate fine AOD from AOD for DOD over the ocean. Since Terra has a relatively short period of data availability (2000-2007) due to the lack of polarization corrections to the L1B data, I use the Aqua Atmosphere Level 3 daily product to examine how the spatial pattern of DOD over North Africa and the tropical Atlantic varies with the strength of the SHL in summertime from 2003 through 2015.

In order to examine the vertical distribution of dust I use data from the Cloud-Aerosol Lidar and Infrared Pathfinder Satellite Observation (CALIPSO). I use both the Level 2 5-km aerosol layer product and the 5-km aerosol profile product to construct vertical profiles of dust. I construct vertical profiles of DOD at 60 m vertical resolution using the following method: The column DOD (τ) identified by the VFM in the aerosol layer product is given by

$$\tau = \alpha \times z$$

where α is the extinction coefficient of the total number of integrated layers with 60 m resolution within the dust plume.. Here the depth of each layer (Δz) is 60 m, which is the vertical resolution of the CALIOP Level 2 aerosol profile product. The DOD of a single 60 m layer (τ_i) is approximately

$$\tau_i = \alpha_i \times \Delta z$$

and from (1) and (2) I define the DOD at a 60 m resolution as

$$\tau_i = \frac{\tau \alpha_i}{\alpha}$$

where τ and α are given in the aerosol layer product and thus represent values integrated over depth, and a_i is reported in the aerosol profile product.

I average the daytime and nighttime CALIOP data in summertime from 2007 through 2015 over several regions in North Africa to examine how the layer-derived DOD varies with the strength of the SHL. I use DOD instead of extinction to be consistent with MOIDS and AERONET.

3.3 Results

I first describe the periodicity of the SHL index and how the LLAT in North Africa evolves with the SHL index. I then examine how DOD from MODIS and surface winds vary with the SHL index in the summertime for the period of 2003-2015. This is followed by an analysis of the differences in the vertical distribution of DOD as the strength of the SHL varies.

3.3.1 Variability of the SHL index

To examine the variability of the SHL index on synoptic time scale, I first apply a 15-day filter to the daily time series of the SHL and subset July and August. Then I select 25% of the days with the warmest SHL index and 25% of the days with the coolest SHL index (62 days/year × 13 years × 25% = 202 days each). Next, I average the SHL index for all warm days and the SHL index for all cool days and subtract the difference (warm - cool). For lead (lag) days we calculate the average SHL index for all days (202 days in total) that are leading (or lagging) the 25% warmest SHL days by the number of lead/lag days specified. I similarly calculate the average SHL index for all days (202 days) that are leading (or lagging) the 25%

coolest SHL days by the number of lead (lag) days. I then subtract the difference between these two time series (warm lead/lag – cool lead/lag) to examine the variability of the SHL index. I repeated this analysis by using the 10% and 50% warmest and coolest days, obtaining qualitatively similar results.

Figure 3.2 shows the difference of the SHL index from 10-day lead to 10-day lag. Two local minima are found at 7-day lead and 7-day lag, indicating the SHL index varies on a timescale of about two weeks. In this chapter, I focus on a 11-day period, which is from 5 days before the SHL is warm to 5 days after the SHL is warm, as during this period the effect of the SHL on dust emission and transport and winds is notably seen.

3.3.2 The LLAT and the SHL index

I composite the LLAT around the 25% warmest and coolest SHL index for the analysis, which amounts to a total of 404 days. I examine the difference in the LLAT when the LLAT leads and lags the 25% warmest and the coolest SHL days for 0 to 5 days. I make the SHL-composited LLAT maps following the method described in chapter 3.3.1.

To make sure that my analysis is not affected by secular trends or seasonality, I examine the distribution of anomalously warm and anomalously cool days. Anomalously warm and anomalously cool days are homogenously distributed through the time period with 50.4% of anomalously cool days and 49.6% of anomalously warm days in the first half of time period (July 2003-July 2009), and 49.6% of anomalously cool days and 50.4% of anomalously warm days in the second half of

time period (August 2009-August 2015). Anomalously warm and anomalously cool days are also evenly distributed throughout the July-August period with 46.7% of anomalously cool days and 53.1% of anomalously warm days in July and 53.1% of anomalously warm days and 46.7% of anomalously cool days in August.

Between 5 and 4 days prior to the maximum in LLAT, a negative anomaly in the LLAT is observed over Mauritania, northern Mali and southern Algeria, indicating anomalous cooling between 925 and 700 hPa over this region (Fig. 3.3a, b). A positive anomaly in the LLAT is observed over Libya between 5 and 4 days prior to the maximum in LLAT (Fig. 3.3a, b). The positive anomaly of the LLAT over Libya extends westward to Algeria and southward to Chad, Niger and Mali at 3-2 day leads (Fig. 3.3c). The east-west transition of the SHL is driven by mid-latitude Rossby waves propagating along the North Atlantic-North African waveguide (*Chauvin et al*., 2010). At 1-day lead the anomaly becomes stronger and the largest positive anomaly of the LLAT is observed over northern Mali and southern Algeria (Fig. 3.3e). The positive LLAT anomaly then migrates westward and is situated over western Mauritania, eastern Mali and southern Algeria at 0-day lead (Fig. 3.3f). This migration could be induced by the cyclonic circulation associated with the low pressure system that brings dry and warm advection from the North on the western edge of the low pressure and cold and moist air, with most of the time deep convective systems, along the eastern edge (*Lavaysse et al*., 2010). The positive anomaly of the LLAT continues to migrate westward and weakens at 1-2 day lags (Fig. 3.3g, h) (*Chauvin et al*., 2010). Once the low pressure becomes close to the coast, the humid and cold advections

generally induce the collapsing of the SHL. At 1-2 day lags a negative anomaly of the LLAT is observed over Lybia, due to the entry of cool air from the Mediterranean where the prevailing flow pattern is from north to south (*Millan et al*., 1997; *Kallos et al*., 1998; *Gangoiti et al*., 2006). At 3-day lag negative anomalies of the LLAT are seen over Libya and Chad (Fig. 3.3i), and those negative anomalies extend across the Sahara at 4-5 day lags (Fig. 3.3j, k). It is noticeable that the 925 hPa wind vectors and the LLAT are strongly correlated with anomalous southwesterlies corresponding to positive anomalies of the LLAT (Fig. 3.3). Chauvin et al. (2010) used 850 hPa potential temperature and winds to study the variability of the SHL and winds on intraseasonal scale, obtaining similar correlation between the SHL and low-level winds.

3.3.3 DOD and the SHL

In order to examine how DOD varies with the SHL, I examine MODIS-derived DOD over North Africa and the tropical Atlantic composited around warm and cool phases of the SHL and for the entire analysis period following the same methodology used in chapter 3.3.1. Since the strength of the SHL affects the intensity of the AEJ, I also perform an identical composite analysis on 600 hPa winds from reanalysis in order to study the effect of changes in the SHL state on the AEJ, which is typically located between 700 and 600 hPa (*Burpee*, 1972). Only values that are statistically significant at the 90% confidence level are plotted.

I note that there are two ways to interpret our results. A positive DOD anomaly can be due only to changes in the wind speed, or it can be due to changes in emission. From this analysis alone I cannot determine which it is.

For dust leading the SHL by 4 and 5 days, a positive DOD anomaly is observed in the vicinity of the Bodélé depression, which is located between 14-24°E and 14-21°N (Fig. 3.4a). At DOD leading the SHL by 4 days dust appears to be advected westward (Fig. 3.4b). Those positive DOD anomalies are likely to be dust emitted from the Bodélé depression because there are no anomalies in the 600 hPa winds (Fig. 3.4b). Furthermore, there are anomalous northeasterly flows at 925 mb (Fig. 3.3b) and 10 m (Fig. 3.6b) over the Bodélé at the same time. For DOD leading the SHL by 3 days a positive DOD anomaly is seen in the lee of the Aïr and Adrar Mountains (Fig. 3.1, Fig. 3.4c), which is an active dust hot spot (*Schepanski et al*; 2007; *Kocha et al*., 2013; *Evan et al*., 2015b). This positive anomaly is also likely due to local emission as anomalous northeasterly flows at 10 m is observed in the lee of the Aïr and Adrar Mountains (Fig.3.1, Fig. 3.6c), facilitating dust emission. For DOD leading the SHL by 2 days a positive DOD anomaly is seen further to the west, over the eastern Mauritania region, while dust from the Bodélé depression and the basin in the lee of the Aïr and Adrar Mountains continues to be advected westward by the intensified AEJ (Fig. 3.1, Fig. 3.4d). For DOD leading the SHL by 1-0 days there is likely dust emission in Mali and Mauritania as an anomalous cyclonic circulation is observed at surface (Fig. 3.3e-f, Fig. 3.6e-f). Dust from those three regions have all merged into one large and very optically thick plume over Mali and Mauritania

(Fig.3.1, Fig. 3.4e-f). Associated with westward transport of dust is the intensification of the AEJ between 20°W-0°E and 10-20°N, evidenced by an anomalous increase in wind speeds at 600 hPa (Fig. 3.4e-f). The intensity of the AEJ is modulated by the anticyclonic circulation associated with the diverging flow at the top of the SHL (*Lavaysse et al*., 2010a; *Kalapureddy et al*., 2010). As the SHL warms, the anticyclonic circulation in the mid-troposphere intensifies and so does the AEJ, consequently, facilitating the westward transport of dust (Fig. 3.4a-f). Therefore, the positive DOD anomaly over Mali and Mauritania is a combination of dust advected from east and local emission. An increase in dust load is observed in Fig. 3.4e north of the SHL, which is possibly related to the enhancement of the North African high as in *Rodriguez et al*. (2015).

Additionally, for DOD leading the SHL by 1-0 days, a negative DOD anomaly is seen off the coast of Western Sahara and Morocco, which is likely associated with anomalous 600 hPa westerlies that are bringing cleaner marine air onshore (Fig.3.1, Fig. 3.4e-f). I repeated this analysis using 850 hPa winds, also noting anomalously strong westerlies at this pressure level (not shown).

For DOD lagging the SHL by 1 day, the positive DOD anomaly, which was centered on 10°W and 15°N at a 0-day lead/lag, appears to propagate westward into the tropical North Atlantic (Fig. 3.4g), reaching 40°W at a 2-day lag (Fig. 3.4h) and 50°W at a 3-day lag (Fig. 3.4i). For dust lagging the SHL by 4-5 days the high DOD anomalies within the Saharan air layer essentially extends beyond 50°W, which is the westernmost edge of our region of study (Fig. 3.4j-k).

However, I cannot be entirely certain with regard to the causality between dust and easterlies. It is possible that the winds along are changing the dust concentration, rather than anomalously high dust concentrations to the east being advected by the anomalously strong easterlies.

Coincident with the westward propagation of this region of high DOD anomalies, from the ERA Interim data I see anomalously strong 600 hPa easterlies that very closely match the spatial structure of this positive DOD anomaly (Fig. 3.4e-i). These positive DOD anomalies in Figures 3.4e-i are bounded to the north by a region of negative DOD anomalies, which are found within a region where the 600 hPa flow is anomalously westerly. Thus, in the tropical North Atlantic and at around 20°N the sign change of the zonal wind is also where the sign of the DOD anomalies change, in the meridional direction. It is important to note that the DOD and wind data are completely independent, thus I can conclude with a high degree of confidence that advection of dust across the tropical North Atlantic, associated with the state of the SHL, is likely due to the SHL-forced strengthening of the AEJ.

At 1-0 day leads and 1-2 lags there is a positive DOD anomaly surrounding and within the SHL (Fig. 4e-h). This area, which includes northern Mali, southern Algeria, and eastern Mauritania (Fig. 3.1), is considered to be one of the major North African dust source regions; DOD from the MODIS Deep Blue product is observed to be above 0.2 for more than 75% of the time in June, July and August from 2003 through 2009 (*Ginoux et al*., 2012). Other satellite products, such as the Ozone Monitoring Instrument (*Schepanski et al*., 2007), the Total Ozone Mapping

Spectrometer Aerosol Indices (*Engelstaedter et al*., 2006) and the Multiangle Imaging Spectroradiometer (*Knippertz and Todd*, 2010), also identify this region as one of the most active dust hot spots in North Africa. The assumption made in the above cited papers is that the high vertically integrated dust concentration is due to strong surface emission. However, such an assumption may not be justified as dust mobilized further east is likely advected into this area; Niger, Mali and Mauritania are downwind of the Bodélé and Aïr and Adrar source regions (Fig. 3.1). *Ashpole and Washington* (2013) find two dominant sources in the central and western Sahara, one in southwest Algeria and northwest Mali, and the other in southern Algeria, northwest Niger, and northeast Mali using Spinning Enhanced Visible and Infrared Imager (SEVIRI) dust flag, but one of the caveats of their method is that it cannot distinguish dust advected from elsewhere from local dust emission. *Schenpanski et al.* (2013) identify dust source regions using fifteen-minute Meteosat Second Generation (MSG) SEVIRI infrared dust index images and find large fraction of dust source activations in the Bodélé and the foothills of the Saharan mountain area, which agrees with our findings here. I will further investigate this later in this section and in Chapter 3.3.5. I repeated the analysis shown in Figure 3.4 using winds from Modern Era Retrospective-Analysis for Research and Applications (MERRA), obtaining results are consistent with those from ERA Interim (not shown).

In order to examine the convective pattern associated with dust within the SHL region I analyze the composite of divergence at 925 hPa and 600 hPa over the SHL center, which is defined here as 10°-0°W and 15°-25°N. I first average divergence and

DOD over the SHL center, and then perform the analysis in the same way as the lead/lag composites of DOD. For divergence leading and lagging the SHL by 1-0 day, anomalous convergence at 925 hPa and divergence at 600 hPa (Fig. 3.5a) are observed over the SHL center. The differences in convergence at 925 hPa and divergence at 600 hPa reach a maximum at 0-day lead/lag (Fig. 3.5a). Anomalous convergence at 925 hPa associated with the warm SHL results in convergence of dust into the SHL center (Fig. 3.5c), and the anomalous upper level divergence directs dust around the SHL center, both contributing to the positive DOD anomaly over the SHL center at 1-0 day lead/lags (Fig. 3.5b, Fig. 3.4e-g). However, I still cannot exclude the possibility that there is emission over the SHL center.

When DOD leads the SHL by 5 to 3 days, a negative DOD anomaly is observed over the SHL center (Fig. 5b). When DOD leads the SHL by 2-0 day and lags the SHL by 1-4 days, a positive DOD anomaly is seen over the SHL center (Fig. 3.5b). Our analysis shows that DOD over the SHL center varies in phase with the SHL index (Fig. 5b, c). When the SHL is cool, dust is emitted from the Bodélé depression and the basin in the lee of the Aïr and Adrar Mountains, and as the SHL warms, dust from these two source regions is likely advected westward to Mali and Mauritania. At a 0-day lead/lag the difference in DOD reaches a maximum over the SHL center (Fig. 3.5b). As the SHL cools and convergence at 925 hPa weakens, the difference in DOD over the SHL center decreases at 1-4 day lags (Fig. 3.5b, c).

3.3.4 Surface winds

It is known that most dust emission in North Africa occurs within major topographic depressions (*Prospero et al*., 2002; *Evan et al*., 2016), where flow through the mountain gaps can accelerate and induce dust storms. It is estimated that nearly 85% of dust emission in North Africa occurs in the downwind directions of mountain gaps (*Evan et al*. 2015), and thus the variability in gap flow significantly affects dust emission. In order to understand how the variability in the SHL affects the gap flow, and in turn dust emission, here I examine the 10m winds from ERA Interim. For dust leading the SHL by 5 to 4 days, anomalous northeasterly surface flow is observed downwind of the gap between the Tibesti mountains (labeled c in Fig. 3.6) and Ennedi plateau (e) as well as the gap between the Tibesti (c) and Ahaggar mountains (b), and thus positive DOD anomaly is seen in the downwind region over the Bodélé depression (Fig. 3.6a). For dust leading the SHL by 3 to 2 days, anomalous northeasterly surface flow is observed downwind of the gap between the Tibesti (c) and Ahaggar mountains (b) as well as the gap between Aïr massif (d) and Ahaggar mountains (b), that contributes to the positive DOD anomaly over the Bodélé depression and the lee of Aïr and Ahaggar mountains (Fig. 3.6c, d). For dust leading the SHL by 4 to 2 days anomalous southwesterly flow is observed between Atlas (a) and Ahaggar mountains (b), and positive DOD is seen over Algeria and Libya (Fig.3.1, Fig. 3.6a-d). For dust leading the SHL by 1 day an anomalous cyclonic circulation is observed at the surface over Mali and Eastern Mauritania, and gap flows weaken between the Tibesti mountains (c) and Ennedi plateau (e) as well as between the

Tibesti (c) and Ahaggar mountains (b) (Fig. 3.6e). For dust leading the SHL by 0 day surface winds converge from all sides in the SHL center, and a positive dust anomaly overlaps with an anomalously strong cyclonic circulation located in Mali and Mauritania (Fig. 3.6f). Our analysis indicates that dust emission in North Africa increases with anomalously strong down-gap winds, which are associated with the cool phases of the SHL.

3.3.5 Dust vertical profiles

Dust vertical profiles provide useful information on dust emission and transport, and CALIPSO is the only satellite that measures vertical profiles of aerosols globally. Since MODIS products do not provide information on the vertical profiles of dust, I use CALIPSO to examine the surface and upper level dust over the SHL center in summer. I examine how the vertical profiles of DOD vary with the SHL strengthen over the SHL center in summer from 2007 through 2015. *Ma et al*. (2013) showed that the climatology of DOD from CALIPSO is significantly lower than MODIS over the Saharan region, which we have also noted (not shown). Here I normalize daily CALIPSO DOD, averaged over the SHL center (10°-0°W, 15°-25°N) so that the daily column integrated DOD from CALIPSO equals the daily mean MODIS DOD over the SHL center. For dust leading the SHL by 5-4 days a negative DOD anomaly is located above 1 km (Fig. 3.7). For dust leading the SHL by 3 days a positive DOD anomaly is observed below 2 km (Fig. 3.7), indicating there is likely dust emission in the SHL center. For dust leading the SHL by 2 days a positive DOD anomaly extends to 3.5 km, suggesting that as the SHL warms, more dust is building up over the SHL center.

Since the positive anomaly is found in the lower troposphere, there is likely dust emission in the SHL center at 2-day lead. For dust leading the SHL by 1-0 day a positive DOD anomaly is seen from the surface up to 6 km due to the anomalous convergence at 925 hPa associated with the warm SHL (Fig. 3.5a, Fig. 3.7), which results in dust being advected into the SHL. The largest difference in DOD is located between 0.5-3.5 km at 1-0 days leads and 1 day lag (Fig. 3.7). For dust lagging the SHL by 3-5 days a positive DOD anomaly is mainly found above 2.5 km (Fig. 3.7), which is likely the residual of dust.

To further examine how dust emission and transport are associated with the strength of the SHL in North Africa in summer, I construct the vertical profiles of DOD for warm and cool SHL cases in regions where DOD anomalies are observed in Fig. 3.4, and calculate the difference in DOD (warm - cool) from the surface to 8 km. Then I normalized the difference in DOD to 1 as I focus on the shape of the profiles rather than the magnitude. For DOD leading the SHL by 2 days a positive DOD anomaly is observed over the lee of the Aïr and Adrar Mountains (Fig. 3.8a), and positive DOD anomalies from CALIPSO (3W-8°E and 15-20°N) occur between 1 to 4 km above sea level with the largest anomaly around 2 km (Fig. 3.8b), indicating there is dust emission over the lee of the Aïr and Adrar Mountains. For DOD leading the SHL by 1 day, positive and statistically significant DOD anomalies (Fig. 3.8c, 10W-2°E, 15-20°N) are seen from the surface up to 6 km (Fig. 3.8d). The vertical profile exhibits a bimodal distribution, with one peak below 1 km and another peak at 2 km, indicating dust in this region could be a mixture of local emissions linked to the gap

flow (Fig. 3.6e) and dust advected from the east. For DOD leading the SHL by 0 day positive DOD anomalies (Fig. 3.8e, 15-5°W, 15-20°N) extend above 6 km (Fig. 3.8f). Surface temperature over the Sahara is high in summer, and thus dry convection produces a deep mixed layer that can extend up to ~450 hPa (6.0 km) (*Carlson and Prospero,* 1972; *Adams et al.*, 2012) when it is fully developed late in the day. Positive DOD anomalies are seen throughout the deep mixed layer, indicating there is strong dry convection to the west of the lee of the Aïr and Adrar Mountains. CALIPSO DOD differences are statistically significant from below 1 km to above 6 km (Fig. 3.8f). The occurrence of dust at high altitudes in this region indicates advection of dust over Mali and Mauritania when the SHL is warm whereas the positive anomaly below 1 km indicates there is dust emission from the surface (Fig. 3.8f). As this dust plume is advected to the western coast of North Africa (1-day lag, Fig. 3.8g, 17-10°W, 15-20°N), CALIPSO DOD differences are statistically significant from near the surface to 7 km (Fig. 3.8h), suggesting dust emission still occurs at the surface at 1-day lag. For DOD lagging the SHL by 2 days (Fig. 3.8i, 17-10°W, 15-20°N), positive and statistically significant DOD anomalies are mainly seen in layers from 4 and 7 km and below 1 km altitude (Fig. 3.8j). The positive anomaly from 4 and 7 km is the residual dust layer while the one below 1 km is attributable to surface emission. Differences in DOD between 1 to 4 km are not statistically significant at 95% confidence level (Fig. 3.8j), and this could be due to the penetration of marine air.

3.4 Conclusions

The purpose of this chapter is to examine the effect of the SHL on dust emission and transport on synoptic scale in North Africa in summer. Combining satellite data and reanalysis product, I have shown that cool phases of the SHL are associated with more dust emission over the major dust hotspots in North Africa through the intensification of the gap flows in mountainous regions upstream. As the SHL warms, dust is likely advected westward by the AEJ, which strengthens with the warm SHL. Positive anomalies in DOD are observed over Mali, Mauritania and Algeria when the SHL is warm, and such large anomalies are due to the westward transport of dust from the Bodélé depression and the lee of Aïr and Adrar Mountains and local emissions as well as the anomalously strong convergence in the lower troposphere over the SHL center that sustains the advection of dust. This region has been identified as one of the major dust hot spots by previous studies (e.g. *Ginoux et al*., 2012). However, my analysis shows that high DOD there is a combination of local emissions and dust advection from east, although the relative contribution of local and upstream sources requires further investigation. As the SHL cools, dust is advected westward over the North tropical Atlantic.

This chapter presented an observational analysis of dust variability on synoptic scale associated with the strength of the SHL in summer over North Africa. Highlighting this relationship between the SHL and dust emission and transport helps identify the source regions of dust and mechanisms that govern dust emission and transport. Climate models in the framework of the 5th Coupled Models

Intercomparison Project (CMIP5) shows large variability in the SHL temperature and discrepancies in the spatial and temporal evolution of the SHL (*Lavaysse et al*., 2015; *Dixon et al*., 2017). In addition, dust emission is systematically underestimated in these models (*Evan et al*., 2014). This study contributes to our understanding of the role the SHL plays in dust emission and transport, and highlights the importance of the correct representations of dust source regions, mechanisms that govern dust transport, as well as the parameterization of the SHL in climate models in predicting dust emission and transport in the future.

Acknowledgements

Chapter 3, in part, has been submitted for publication of the material as it may appear in The Role the Saharan Heat Low Plays in Dust Emission and Transport during Summertime in North Africa. Wang, Weijie; Evan, Amato; Flamant, Cyrille; Lavaysse, Christophe, Aeolian Research, 2017. The dissertation author was the primary investigator and author of this paper.

3.5 Figures

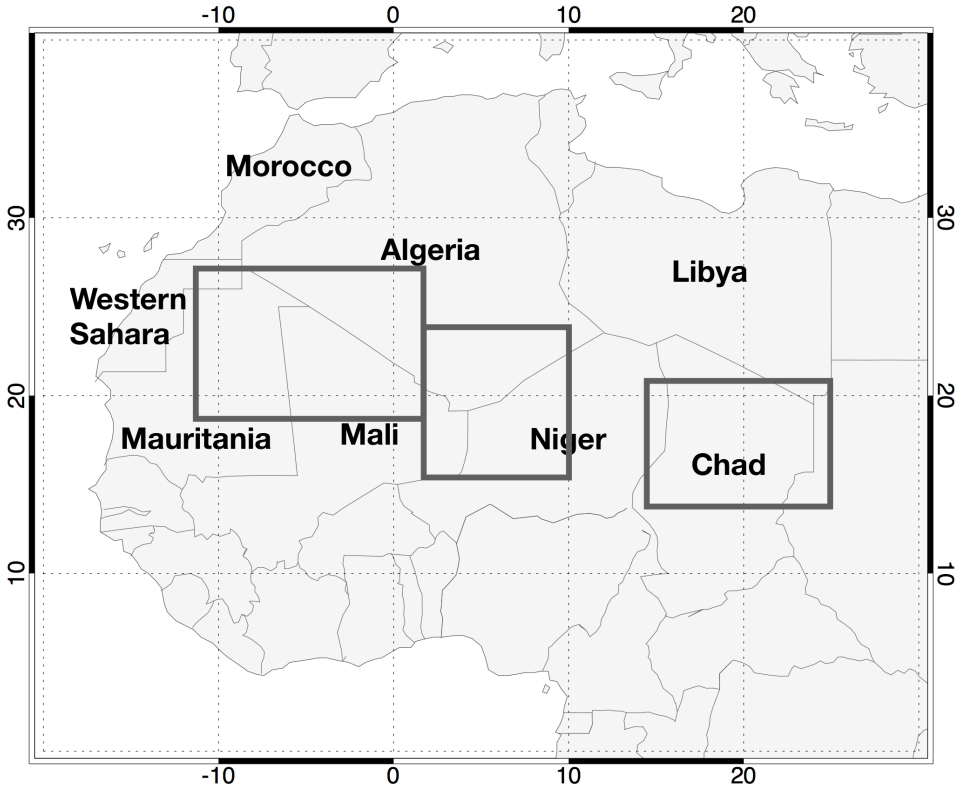

Figure 3.1 Map of North Africa. The gray boxes are the major dust source regions of the Bodélé Depression (14° to 24° E, 14° to 21° N), the depression in the lee of Aïr and Adrar Mountains (2° to 10° E, 16° to 24° N), and the Mauritania and Western Sahara source region (12°W to 2° E, 18° to 27° N).

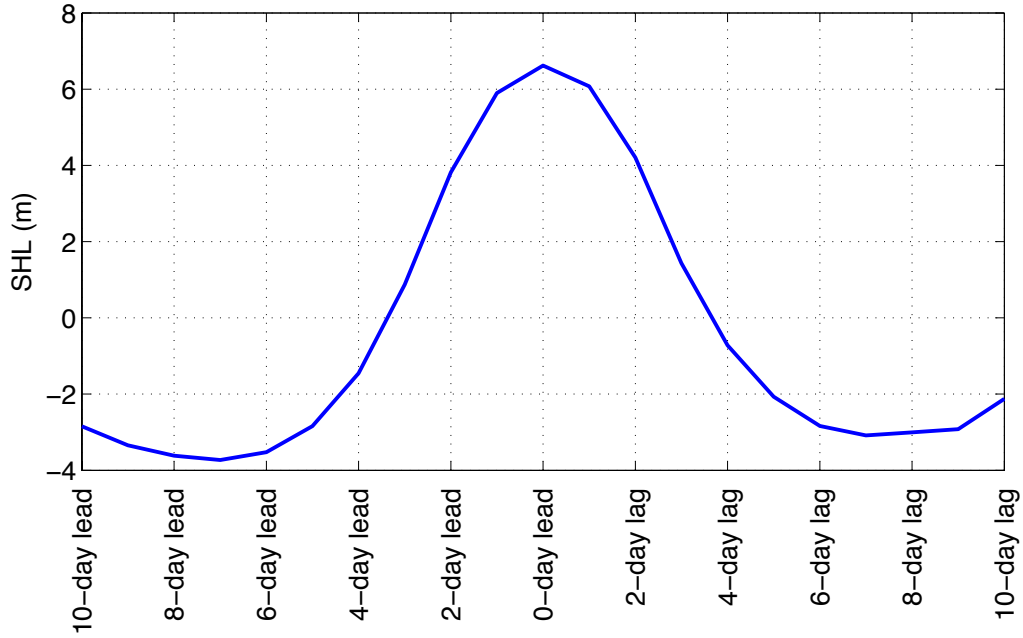

Figure 3.2 Difference in the SHL for 25% of the warmest minus 25% of the coolest SHL cases in July and August from 2003 through 2015 from 10-day lead to 10-day lag.

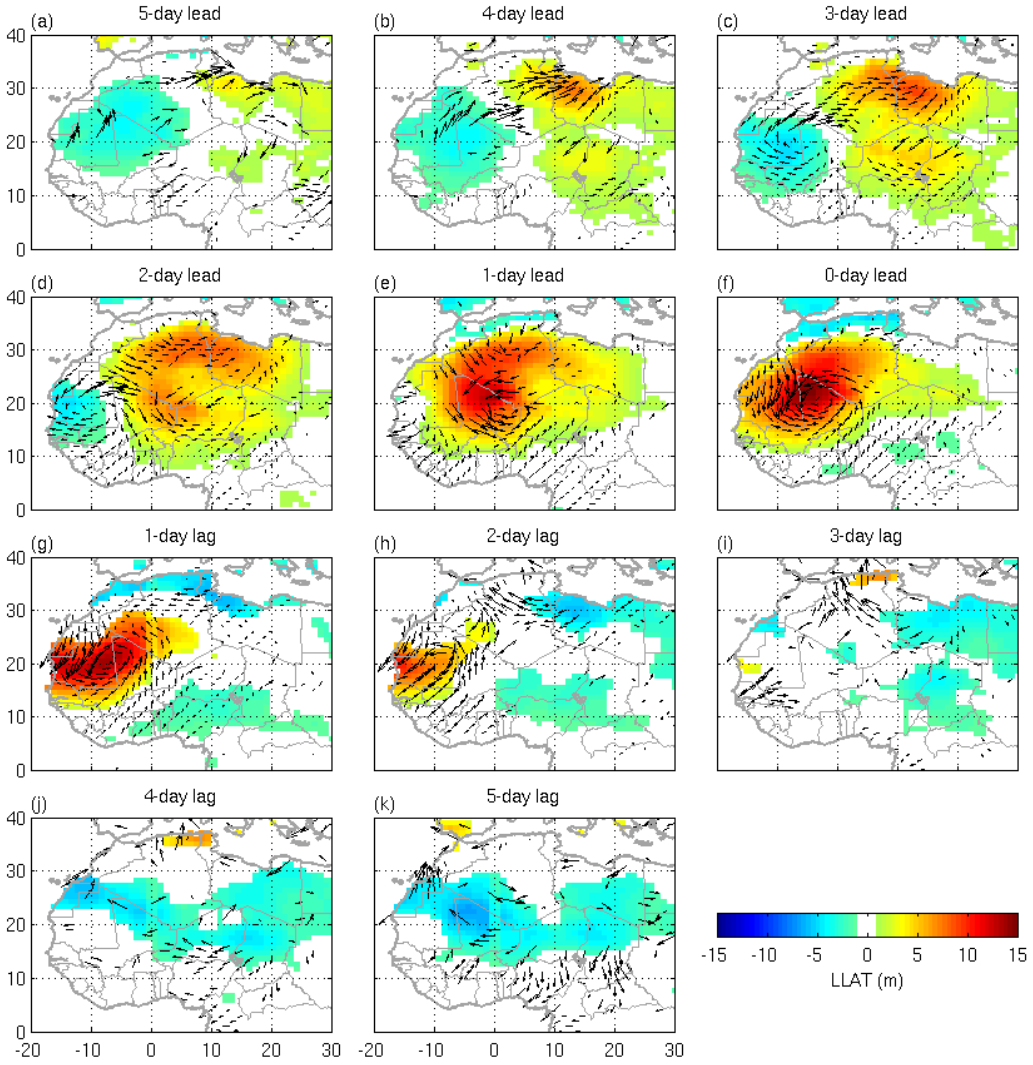

Figure 3.3 Differences in the LLAT and wind vectors at 925 hPa for the 25% warmest minus 25% coolest SHL cases in July and August from 2003 through 2015 using 15-day filter. 925 hPa wind vectors are from ERA Interim daily product. (a)-(f) winds lead the SHL for 5 to 0 days. (g)-(k) winds lag the SHL for 1 to 5 days. Only differences statistically significant at the 90% confidence level are shown.

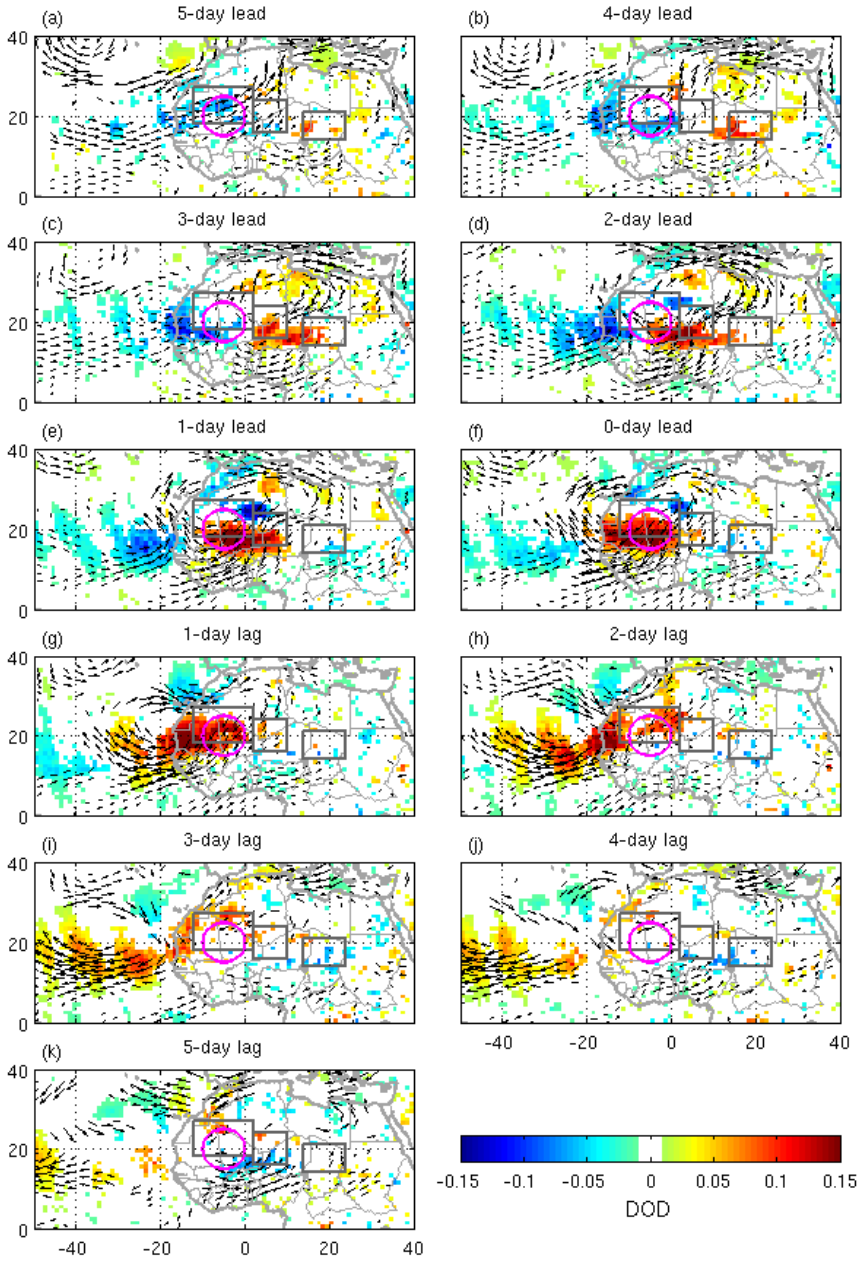

Figure 3.4 Differences in DOD and wind vectors at 600 hPa for the 25% warmest minus 25% coolest SHL cases in July and August from 2003 through 2015 using 15-day filter. DOD is from MODIS dark target and deep blue combined at 550 nm and 600 hPa wind vectors are from ERA Interim daily product. (a)-(f) DOD leads the SHL for 5 to 0 days. (g)-(k) DOD lags the SHL for 1 to 5 days. Only differences statistically significant at the 90% confidence level are shown. The gray boxes are the major dust source regions. The magenta circle indicates the location of the mean seasonal position of the SHL.

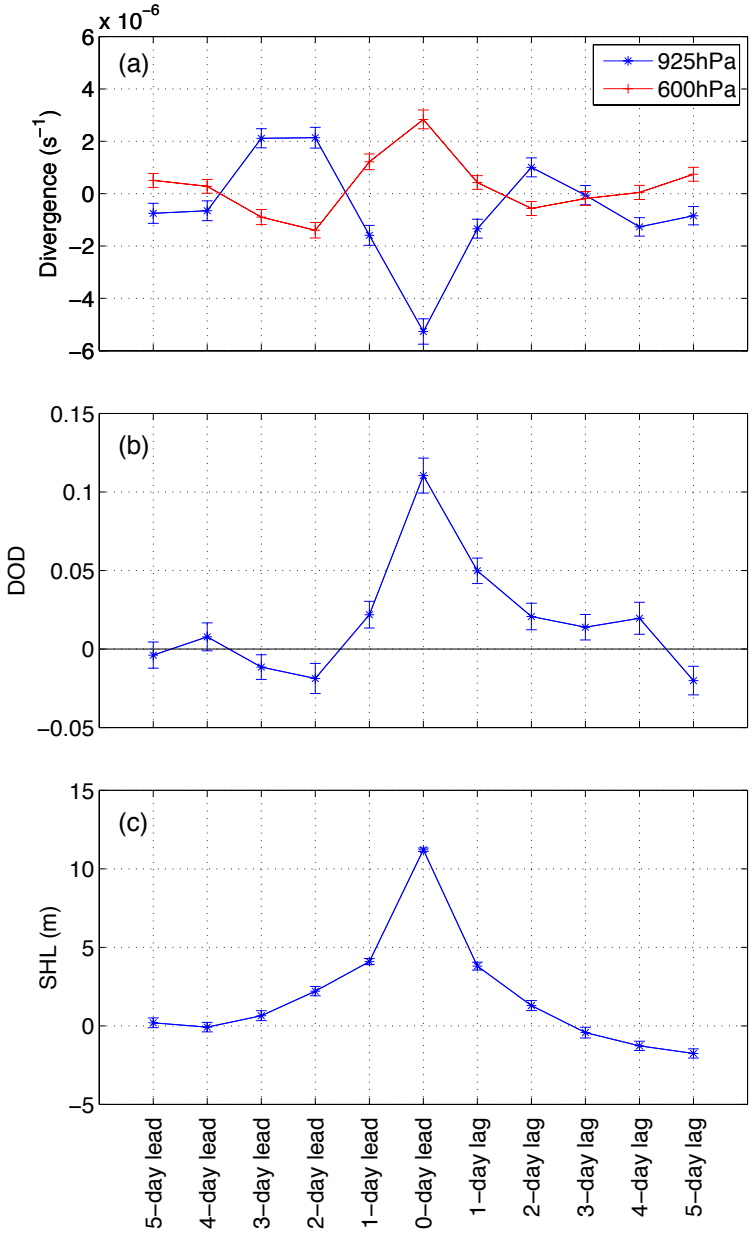

Figure 3.5 Differences in (a) divergence at 925 hPa and 600 hPa, (b) MODIS DOD over the SHL center, and (c) the SHL for the 25% warmest minus 25% coolest SHL cases in July and August from 2003 through 2015 using 15-day filter when divergence and DOD lead or lag the SHL for 0-5 days. Also shown is the error bars of divergence, DOD and the SHL. Divergence and DOD are averaged over 10° to 0°W and 15°-25°N. Divergence is from ERA Interim daily product.

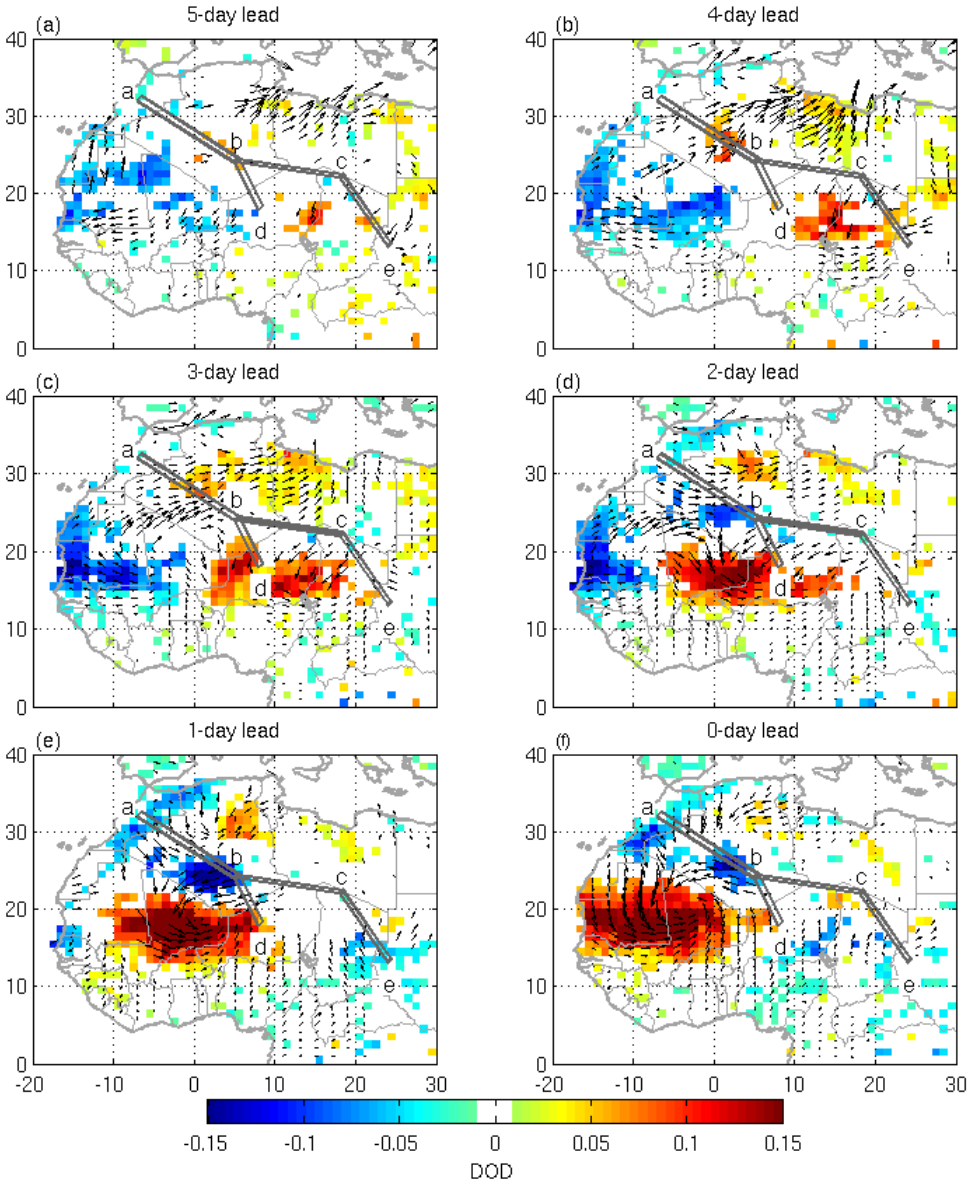

Figure 3.6 Difference of the 10m wind vectors from ERA-Interim and DOD from MODIS for the 25% warmest minus 25% coolest SHL cases at 5-0 day leads in the summertime from 2007 through 2015 using 15-day filter. Only differences statistically significant at the 90% confidence level are shown. Transects indicate gaps between mountains. a-e represent Atlas Mountains, Ahaggar mountains, Tibesti mountains, Aïr massif and Ennedi plateau, respectively.

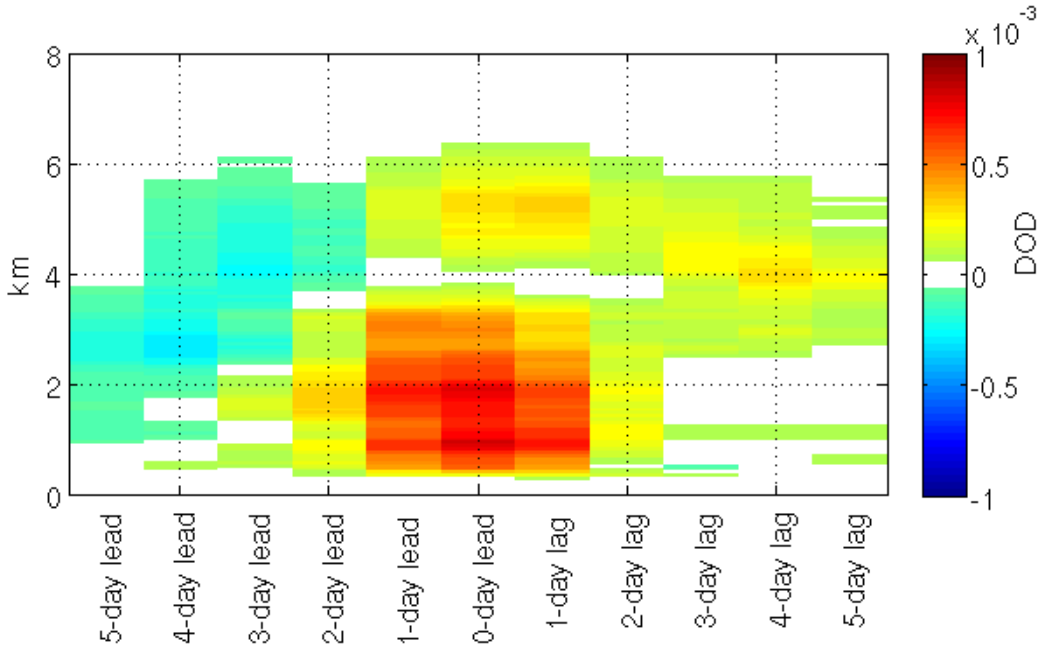

Figure 3.7 Difference in the vertical distribution of DOD from CALIPSO for the 25% warmest minus 25% coolest SHL cases in the summertime from 2007 through 2015 averaged over the SHL center (10-0°W and 15-25°N) for 5-0 day leads and 1-5 day lags. Daily DOD from CALIPSO averaged over the SHL center is normalized to equal daily mean DOD from MODIS averaged over the SHL center.

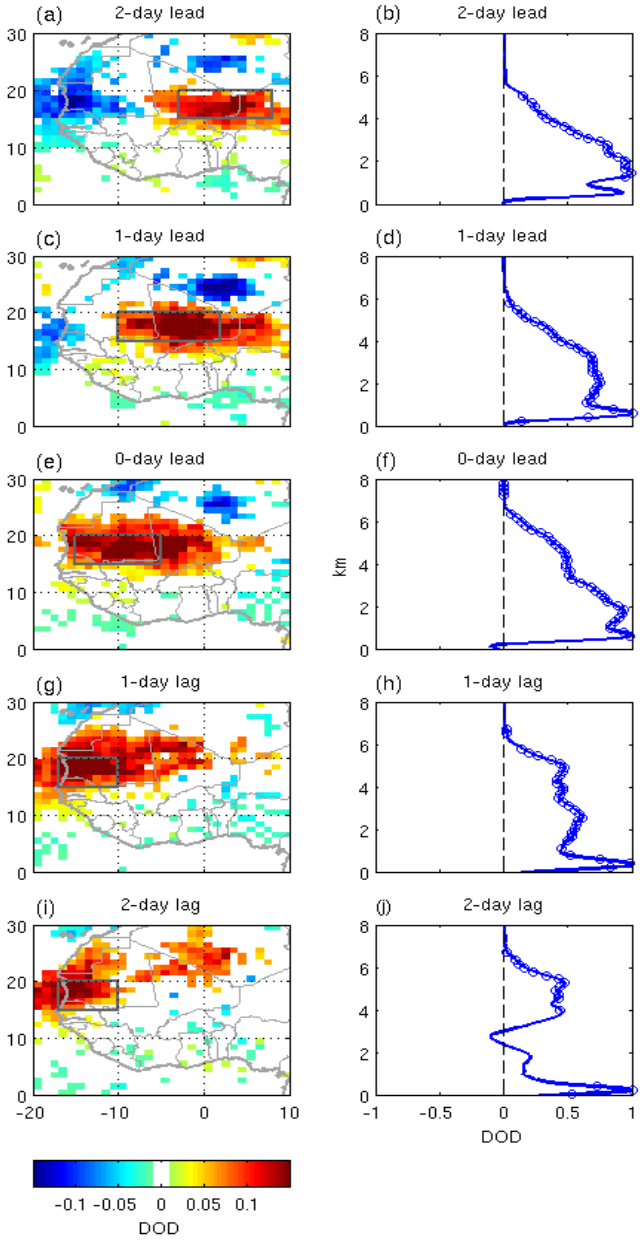

Figure 3.8 Differences in the vertical distribution of DOD from CALIPSO for the 25% warmest minus 25% coolest SHL cases in the summertime from 2007 through 2015 averaged over (b) 3W-8°E and 15-20°N at a 2-day lead, (d) 10W-2°E and 15-20°N at a 1-day lead, (f) 15W-5°E and 15-20°N at a 0-day lead, (h) 17-10°W and 15-20°N at a 1-day lag, and (j) 17-10°W and 15-20°N at a 2-day lag. Vertical profiles of DOD are normalized to 1. Circles indicate where the difference in DOD is significantly different at the 95% confidence level. Figures (a), (c), (e), (g), and (i) are the same as figures 4 (d)-(h). Gray boxes indicate the regions where CALIPSO profiles are constructed.

Chapter 4

Identifying the Bias in a Dust Source Function in North Africa using the WRF-Chem Model

Abstract

The Sahara is the largest desert in the world that accounts for more than 50% of the global dust emission. However, it is difficult to identify dust source regions as the Sahara is vastly uninhabited. Previous works have used satellite data to construct dust source functions. In this chapter, I examine an existing dust source function in North Africa constructed with Deep Blue AOD from MODIS. I find the dust source function made with MODIS data is biased in the Sahel and western Sahara as satellite cannot distinguish local emission from dust advection. By using dust emission flux and DOD from the Weather Research and Forecasting with Chemistry (WRF-Chem) model, I find the current dust source function overestimates DOD in the Sahel and the western Sahara region in all seasons. To eliminate the biases of the dust source function due to advection, I develop a new source function using DOD in the lowest 1km from the model. Using DOD below 1km reduces the biases in the source function in the Sahel. However, no significant improvement is observed in the western Sahara region. This work suggests that dust source functions constructed with satellite observations may overestimate dust emission in the downwind regions and DOD may not be a good proxy for the source function.

4.1 Introduction

Dust plays an important role in the global and regional climate system (e.g. *Tegen et al*., 1996; *Ramanathan et al*., 2001; *Woodward*, 2001). In order to estimate the impacts of dust on the climate, dust sources need to be properly identified. Dust emission from North Africa accounts for more than 50% of the total global dust emission (*Engelstaedter et al.,* 2006; *Ginoux et al.,* 2012). However, it is difficult to identify dust source regions in North Africa due to the lack of ground-based observations in the Sahara. Previous studies have used satellite observations to derive dust source regions in North Africa (*Schepanski et al*., 2007; *Ginoux et al*., 2012; *Ashpole and Washington*, 2013a). For example, *Ginoux et al*. (2012) made a dust source function in North Africa using Deep Blue AOD from MODIS. However, satellite products cannot distinguish between local dust emission and dust transport, and thus dust source functions derived from satellite observations may be biased. In the past decades, there has been increasing efforts to improve dust modeling (e.g. *Ginoux et al*., 2001; *Zender et al*., 2003; *Zhao et al*., 2010). Although climate models show a wide range of dust emission due to uncertainties in model processes (*Evan et al*., 2014), they provide a unique opportunity to examine how dust emission flux and dust concentrations are related to each other.

The aim of this chapter is threefold. First, I examine the dust climatology from satellite products. Second, I use dust emission and DOD from the Weather Research and Forecasting with Chemistry (WRF-Chem) model (*Grell et al*., 2005; *Skamarock et al*., 2008) to examine the biases in the dust source function developed by *Ginoux et al*.

(2012). Then I develop a new dust function to examine whether that improves dust source mapping in North Africa.

This chapter is organized as follows. Chapter 4.2 details the satellite products and model used in this work. Chapter 4.3 compares dust climatology from two satellites. Chapter 4.4 examines dust emission frequency from the WRF-Chem model using three criteria. Conclusions are provided in Chapter 4.5.

4.2 Data and Method

4.2.1 Dust Climatology

I use monthly mean MODIS Aqua Deep Blue product to derive DOD as described in Chapter 3.2.2. I construct the seasonal mean DOD climatology from monthly mean MODIS at 1° × 1° from 2003 through 2015. I also use CALIPSO Level 3 monthly mean DOD under cloud free conditions from 2007 through 2015 at 5° × 2° to construct the seasonal mean dust climatology in North Africa.

4.2.2 Model

I use DOD and emission flux from a dust simulation (*Zhao et al*., 2013) made with the WRF-Chem model. The WRF-Chem model simulates particulates and trace gases alone with the meteorological fields at 3 hourly intervals. The simulations are conducted at 1° horizontal resolution using a quasi-global channel configuration (180°W-180°E, 60°S-70°N) with 35 vertical layers up to 50hPa. The meteorological initial conditions and lateral boundary are derived from the NNRP data at 6 hourly intervals.

The aerosol scheme implemented in WRF-Chem is the Model for Simulating Aerosol Interactions and Chemistry aerosol model (MOSAIC, *Zaveri et al*., 2008) coupled with the Carbon Bond Mechanism photochemical mechanism (*Zaveri and Peters*, 1999). The MOSAIC aerosol scheme divides aerosol size distribution into discrete size bins (*Fast et al*., 2006) and includes physical and chemical processes such as nucleation, condensation, coagulation, aqueous phase chemistry, and dry and wet deposition.

The dust emission scheme is from the Goddard Chemistry Aerosol Radiation and Transport (GOCART) model (*Ginoux et al*., 2001) coupled with the MOSAIC aerosol scheme (*Zhao et al*., 2013). The GOCART scheme calculates the dust emission flux (*F*) as a function of the horizontal wind speed at 10m (u_{10m}) and a prescribed source function (*S*).

$$F = CSs_p u_{10m}^2 (u_{10m} - u_t) \quad (1)$$

where *C* is the dimensional factor equal to 1 $\mu g s^2 m^{-5}$, u_t is the threshold velocity, and s_p is the fraction of each size class. If u_{10m} is less than u_t, there is no emission. The *S* is the probability to have accumulated sediments defined as

$$S = \left(\frac{z_{max} - z_i}{z_{max} - z_{min}}\right)^5 \quad (2)$$

where z_i is the altitude of grid i, and z_{max} and z_{min} are the maximum and minimum elevations in the surrounding 10° by 10° region, respectively (*Ginoux et al*., 2001).

The *S* is important in estimating dust emission flux. *Ginoux et al*. (2012) use Deep Blue AOD from MODIS to make a *S*. They apply three criteria as described in Chapter 3.2.2 to distinguish dust from other types of aerosols, and they define a dust

event as DOD is larger than 0.2. They construct a S using the annual mean emission frequency in North Africa based on the selected threshold. However, the *S* made by *Ginoux et al*. (2012) may be biased in western Sahara as dust observed over there is a combination of local emission and advection of dust from east.

To examine the biases of the *S* from *Ginoux et al*. (2012), I use model output from 2010 through 2015 to calculate dust emission frequency over North Africa. I use dust emission flux, column integrated DOD, and DOD below 1 km from the model to obtain the dust emission frequency. For dust emission flux a dust event is defined as a 3-hourly mean dust emission flux greater than or equal to 1 $\mu gm^{-2}s^{-1}$ (*Laurent et al*., 2010; *Tegen et al*., 2013). For column integrated DOD a dust event is defined as DOD greater than or equal to 0.235. For DOD below 1 km a dust event is defined as DOD greater than or equal to 0.12. To obtain the dust emission frequency, I divide the total number of events by the total number of days. The thresholds for column integrated DOD and DOD below 1 km are chosen so that the annual mean emission frequency from column integrated DOD (f_{DOD}) and DOD below 1 km (f_{DOD1km}) is equal to that from emission flux (f_{emi}). Then I examine the differences in the dust emission frequency obtained from the above three criteria.

4.3 Dust Climatology

CALIPSO provides monthly mean DOD, which can be used to examine the spatial distribution of dust. Here I compare DOD from CALIPSO with DOD derived from Deep Blue AOD from MODIS Aqua. I first examine the climatology of DOD in North African using Deep Blue DOD from MODIS Aqua. DOD values of 0.7 are

observed over the Bodélé depression in all four seasons, indicating the Bodélé is an active dust source region all year around (Fig. 4.1, *Ridley et al*., 2012). DOD peaks in spring and summer over the Bodélé depression (Fig. 4.1b, c). In summer, DOD values between 0.5 and 0.7 are seen in northern Mali, southern Algeria, and Mauritania (Fig. 4.1b, c), while this region is less active in fall and winter (Fig. 4.1a, d, *Koven et al*., 2008).

In comparison, CALIPSO shows much smaller DOD values over the Bodélé depression in all seasons compared with MODIS (Fig. 4.1, Fig. 4.2), and the difference is largest in summer. This result is consistent with a previous study that found DOD from CALIPSO over the Bodélé is 0.3 smaller compared with MODIS (*Ma et al*., 2013). The differences in the annual means of DOD from MODIS and CALIPSO are consistent with those for the summertime only (Fig. 3.8, Fig. 4.1, Fig 4.2). CALIPSO shows the highest DOD values of 0.6 in northern Mali and southern Algeria in spring and summer (Fig. 4.2b, c), similar as MODIS in this region (Fig. 4.1b, c).

The major differences in DOD between those two products are mainly attributable to two reasons. First, the lidar ratio used by CALIPSO for dust retrieval may be inappropriate. Second, the aerosol model used to retrieve MODIS AOD may not work well over heavily dusty regions.

4.4 Dust Emission Frequency

Here I examine the biases of the *S* derived from MODIS using emission flux and DOD from the WRF-Chem model. To eliminate to effect of dust advection to the

biases in the *S*, I use DOD in the below 1 km from the model to make a *S* and examine whether that improves the accuracy of the *S*.

I examine the seasonal f_{emi}, f_{DOD}, and f_{DOD1km} from WRF-Chem. In winter, the highest f_{emi} is found over the Bodélé depression and along the Atlantic coast between 20° to 30°N (Fig. 4.3a). The highest f_{DOD} is also found over the Bodélé in winter although the magnitude is smaller than f_{emi} (Fig. 4.3b). f_{DOD} is lower than f_{emi} across North Africa in winter. f_{DOD1km} shows the highest value over the Bodélé in winter as well, and it shows higher values in western Sahara compared with f_{DOD} (Fig. 4.3b). Both f_{DOD} and f_{DOD1km} are lower than f_{emi} in northern Algeria, Libya, and Egypt (Fig. 4.3).

In spring, high f_{emi} is found along the Mediterranean coast in addition to the Bodélé depression and the Atlantic coast (Fig. 4.4a). In comparison, f_{DOD} and f_{DOD1km} are persistently high over the major dust source regions, including the Bodélé depression, the lee of the Aïr and Adrar Mountains and the western Sahara region, where f_{DOD} and f_{DOD1km} are close to 100% (Fig. 4.4b, c).

In summer, the highest f_{emi} is seen in Libya and Egypt as well as along the Atlantic coast while over the Bodélé depression it is between 50% to 60%, lower than that in winter, spring and fall (Fig. 4.3-4.7a). In western Sahara, f_{emi} is between 60% to 80% whereas f_{DOD} and f_{DOD1km} are 100% (Fig. 4.5b, c). f_{DOD} and f_{DOD1km} are also 100% over the Bodélé depression and the lee of the Aïr and Adrar Mountains in summer (Fig. 4.5b, c). f_{DOD1km} is 0 south of 12°N while f_{DOD} is above 0 between 10° to 12°N (Fig. 4.5b, c).

In fall, emission frequency is highest over the Bodélé depression while it is the lowest in western Sahara among four seasons (Fig. 4.6a). The spatial structure of the seasonal mean f_{DOD1km} is similar to that of f_{DOD} as they both show high emission frequency over the three dust source regions in all four seasons (Fig. 4.6b, c).

To examine the how the emission frequency varies with three criteria, I compare the difference in the spatial structure of f_{emi}, f_{DOD}, and f_{DOD1km}. Figure 4.7 shows the difference between f_{emi} and f_{DOD} ($f_{DOD} - f_{emi}$). In winter, f_{emi} is higher than f_{DOD} in the Sahara whereas in the Sahel f_{emi} is lower than f_{DOD} (Fig. 4.7a). In spring, f_{emi} is higher in the coastal regions and Egypt while f_{DOD} is higher everywhere else in North Africa. The difference between f_{DOD} and f_{emi} is up to 0.5 between 10° to 20°N (Fig. 4.7b). When compared with the emission flux from the WRF-Chem model, such method overestimates dust emissions in the Sahel. In summer, f_{DOD} is higher than f_{emi} throughout North Africa except in Egypt and Libya (Fig. 4.7c). Large difference between f_{DOD} and f_{emi} is found between 10° to 20°N and between 20° to 30°N east of 10°E (Fig. 4.7c), indicating DOD might be overestimated in western Sahara by *Ginoux et al.* (2012). In fall, f_{emi} is higher than f_{DOD} in northern Algeria, Libya and Egypt whereas f_{DOD} is higher between 10° to 20°N (Fig. 4.7d).

Figure 4.8 shows the difference between f_{emi} and f_{DOD1km} ($f_{DOD1km} - f_{emi}$). f_{DOD1km} is higher than f_{emi} over the major dust emission regions in spring, summer and fall (Fig. 4.8b, c, d). In winter, the difference between $f_{DOD1km} - f_{emi}$ is smaller compared with $f_{DOD} - f_{emi}$ in the Sahara (Fig. 4.7a, Fig. 4.8a), suggesting using DOD under 1 km can reduce the biases in dust emission in winter. By using a threshold of

DOD > 0.2 to identify dust emission events, *Ginoux et al*. (2012) may underestimated dust emission in North Africa in winter. In summer, the difference between $f_{DOD1km} - f_{emi}$ is smaller compared with $f_{DOD} - f_{emi}$ in the Sahel (Fig. 4.7c, Fig. 4.8c), suggesting using DOD below 1 km may reduce the biases in DOD and improve dust modeling in the Sahel.

Figure 4.9 shows the difference between f_{DOD} and f_{DOD1km} ($f_{DOD} - f_{DOD1km}$). In winter, f_{DOD} is lower than f_{DOD1km} over North Africa (Fig. 4.9a). In spring, summer and fall, f_{DOD} is higher than f_{DOD1km} in the Sahel (Fig. 4.9b, c, d).

The root mean squared error of f_{emi} minus f_{DOD} is 0.28 while it is 0.24 for f_{emi} minus f_{DOD1km}. Using DOD below 1 km is slightly better than column integrated DOD, but the root mean squared error is still large. My results suggest that DOD in general is not a good proxy for the *S* in North Africa.

4.5 Conclusions

I examine the annual and seasonal mean dust climatology over North Africa using MODIS and CALIPSO. CALIPSO has lower seasonal mean DOD compared with MODIS over North Africa, especially in summer. I then examine the dust *S* developed by *Ginoux et al*. (2012) using dust emission flux and DOD from the WRF-Chem model. My results suggest that the *S* by *Ginoux et al*. (2012) may significantly overestimate dust in the Sahel and western Sahara. I use DOD below 1 km instead of the column integrated DOD to eliminate the effect of advection on determining dust source regions. Such method does reduce the biases in dust emission in the Sahel. However, it does not show notable improvement in reducing the biases in DOD over

the western Sahara region. In general, DOD is not a good proxy for the *S*. I note that this result is model specific. Future work should use dust output from various models to examine the reliability of dust source functions made from satellite observations.

Schepanski et al. (2007) made a *S* by visual determination of dust emission using 15-minute composite images of SEVIRI. However, their method is also likely biased in that a dust emission event cannot be seen if the column DOD is too high. Thus, DOD in western Sahara is lower from *Schepanski et al*. (2007) compared with *Ginoux et al*. (2012).

The biases in the *S* from *Ginoux et al*. (2012) are largely due to dust advection from east. This *S* is implemented in global climate models and MERRAero reanalysis, indicating the climate models and reanalysis may also overestimate dust emission in western Sahara. It will be necessary to develop a dust source function that correctly represents dust emission in North Africa so as to better estimate global dust emission as well as to assess the impact of dust on the climate.

Acknowledgements

Chapter 4, in part, is currently being prepared for submission for publication of the material. Wang, Weijie; Evan, Amato; Zhao, Chun. The dissertation author was the primary investigator and author of this paper.

4.6 Figures

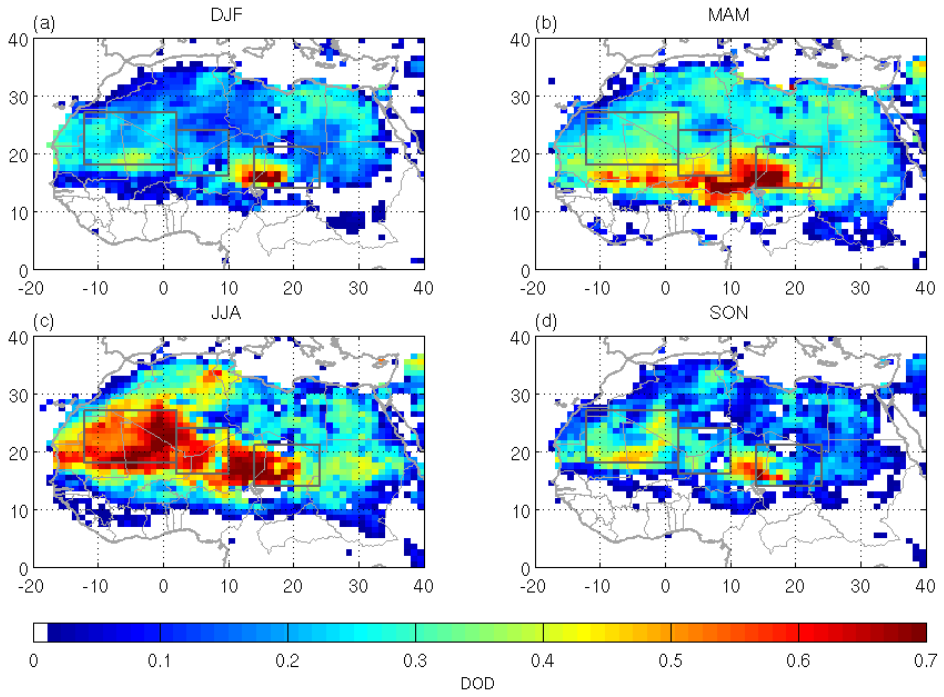

Figure 4.1 Seasonal mean DOD from monthly mean MODIS Aqua Deep Blue in North Africa averaged over 2003 through 2015.

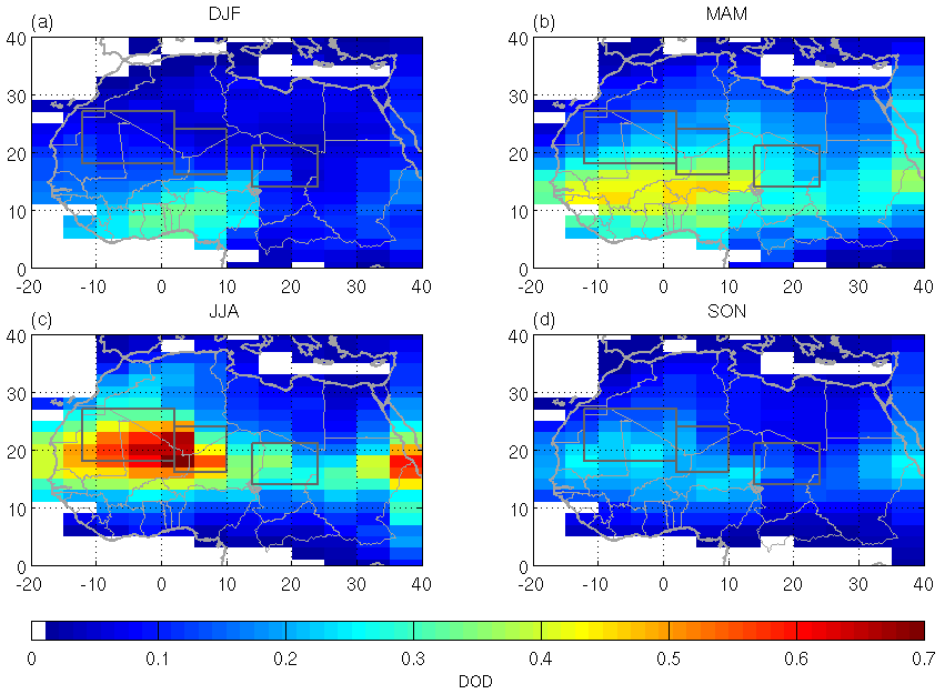

Figure 4.2 Seasonal mean DOD from monthly mean CALIPSO Level 3 cloud free product in North Africa averaged over 2007 through 2015.

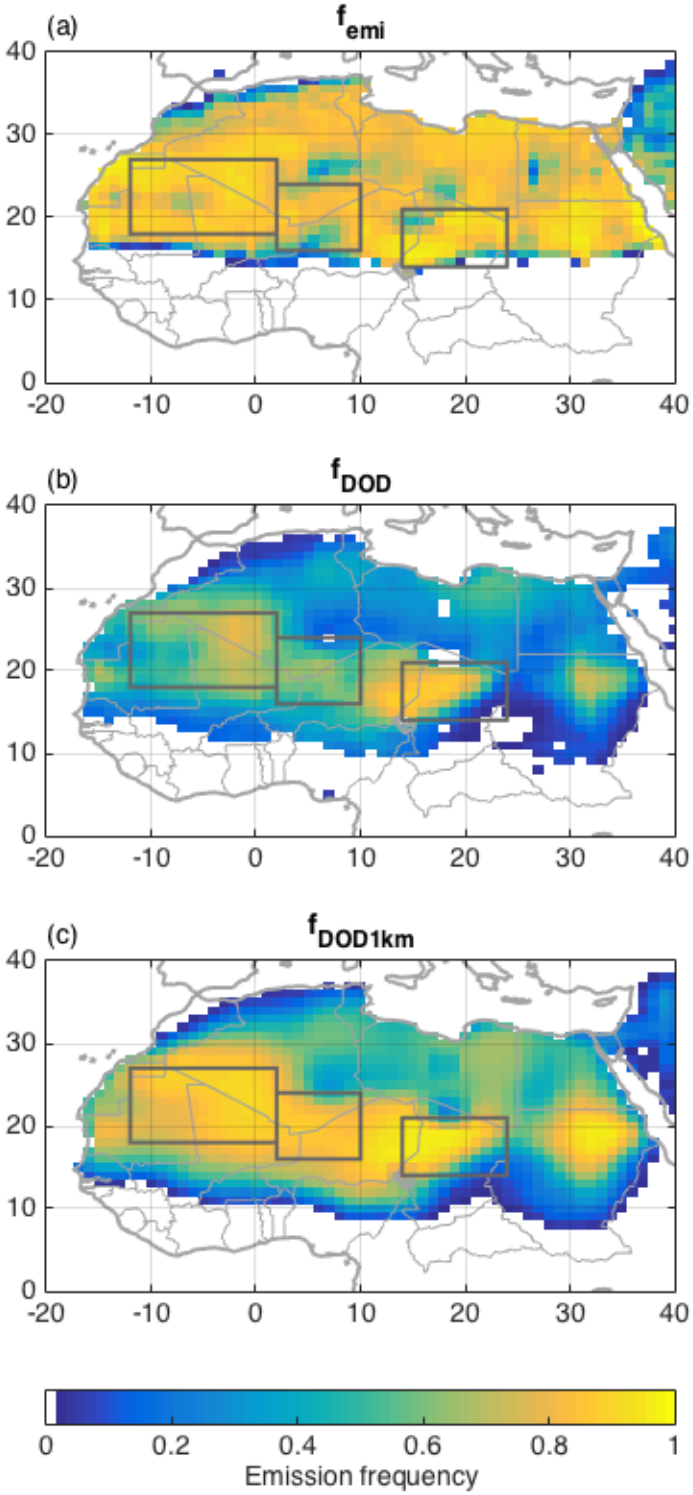

Figure 4.3 Seasonal mean f_{emi}, f_{DOD} and f_{DOD1km} from WRF-Chem in winter North Africa from 2010 through 2015.

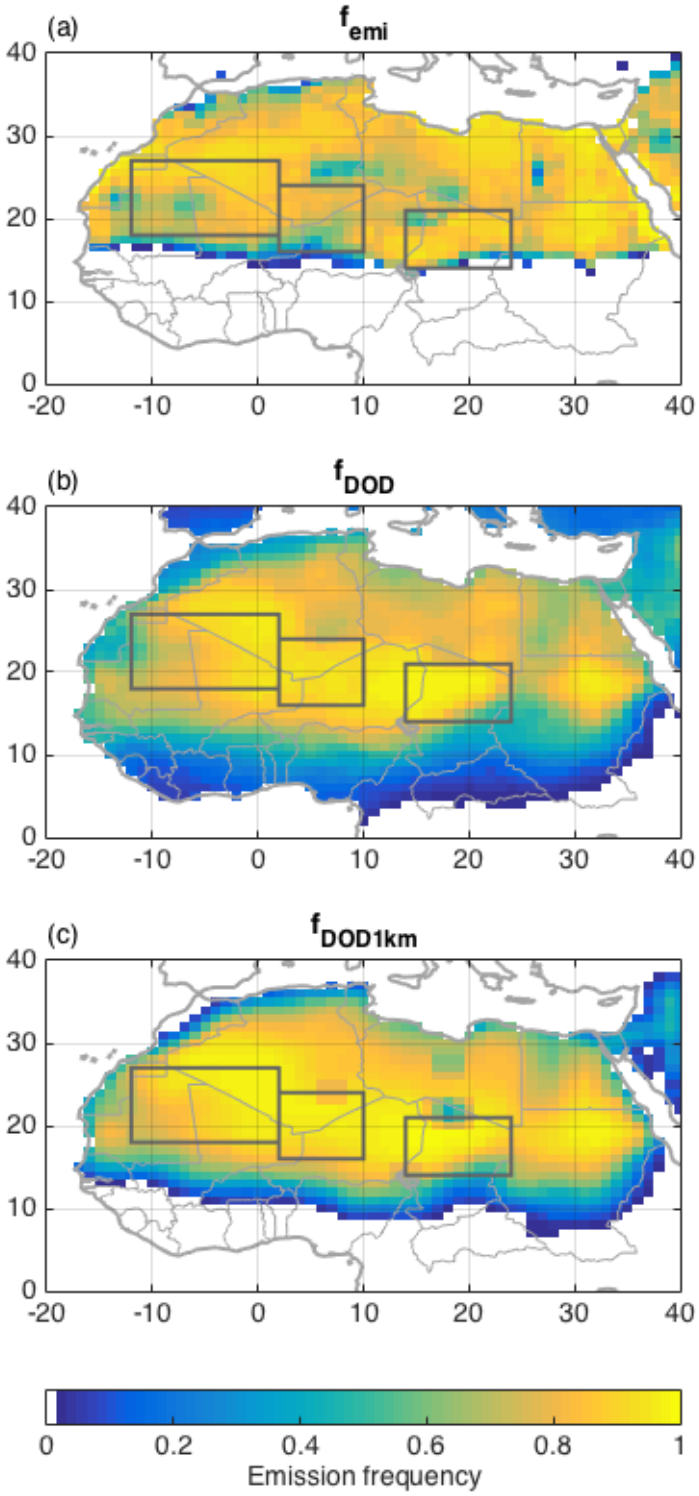

Figure 4.4 Same as Figure 4.3 but in spring.

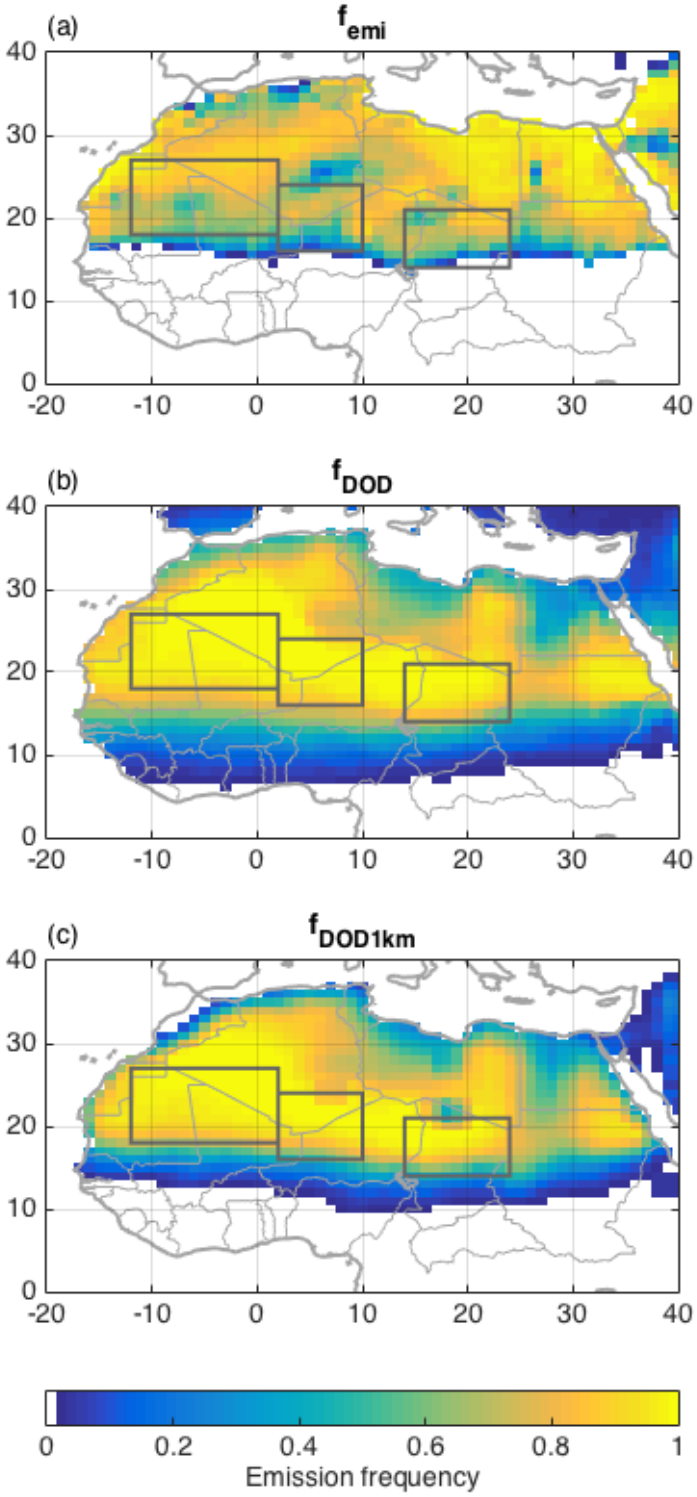

Figure 4.5 Same as Figure 4.3 but in summer.

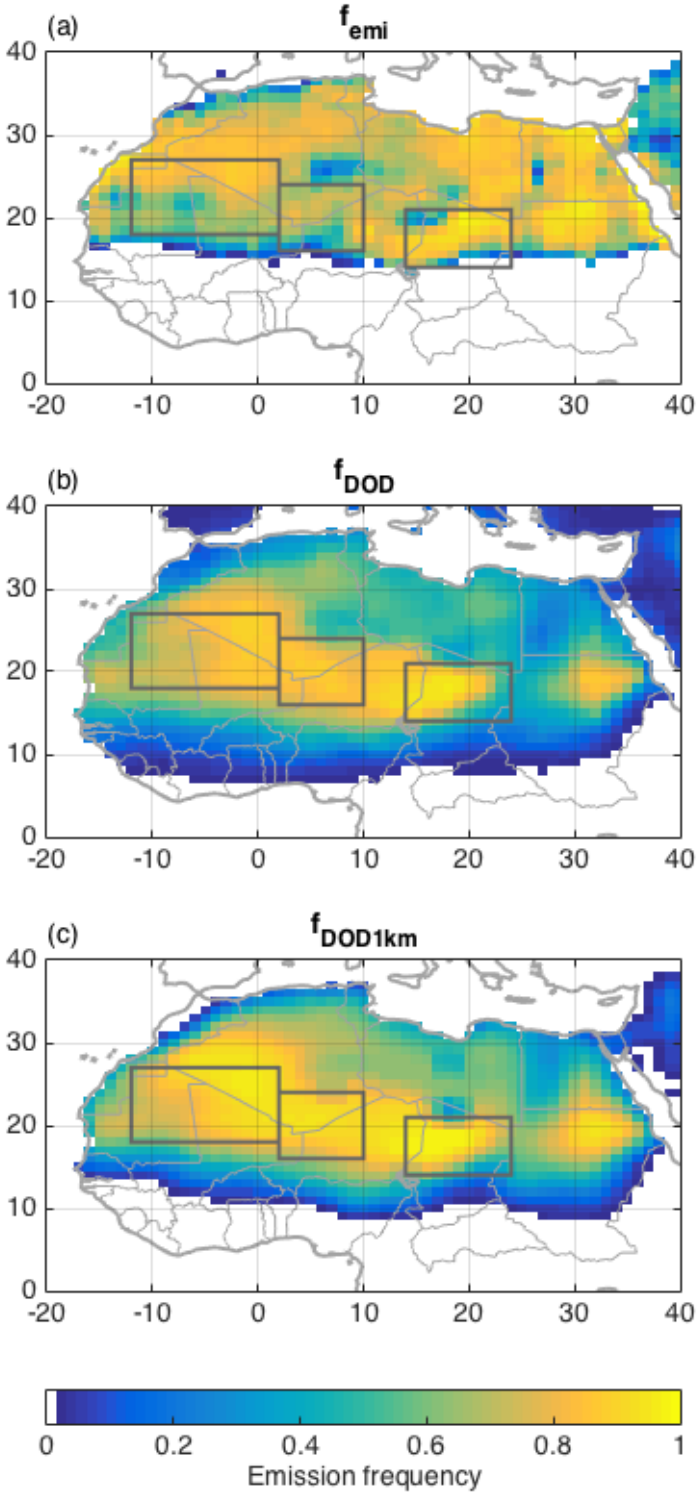

Figure 4.6 Same as Figure 4.3 but in fall.

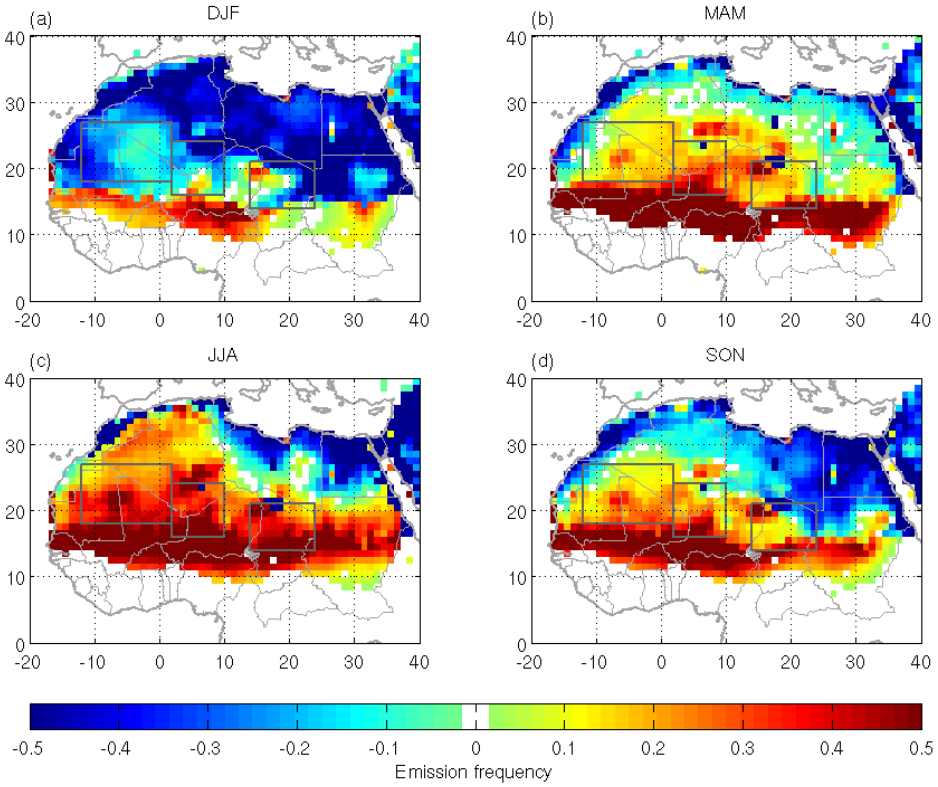

Figure 4.7 Seasonal mean difference in emission frequency (f_{DOD}- f_{emi}) over bright surfaces in North Africa from WRF-Chem from 2010 through 2015.

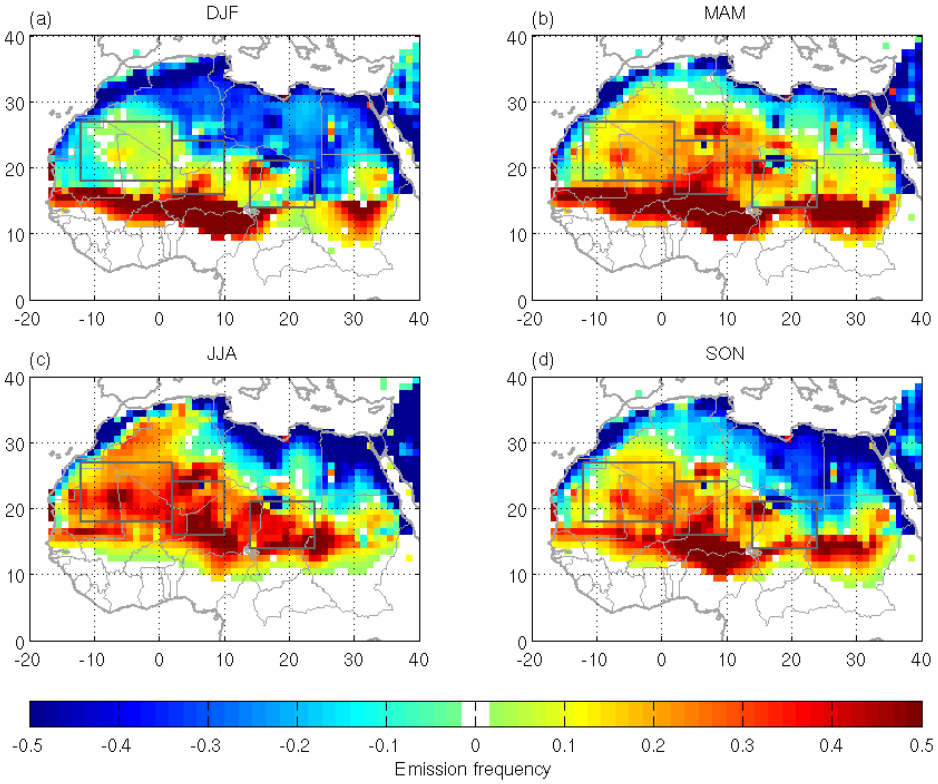

Figure 4.8 Seasonal mean difference in emission frequency (f_{DOD1km}- f_{emi}) over bright surfaces in North Africa from WRF-Chem from 2010 through 2015.

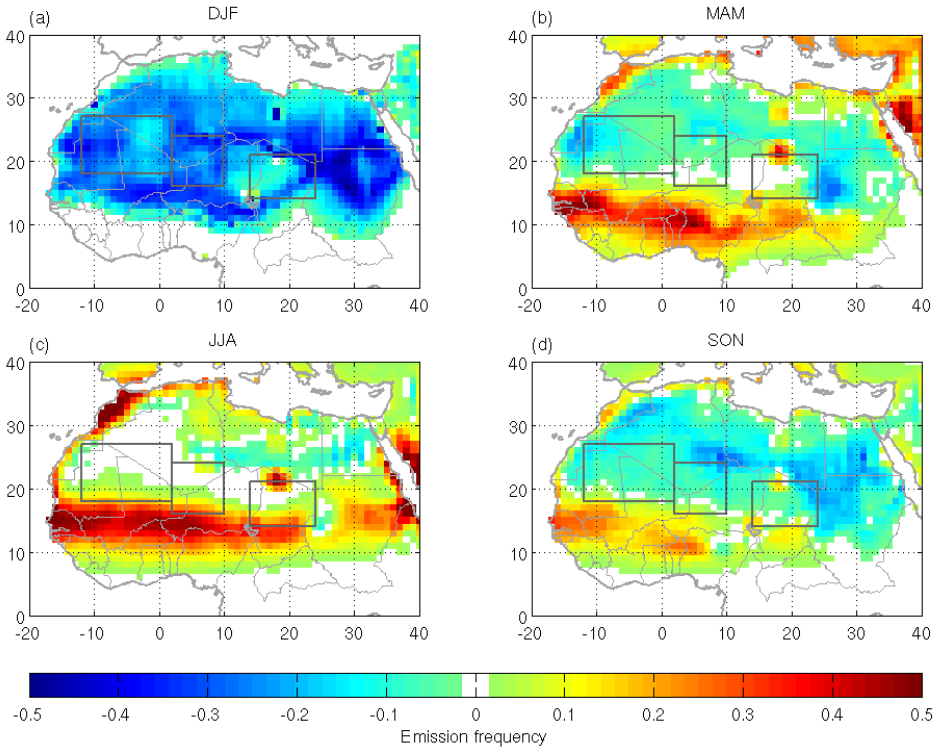

Figure 4.9 Seasonal mean difference in emission frequency (f_{DOD}- f_{DOD1km}) over bright surfaces in North Africa from WRF-Chem from 2010 through 2015.

Chapter 5

Summary

In this thesis, I first explore the role the SHL plays in dust emission in the Sahara and precipitation in the Sahel over the past three decades. By using satellite observations and reanalysis products, I found the upward trend in Sahelian precipitation and the downward trend in dust emission in the Sahara can be explained by the warming of the SHL. As the SHL warms, the anomalous low level cyclonic circulation associated with the SHL strengthens the southwesterly flow, bringing moisture from the Gulf of Guinea inland, and thus leads to increased precipitation in the Sahel. Meanwhile, the anomalous southwesterlies weaken the climatological northeastlies, resulting in less dust emission over the major dust source regions in the Sahara.

Next I examine how the SHL affects dust emission and transport on the synoptic scale using 13 years of satellite data. During the cool phases of the SHL, dust is preferentially emitted from the Bodélé depression. As the SHL warms, dust is advected westward to the western Sahara by the intensified AEJ. And as the SHL cools, dust is further advected over the tropical north Atlantic. The SHL contributes to 10% of the variability of dust over western Sahara.

Finally, the western Sahara region is identified as a major dust source region by satellite observations. I analyze the emission flux and DOD in North Africa from WRF-Chem model and show that the existing dust source function overestimates dust emission in the Sahel and the western Sahara.

Over the past three decades, temperature over North Africa has been rising steadily. The warming of the Sahara and the Sahel can change circulation patterns from microscale to mesoscale and will affect dust emission and transport and precipitation in North Africa. Yet up-to-date climate models are unable to reproduce the historical trend of dust over the tropical north Atlantic and dust source regions are misrepresented in the models. My results suggest future efforts should be made to improve the parameterization of dynamic features such as the SHL as well as dust source regions so as to better predict how climate change will affect North Africa in the 21st century.

Bibliography

Adler, R. F., G. J. Huffman, A. Chang, R. Ferraro, P. P. Xie, J. Janowiak, B. Rudolf, U. Schneider, S. Curtis, D. Bolvin, A. Gruber, J. Susskind, P. Arkin and E. Nelkin, The Version-2 Global Precipitation Climatology Project (GPCP) Monthly Precipitation Analysis (1979–Present). *J. Hydrometeor.*, **4** (2003).

Alley, R. B., Wally was right: predictive ability of the North Atlantic ‘‘conveyor belt’’ hypothesis for abrupt climate change, *Annu. Rev. Earth. Planet Sci*., **35**, 241–272 (2007).

Andreae, M. O., and D. Rosenfeld, Aerosol-cloud-precipitation interaction. Part 1. The nature and sources of cloud-active aerosols, *Earth-Sci. Rev*. **89**, 1-2 (2008).

Ansmann, A., A. Petzold, K. Kandler, I. Tegen, M. Wendisch, D. Müller, B. Weinzierl, T. Müller, J. Heintzenberg, Saharan Mineral Dust Experiments SAMUM-1 and SAMUM-2: What have we learned? *Tellus*, **63B**, 403–429 (2011).

Ashpole, I., and R. Washington, A new high-resolution central and western Saharan summertime dust source map from automated satellite dust plume tracking, *J. Geophys. Res. Atmos*., **118**, 6981–6995, doi:10.1002/jgrd.50554 (2013a).

Ashpole, I., and R. Washington, Intraseasonal variability and atmospheric controls on daily dust occurrence frequency over the central and western Sahara during the boreal summer, *J. Geophys. Res. Atmos*., **118**, 12915–12926, doi:10.1002/2013JD020267 (2013b).

Ben-Ami, Y., I. Koren, and O. Altaratz, Patterns of North African dust transport over the Atlantic: winter vs. summer, based on CALIPSO first year data, *Atmos. Chem. Phys*., **9**, 7867-7875, doi:10.5194/acp-9-7867-2009 (2009).

Bergametti, G., L. Gomes, G. Coudé-Gaussen, P. Rognon, M.-N. Le Coustumer, African dust observed over Canary Islands: Source-regions identification and transport pattern for some summer situations, *J. Geophys. Res.*, **94**, D12, 14855–14864 (1989).

Broecker, W. S., D. M. Peteet, and D. Rind, Does the ocean–atmosphere system have more than one stable mode of operation? *Nature,* **315**, 21-26. doi:10.1038/315021a0 (1985).

Brooks, N. and M. Legrand, Dust variability over North Africa and rainfall in the Sahel, in: Linking climate change to land surface change, *Adv. Global Change Res*., Kluwer Academic Publishers, Dordrecht, 1–25 (2003).

Buchard, V., A. M. da Silva, P. R. Colarco, A. Darmenov, C. A. Randles, R. Govindaraju, O. Torres, J. Campbell, and R. Spurr, Using the OMI aerosol index and

absorption aerosol optical depth to evaluate the NASA MERRA Aerosol Reanalysis, *Atmos. Chem. Phys*., **15**, 5743-5760, doi:10.5194/acp-15-5743-2015 (2015).

Buchard, V., A. M. da Silva, C. A. Randles, P. Colarco, R. Ferrare, J. Hair, C. Hostetler, J. Tackett, and D. Winker: Evaluation of the surface PM2.5 in Version 1 of the NASA MERRA Aerosol Reanalysis over the United States, *Atmos. Environ.*, **125**, 100-111, doi:10.1016/j.atmosenv.2015.11.004 (2016).

Cakmur, R. V., R. L. Miller, and I. Tegen, A comparison of seasonal and interannual variability of soils dust aerosols over the Atlantic Ocean as inferred by the TOMS AI and AVHRR AOT retrievals, *J. Geophys. Res*., **106**(D16), 18287–18303 (2001).

Caquineau, S., A. Gaudichet, L. Gomes, and M. Legrand, Mineralogy of Saharan dust transported over northwestern tropical Atlantic Ocean in relation to source regions, *J. Geophys. Res*., 107, 4251, doi:10.1029/2000jd000247 (2002).

Charney, J. G., Dynamics of deserts and drought in the Sahel, *Q. J. R. Meteorol. Soc*. **101**, 193 (1975).

Chauvin, F., R. Roehrig, and J.-P. Lafore, Intraseasonal variability of the Saharan heat low and its link with midlatitudes. *J. Clim*., **23**, 2544–2561, doi:10.1175/2010JCLI3093.1 (2010).

Chiapello, I., G. Bergametti, B. Chatenet, P. Bousquet, F. Dulac, and E. Santos Soares, Origins of African dust transported over the northeastern tropical Atlantic, *J. Geophys. Res*., **102**, D12, 13701–13709 (1997).

Chiapello, I., J. M. Prospero, J. R. Herman, and N. C. Hsu, Detection of mineral dust over the North Atlantic Ocean and Africa with the Nimbus 7 TOMS, *J. Geophys. Res*., **104**, 9277–9292 (1999).

Chiapello, I., and C. Moulin, TOMS and METEOSAT satellite records of the variability of Saharan dust transport over the Atlantic during the last two decades (1979-1997), *Geophys. Res. Lett*., **29**(8), 1176, doi:10.1029/2001GL013767 (2002).

Chu, D. A., Y. J. Kaufman, C. Ichoku, L. A. Remer, D. Tanré, and B. N. Holben, Validation of MODIS aerosol optical depth retrieval over land, *Geophys. Res. Lett*., **29**(12), doi:10.1029/2001GL013205 (2002).

COHMAP Members, Climatic changes of the last 18,000 years: Observations and model simulations, *Sci.*, **241**, 1043-1052 (1988).

Cook, K. H., Generation of the African easterly jet and its role in determining West African precipitation, *J. Clim*., **12**, 1165–1184 (1999).

Cowie, S. M., P. Knippertz and J. H. Marsham, Are vegetation-related roughness

changes the cause of the recent decrease in dust emission from the Sahel? *Geophys. Res. Lett*., **40** (2013).

Creamean, J. M., K. J. Suski, D. Rosenfeld, A. Cazorla, P. J. DeMott, R. C. Sullivan, A. B. White, F. M. Ralph, P. Minnis, J. M. Comstock, J. M. Tomlinson, and K. A. Prather, Dust and biological aerosols from the Sahara and Asia influence precipitation in the Western US. *Sci*. **339**, 6127 (2013).

Cuevas, E., C. Camino, A. Benedetti, S. Basart, E. Terradellas, J. M. Baldasano, J. J. Morcrette, B. Marticorena, P. Goloub, A. Mortier, A. Berjón, Y. Hernández, M. Gil-Ojeda, and M. Schulz, The MACC-II 2007–2008 reanalysis: atmospheric dust evaluation and characterization over northern Africa and the Middle East, *Atmos. Chem. Phys*., **15**, 3991–4024 (2015).

Dahl, K., A. J. Broccoli, and R. J. Stouffer, Assessing the role of North Atlantic freshwater forcing in millennial scale climate variability: A tropical Atlantic perspective, *Clim. Dyn*., **24**, 325-346, doi:10.1007/s00382-004-0499-5 (2005).

deMenocal, P. B, J. Ortiz, T. Guilderson, J. Adkins, M. Sarnthein, L. Baker, and M. Yarusinski, Abrupt onset and termination of the African Humid Period: Rapid climate response to gradual insolation forcing, *Quat. Sci. Rev*, **19**, 347-361 (2000).

Das, R., A. T. Evan and D. Lawrence, Contributions of long-distance dust transport to atmospheric P inputs in the Yucatan Peninsula. *Global Biogeochem. Cycles* **27** (2013).

Dee, D. P., S. M. Uppala, A. J. Simmons, P. Berrisford, P. Poli, S. Kobayashi, U. Andrae, M. A. Balmaseda, G. Balsamo, P. Bauer, P. Bechtold, A. C. M. Beljaars, L. van de Berg, J. Bidlot, N. Bormann, C. Delsol, R. Dragani, M. Fuentes, A. J. Geer, L. Haimberger, S. B. Healy, H. Hersbach, E. V. Hólm, L. Isaksen, P. Kållberg, M. Köhler, M. Matricardi, A. P. McNally, B. M. Monge-Sanz, J.-J. Morcrette, B.-K, Park, C. Peubey, P. de Rosnay, C. Tavolato, J.-N. Thépaut, and F. Vitart, The ERA-Interim reanalysis: configuration and performance of the data assimilation system. *Q. J. R. Meteorol. Soc*., **137**, 656 (2011).

DeFlorio, M. J., I. D. Goodwin, D. R. Cayan, A. J. Miller, S. J. Ghan, D. W. Pierce, L. M. Russell, and B. Singh, Interannual modulation of subtropical Atlantic boreal summer dust variability by ENSO, *Clim. Dyn*., **46**: 585. doi:10.1007/s00382-015-2600-7 (2016).

DeMott, P. J., K. Sassen, M. R. Poellot, D. Baumgardner, D. C. Rogers, S. D. Brooks, A. J. Prenni, and S. M. Kreidenweis, African dust aerosols as atmospheric ice nuclei. *Geophys. Res. Lett*., **30**(14), 1732 (2003).

Diner, D.J, C.J. Bruegge, J.V. Martonchik, T.P. Ackerman, R. Davies, S.A.W. Gerstl, H.R. Gordon, P.J. Sellers, and J. Clark, J.A. Daniels, E.D. Danielson, V.G. Duval, K.P.

Klassen, G.W. Lilienthal, D.I. Nakamoto, R. Pagano, T.H. Reilly, MISR: A Multi-angle Imaging SpectroRadiometer for geophysical and climatological research from EOS. *IEEE Trans. Geoscience and Remote Sens.*, **27** (2), 200-214 (1989).

Diner, D. J., C. J. Bruegge, J. V. Martonchik, G. W. Bothwell, E. D. Danielson, E. L. Floyd, V. G. Ford, L. E. Hovland, K. L. Jones, and M. L. White, A multiangle imaging spectroradiometer for terrestrial remote sensing from the earth observing system. *Int. J. Imaging Syst. Technol*., **3**, 92–107. doi:10.1002/ima.1850030206 (1991).

Doherty, O. M., N. Riemer, and S. Hameed, Control of Saharan mineral dust transport to Barbados in winter by the Intertropical Convergence Zone over West Africa, *J. Geophys. Res.*, **117**, D19117 (2012).

Doherty, O. M., N. Riemer, and S. Hameed, Role of the convergence zone over West Africa in controlling Saharan mineral dust load and transport in the boreal summer, *Tellus B*, **66**, 23191 (2014).

Dupont, L. M., Vegetation zones in NW Africa during the Brunhes chron reconstructed from marine palynological data. *Quat. Sci. Rev*. **12**, 189-202, (1993).

Eck, T. F., B. N. Holben, J. S. Reid, O. Dubovik, A. Smirnov, N. T. O'Neill, I. Slutsker, and S. Kinne, Wavelength dependence of the optical depth of biomass burning, urban, and desert dust aerosols, *J. Geophys. Res*., **104**, D24, 31333–31349 (1999).

Engelstaedter, S., I. Tegen, and R. Wahsington, North African dust emissions and transport. *Earth-Sci. Rev*., **79**, 1 (2006).

Engelstaedter, S. and R. Washington, Temporal controls on global dust emissions: The role of surface gustiness. *Geophys. Res. Lett*., **34**, L15805 (2007).

Evan, A. T., A. K. Heidinger, and M. J. Pavolonis, Development of a new over– water advanced very high resolution radiometer dust detection algorithm. *Int. J. Remote Sens*., **27**, 3903-3924 (2006).

Evan, A. T. D. J. Vimont, A. K. Heidinger, J. P. Kossin and R. Bennartz, The role of aerosols in the evolution of tropical North Atlantic Ocean temperature anomalies. *Sci*., **324**, 5928 (2009).

Evan, A. T. and S. Mukhopadhyay, African dust over the northern tropical Atlantic: 1955-2008. *J. Appl. Meteor. Climatol*. **49**, 2213-2229 (2010).

Evan, A. T., C. Flamant, S. Fiedler, and O. Doherty, An analysis of aeolian dust in climate models. *Geophys. Res. Lett.*, **41**, 5996-6001 (2014).

Evan, A. T., C. Flamant, C. Lavaysse, C. Kocha, and A. Saci, Water Vapor–Forced

Greenhouse Warming over the Sahara Desert and the Recent Recovery from the Sahelian Drought. *J. Clim*., **28**, 108–123, doi: http://dx.doi.org/10.1175/JCLI-D-14-00039.1 (2015).

Evan, A. T., S. Fiedler, C. Zhao, L. Menut, K. Schepanski, C. Flamant and O. Doherty, Derivation of an observation-based map of North African dust emission. *Aeol. Res*., **16**, 153-162 (2015).

Fast, J. D., W. I. Gustafson, R. C. Easter, R. A. Zaveri, J. C. Barnard, E. G. Chapman, G. A. Grell, and S. E. Peckham, Evolution of ozone, particulates, and aerosol direct radiative forcing in the vicinity of Houston using a fully coupled meteorology-chemistry- aerosol model, *J. Geophys. Res*., **111**, D21305, doi:10.1029/2005JD006721 (2006).

Fecan, F., B. Marticorena and G. Bergametti, Parameterization of the increase of the aeolian erosion threshold wind friction velocity due to soil moisture for arid and semi-arid areas. *Ann. Geophys. Atmos. Hydr*., **17**, 149-157 (1999).

Folland, C. K., T. N. Palmer, and D. E. Parker, Sahel rainfall and worldwide sea temperature 1901–1985. *Nature*, **320**, 602–607 (1986).

Foltz, G. R. and M. J. McPhaden, Impact of Saharan Dust on Tropical North Atlantic SST. *J. Clim*., **21** (2008).

Fontaine, B., S. Janicot, and V. Moron, Rainfall anomaly pat- terns and wind field signals over West Africa in August (1958– 1989). *J. Clim.,* **8,** 1503–1510 (1995).

Formenti, P., M. O. Andreae, L. Lange, G. Roberts, J. Cafmeyer, I. Rajta, W. Maenhaut, B. N. Holben, P. Artaxo, and J. Lelieveld, Saharan dust in Brazil and Suriname during the Large-Scale Biosphere-Atmosphere Experiment in Amazonia (LBA) - Cooperative LBA Regional Experiment (CLAIRE) in March 1998, *J. Geophys. Res*., **106**(D14), 14919–14934, doi:10.1029/2000JD900827 (2001).

Formenti, P., L. Schutz, Y. Balkanski, K. Desboeufs, M. Ebert, K. Kandler, A. Petzold, D. Scheuvens, S. Weinbruch, and D. Zhang, Recent progress in understanding physical and chemical properties of African and Asian mineral dust, *Atmos. Chem. Phys*., **11**, 8231–8256 (2011).

Formenti, P., S. Caquineau, K. Desboeufs, A. Klaver, S. Chevaillier, E. Journet, and J. L. Rajot, Mapping the physico-chemical properties of mineral dust in western Africa: mineralogical composition, *Atmos. Chem. Phys*., **14**, 10663–10686 (2014).

Giannini, A., R. Saravanan, and P. Chang, Oceanic forcing of Sahel rainfall on interannual to interdecadal time scales. *Sci*., **302**, 1027–1030, doi:10.1126/science.1089357 (2003).

Gangoiti, G., L. Alonso, M. Navazo, J. A. García, and M. M. Millán, North African soil dust and European pollution transport to America during the warm season: Hidden links shown by a passive tracer simulation, *J. Geophys. Res*., **111**, D10109, doi:10.1029/2005JD005941 (2006).

Ginoux, P., M. Chin, I. Tegen, J. M. Prospero, B. Holben, O. Dubovik, and S. J. Lin, Sources and distributions of dust aerosols simulated with the GOCART model. *J. Geophys. Res. Atmos*. **106** (D17), 20255–20273 (2001).

Ginoux, P., J. M. Prospero, T. E. Gill, N. C. Hsu, and M. Zhao, Global-scale attribution of anthropogenic and natural dust sources and their emission rates based on MODIS Deep Blue aerosol products. *Rev. Geophys*. **50**, RG3005 (2012).

Goudie, A. S.: Great warm deserts of the world, Oxford University Press, Oxford (2003).

Haywood, J. M., B. T. Johnson, S. R. Osborne, A. J. Baran, M. Brooks, S. F. Milton, J. Mulcahy, D. Walters, R. P. Allan, A. Klaver, P. Formenti, H. E. Brindley, S. Christopher, P. Gupta, Motivation, rationale and key results from the GERBILS Saharan dust measurement campaign. *Q. J. R. Meteorol. Soc*. **137**, 1106–1116. Doi:10.1002/qj.797 (2011).

Grell, G.A., Peckham, S.E., Schmitz, R., McKeen, S.A., Frost, G., Skamarock, W.C., and Eder, B., Fully coupled ‘‘online’’ chemistry within the WRF model. *Atmos. Environ*. **39** (37), 6957–6975 (2005).

Israelevich, P. L., Levin, Z., Joseph, J. H., and Ganor, E.: Desert aerosol transport in the Mediterranean region as inferred from the TOMS aerosol index, *J. Geophys. Res*., **107**, 4572, doi:10.1029/2001jd002011 (2002).

Heintzenberg, J., The SAMUM-1 experiment over Southern Morocco: Overview and introduction, *Tellus*, **61**, 2–11 (2009).

Held, I. M., T. L. Delworth, J. Lu, K. L. Findell, and T. R. Knutson, Simulation of Sahel drought in the 20th and 21st centuries, *PNAS*, **102**(50), 17891-17896, doi: 10.1073/pnas.0509057102 (2005).

Herman, J. R., P. K. Bhartia, O. Torres,C. Hsu, C. Seftor, and E. Celarier, Global distribution of UV-absorbing aerosols from Nimbus-7/TOMS data, *J. Geophys. Res*., **102**, 16911-16922 (1997).

Holben, B. N., T. F. Eck, I. Slutsker, D. Tanré, J. P. Buis, A. Setzer, E. Vermote, J. A. Reagan, Y. J. Kaufman, T. Nakajima, F. Lavenu, I. Jankowiak, and A. Smirnov, AERONET-A federated instrument network and data archive for aerosol characterization, *Remote Sens. Environ*., **66**, 1–16 (1998).

Hollingsworth, A., Engelen, R. J., Textor, C., Benedetti, A., Boucher, O., Chevallier, F., Dethof, A., Elbern, H., Eskes, H., Flemming, J., Granier, C., Kaiser, J. W., Morcrette, J.-J., Rayner, R., Peuch, V.-H., Rouil, L., Schultz, M. G., Sim- mons, A. J., and The GEMS Consortium: Toward a mon- itoring and forecasting system for atmospheric composition: the GEMS project, B. *Am. Meteorol. Soc*., **89**, 1147–1164, doi:10.1175/2008BAMS2355.1 (2008).

Huang, J., Minnis, P., Yan, H., Yi, Y., Chen, B., Zhang, L., and Ayers, J. K., Dust aerosol effect on semi-arid climate over Northwest China detected from A-Train satellite measurements, *Atmos. Chem. Phys*., **10**, 6863-6872, doi:10.5194/acp-10-6863-2010 (2010).

Hurrell, J. W., Decadal trend in the North Atlantic Oscillation: Regional temperatures and precipitations. *Sci.,* **269**, 676–679 (1995).

Inness, A., F. Baier, A. Benedetti, I. Bouarar, S. Chabrillat, H. Clark, C. Clerbaux, P. Coheur, R. J. Engelen, Q. Errera, J. Flemming, M. George, C. Granier, J. Hadji-Lazaro, V. Huijnen, D. Hurtmans, L. Jones, J. W. Kaiser, J. Kapsomenakis, K. Lefever, J. Leitao, M. Razinger, A. Richter, M. G. Schultz, A. J. Simmons, M. Suttie, O. Stein, J.-N. Thépaut, V. Thouret, M. Vrekoussis, C. Zerefos, and the MACC team, The MACC reanalysis: an 8 yr data set of atmospheric composition, *Atmos. Chem. Phys*., **13**, 4073–4109 (2013).

IPCC, Climate Change 2013: The Physical Science Basis. Contribution of Working Group I to the Fifth Assessment Report of the Intergovernmental Panel on Climate Change [Stocker, T.F., D. Qin, G.-K. Plattner, M. Tignor, S.K. Allen, J. Boschung, A. Nauels, Y. Xia, V. Bex and P.M. Midgley (eds.)]. Cambridge University Press, Cambridge, United Kingdom and New York, NY, USA, 1535 pp, doi:10.1017/CBO9781107415324 (2013).

Israelevich, P. L., Z. Levin, J. H. Joseph, and E. Ganor, Desert aerosol transport in the Mediterranean region as inferred from the TOMS aerosol index, *J. Geophys. Res*., **107**, 4572, doi:10.1029/2001jd002011 (2002).

Joussaumen. S., K. E. Taylor, P. Braconnot, J. F. B. Mitchell, J. E. Kutzbach, S. P. Harrison, I. C. Prentice, A. J. Broccoli, A. Abe-Ouchi, P. J. Bartlein, C. Bonfils, B. Dong, J. Guiot, K. Herterich, C. D. Hewitt, D. Jolly, J. W. Kim, A. Kislov, A. Kitoh, M. F. Loutre, V. Masson, B. McAvaney, N. de Nobelt, W. R. Peltier, J. Y. Peterschmitt, D. Pollard, D. Rind, J. F. Royer, M. E. Schlesinger, J. Syktus, S. Thompson, P. Valdes, G. Vettoretti, R. S. Webb, and U. Wyputta, Monsoon changes for 6000 years ago: Results of 18 simulations from the Paleoclimate Modeling Intercomparison Project (PMIP), *J Geophys. Res*., **26**(7), 859-862 (1999).

Kallos, G., V. Kotroni, K. Lagouvardos, and A. Papadopoulos, On the long-range transport of air pollutants from Europe to Africa, *Geophys. Res. Let*t., **25**, 5 619-622

(1998).

Kalnay, E., M. Kanamitsu, R. Kistler, W. Collins, D. Deaven, L. Gandin, M. Iredell, S. Saha, G. White, J. Woollen, Y. Zhu, A. Leetmaa, R. Reynolds, M. Chelliah, W. Ebisuzaki, W. Higgins, J. Janowiak, K. C. Mo, C. Ropelewski, J. Wang, R. Jenne and D. Joseph, The NCEP/NCAR 40-year reanalysis project, *Bull. Amer. Meteor. Soc*., **77**, 437-470 (1996).

Kanamitsu, M., W. Ebisuzaki, J. Woollen, S-K Yang, J.J. Hnilo, M. Fiorino and G. L. Potter, NCEP-DOE AMIP-II Reanalysis (R-2), *Bull. Amer. Meteor. Soc.*, **83**, 1631-1643 (2002).

Kaufman, Y. J., I. Koren, L. A. Remer, D. Tanré, P. GInoux, and S. Fan, Dust transport and deposition observed from the Terra-Moderate Resolution Imaging Spectroradiometer (MODIS) spacecraft over the Atlantic Ocean. *J. Geophys. Res*. **110**, D10S12 (2005).

Kröpelin, S., D. Verschuren, A. -M. Lézine, H. Eggermont, C. Cocquyt, P. Francus, J. –P. Cazet, M. Fagot, B. Rumes, J. M. Russell, F. Darius, D. J. Conley, M. Schuster, H. von Suchodoletz, and D. R. Engstrom, Climate-driven ecosystem succession in the Sahara: The past 6000 years, *Sci*., **320**, 5877, 765-768 (2008).

Knippertz, P. and M. C. Todd, Mineral dust aerosols over the Sahara: meteorological controls on emission and transport and implications for modeling. *Rev. Geophys*., **50**, RG1007 (2012).

Kok, J. F., N.M. Mahowald, S. Albani, G. Fratini, J.A. Gillies, M. Ishizuka, J. F. Leys, M. Mikami, M.-S. Park, S.-U. Park, R.S. Van Pelt, D.S. Ward, and T.M. Zobeck

An improved dust emission model with insights into the global dust cycle's climate sensitivity, *Atmos. Chem. Phys*., **14** (5) (2014).

Koven, C. D., and I. Fung, Identifying global dust source areas using high-resolution land surface form, *J. Geophys. Res*., **113**, D22204, doi:10.1029/2008JD010195 (2008).

Kutzbach, J. E., and B. L. Otto-Bliesner, The sensitivity of the African-Asian monsoonal climate to orbital parameter changes for 9000 years B.P. in a low-resolution general circulation model. *J. Atmos. Sci*., **39**, 1177–1188 (1982).

Kutzbach, J. E., and P. J. Guetter, The influence of changing orbital parameters and surface boundary conditions on climate simulations for the past 18000 years, *J. Atmos. Sci*., **43**, 1726–1759 (1986).

Kutzbach, J. E., G. Bonan, J. Foley, and S. P. Harrison, Vegetation and soil feedbacks on the response of the African monsoon to orbital forcing in the early to middle Holocene. *Nature*, **384**, 623-626 (1996).

Kutzbach, J. E., and Z. Liu, Response of the African monsoon to orbital forcing and ocean feedbacks in the middle Holocene, *Sci*, **278**, 5337, 440-443 (1997).

Largeron, Y., F. Guichard, D. Bouniol, F. Couvreux, L. Kergoat and B. Marticorena, Can we use surface wind fields from meteorological reanalyses for Sahelian dust emission simulations? *Geophys. Res. Lett.*, 10.1002/2014GL062938 (2015).

Laurent, B., I. Tegen, B. Heinold, K. Schepanski, B. Weinzierl, and M. Esselborn, A model study of Saharan dust emissions and distributions during the SAMUM-1 campaign. *J. Geophys. Res*., **115**, D21210 (2010).

Lavaysse, C., C. Flamant, S. Janicot, D. J. Parker, J.-P. Lafore, B. Sultan, and J. Pelon, Seasonal evolution of the West African heat low: A climatological perspective. *Clim. Dyn*., **33**, 313-330, doi:10.1007/s00382-009-0553-4 (2009).

Lavaysse, C., C. Flamant and S. Janicot, Regional-scale convection patterns during strong and weak phases of the Saharan heat low. *Atmos. Sci. Let*., **11**, 255-264 (2010).

Levelt, P. F., G. H. J. van den Oord, M. R. Dobber, A. Mälkki, H. Visser, J. de Vries, P. Stammes, J. O. V. Lundell, and H. Saari, The Ozone Monitoring Instrument, *IEEE Trans. on Geos. Rem. Sens*,, **44**, 5, 1093-1101 (2006).

Liang, S., B. Zhong, and H. Fang, Improve estimation of aerosol optical depth from MODIS imagery over land surfaces, *Rem. Sens. Envi*. **104**(4), 416-425, (2006).

Liao H., and J.H. Seinfeld, Radiative forcing by mineral dust aerosols: sensitivity to key variables, *J. Geophys. Res*. **103**, D24, 31637-31645 (1998).

Liu, D., Z. Wang, Z. Liu, D. Winker, and C. Trepte, A height resolved global view of dust aerosols from the first year CALIPSO lidar measurements, *J. Geophys. Res*., **113**, D16214, doi:10.1029/2007JD009776 (2008).

Liu, Y., and J. C. H. Chiang, Coordinated Abrupt Weakening of the Eurasian and North African Monsoons in the 1960s and Links to Extratropical North Atlantic Cooling, *J. Clim*., **25**, 3532–3548, doi: http://dx.doi.org/10.1175/JCLI-D-11-00219.1 (2012).

Liu, Y., J. C. H. Chiang, C. Chou, and C. M. Patricola, Atmospheric teleconnection mechanisms of extratropical North Atlantic SST influence on Sahel rainfall, *Clim. Dym*., **43**(9), 2797-2811 (2014).

Liu, Z., Liu, D., Huang, J., Vaughan, M., Uno, I., Sugimoto, N., Kittaka, C., Trepte, C., Wang, Z., Hostetler, C., and Winker, D., Airborne dust distributions over the Tibetan Plateau and surrounding areas derived from the first year of CALIPSO lidar observations, *Atmos. Chem. Phys*., **8**, 5045-5060, doi:10.5194/acp-8-5045-2008 (2008a).

Liu, Z., A. Omar, M. Vaughan, J. Hair, C. Kittaka, Y. Hu, K. Powell, C. Trepte, D. Winker, C. Hostetler, R. Ferrare, and R. Pierce, CALIPSO lidar observations of the optical properties of Saharan dust: A case study of long-range transport, *J. Geophys. Res*., **113**, D07207, doi:10.1029/2007JD008878 (2008b).

Longueville, F. D., P. Ozer, S. Doumbia, and S. Henry, Desert dust impacts on human health: an alarming worldwide reality and a need for studies in West Africa, *Intl. J. Biometeo*. **57**(1), 1-19 (2012).

Lu, J., and T. L. Delworth, Oceanic forcing of the late 20th century Sahel drought, *Geophys. Res. Lett*., **32**, L22706, doi:10.1029/2005GL023316 (2005).

Mahowald, N. M., M. Yoshioka, W.D. Collins, A.J. Conley, D.W. Fillmore, and D.B. Coleman, Climate response and radiative forcing from mineral aerosols during the last glacial maximum, pre-industrial, current and doubled-carbon dioxide climates, *Geophys. Res. Lett*., **33** (20) (2006).

Martonchik, J. V., J. D. David, K. A. Crean, and M. A. Bull, Regional aerosol retrieval results from MISR, IEEE T. *Geosci*. *Remote*, **40**, 1520–1531 (2002).

McConnell, C. L., E. J. Highwood, H. Coe, P. Formenti, B. Anderson, S. Osborne, S. Nava, K. Desboeufs, G. Chen, and M. A. J. Harrison, Seasonal variations of the physical and optical characteristics of Saharan dust: Results from the Dust Outflow and Deposition to the Ocean (DODO) experiment, *J. Geophys. Res*., **113**, D14S05, doi:10.1029/2007JD009606 (2008).

McIntyre, A., W. F. Ruddiman, K. Karlin, and A. C. Mix, Surface water response of the equatorial Atlantic Ocean to orbital forcing, *Paleoceanography*, **4**(1), 19-55 (1989).

Meloni, D., A. D. Sarra, T. D. Iorio, and G. Fiocco, Influence of the vertical profile of Saharan dust on the visible direct radiative forcing, *JQSRT*, **93**, 397-413 (2005).
Miller, R. L. and I. Tegen, Climate Response to Soil Dust Aerosols, *J. Clim*., **11**, 3247–3267 (1998).

Miller, R. L., I. Tegen, and J. Perlwitz, Surface radiative forcing by soil dust aerosols and the hydrological cycle, *J. Geophys. Res*., **105**, D04203, doi:10.1029/2003JD004085 (2004).

Monerie, P. A., B. Fontaine, and P. Roucou, Expected future changes in the African monsoon between 2030 and 2070 using some CMIP3 and CMIP5 models under a medium-low RCP scenario, *J. Geophy. Res*., **117**, D16 (2012).

Monerie, P. A., P. Roucou, and B. Fontaine, Mid-century effects of climate change on African monsoon dynamics using the A1B emission scenario, *Int. J. Climatol*., **33**, 881–896, doi:10.1002/joc.3476 (2013).

Moulin, C., C. E. Lambert, F. Dulac, and U. Dayan, Control of atmospheric export of dust from North Africa by the North Atlantic Oscillation, *Nature,* **387**, 691-694 (1997).

Mulitza, S., M. Prange, J.-B. Stuut, M. Zabel, T. V. Dobeneck, A. C. Itambi, J. Nizou, M. Schulz, and G. Wefer, Sahel mega droughts triggered by glacial slowdowns of Atlantic meridional overturning, *Paleoceanography*, **23**, PA4206, doi:10.1029/2008PA001637 (2008).

Menut, L., C. Perez Garcia-Pando, K. Haustein, B. Bessagnet, C. Prigent, S. Alfaro

Relative impact of roughness and soil texture on mineral dust emission fluxes modeling, *J. Geophys. Res. Atmos*., **118**, 6505–6520 (2013).

Newell, R. E., and J. W. Kidson, African mean wind changes between Sahelian wet and dry periods, *Int. J. Climatol*., **4**, 27-33 (1984).

Nicholson, S. E., Long-term changes in African rainfall, *Weather*, **44**(2), doi: 10.1002/j.1477-8696.1989.tb06977.x (1989).

Nicholson, S. E., B. Some, J. McCollum, E. Nelkin, D. Klotter, Y. Berte, B. M. Diallo, I. Gaye, G. Kpabeba, O. Ndiaye, J. N. Noukpozounkou, M. M. Tanu, A. Thiam, A. A. Toure, and A. K. Traore, Validation of TRMM and other rainfall estimates with a high-density gauge data set for West Africa. Part I: Validation of GPCC rainfall product and pre-TRMM satellite and blended products. *J. Appl. Meteor*., **42**(10), 1337-1354 (2003).

Nicholson, S., On the question of the "recovery" of the rains in the West African Sahel, *J. Arid Envi*., **63**(3), 615-641 (2005).

Norquist, D. C., E. E. Recker, and R. J. Reed, The energetics of African wave disturbances as observed during the phase III of GATE. *Mon. Wea. Rev.,* **105,** 334–342 (1977).

Okin, G. S., A. R. Baker, I. Tegen, N. Mahowald, F. J. Dentener, R. A. Duce, J. N. Galloway, K. Hunter, M. Kanakidou, N. Kubilay, J. M. Prospero, M. Sarin, V. Surapipith, M. Uematsu, and T. Zhu, Impacts of atmospheric nutrient deposition on marine productivity: Roles of nitrogen, phosphorus, and iron. *Global Biogeochem. Cycles* **25**, GB2022 (2011).

Olsson, L., L. Eklundh, and J. Ardö, A recent greening of the Sahel-trends, patterns and potential causes, *J. Arid Env*., **63**, 556‑566 (2005).

Onishi, K., Y. Kurosaki, S. Otani, A. Yoshida, N. Sugimoto, and Y. Kurozawa, Atmospheric transport route determines components of Asian dust and health effects in Japan, *Atmos. Env*. **49**, 94-102 (2012).

Otterman, J., Baring high-albedo soils by overgrazing: A hypothesized desertification mechanism, *Sci*., **185**, 531 (1974).

Petit-Maire, N., and Z. Guo, Mis en evidence de variations climatiques Holocenes rapides, en phase dans les deserts actuels de Chine et de Nord de l'Afrique, *Sciences de la Terre et des Planetes,* **322**, 847-851 (1996).

Prell, W.L., and Kutzbach, J. E., Monsoon variability over the past 150,000 years. *J. Geophys. Res*., **92**, 8411-8425 (1987).

Prospero, J. M., P. Ginoux, O. Torres, S. E. Nicholson, and T. E. Gill, Environmental characterization of global sources of atmospheric soil dust identified with the Nimbus 7 Total Ozone Mapping Spectrometer (TOMS) absorbing aerosol product, *Rev. Geophys*., **40**(1), 1002, doi:10.1029/2000RG000095 (2002).

Prospero, J. M., and P. J. Lamb, African droughts and dust transport to the Caribbean: climate change implications, *Sci.* **302**, 1024 (2003).

Ramanathan, V., P. J. Crutzen, J. T. Kiehl, and D. Rosenfeld, Aerosols, climate, and the hydrological cycle, *Sci*, **294**, 5549, Doi: 10.1126/science.1064034 (2001).

Redelsperger, J.-L., C. D. Thorncroft, A. Diedhiou, T. Lebel, D. J. Parker, and J. Polcher, African Monsoon Multidisciplinary Analysis: An International Research Project and Field Campaign. *Bull. Amer. Meteor. Soc.*, **87**, 1739–1746. doi: http://dx.doi.org/10.1175/BAMS-87-12-1739 (2006).

Remer, L. A., D. Tanré, Y. J. Kaufmann, C. Ichoku, S. Mattoo, R. Levy, D. A. Chu, B. Holben, O. Dubovik, A. Smirnov, J. V. Martins, R.-R. Li, and Z. Ahmad, Validation of MODIS aerosol retrieval over ocean, *Geophys. Res. Lett*., **29**(12), doi:10.1029/2001GL013204 (2002).

Remer, L. A., Y. J. Kaufman, D. Tanré, S. Mattoo, D. A. Chu, J. V. Martins, R.-R. Li, C. Ichoku, R. C. Levy, R. G. Kleidman, T. F. Eck, E. Vermote, and B. N. Holben, The MODIS Aerosol Algorithm, Products, and Validation. *J. Atmos. Sci.*, **62**, 947–973.doi: http://dx.doi.org/10.1175/JAS3385.1 (2005).

Remer, L. A., R. G. Kleidman, R. C. Levy, Y. J. Kaufman, D. Tanré, S. Mattoo, J. V. Martins, C. Ichoku, I. Koren, H. Yu, and B. N. Holben, Global aerosol climatology from the MODIS satellite sensors, *J. Geophys. Res*., **113**, D14S07, doi:10.1029/2007JD009661 (2008).

Ridley, D. A., C. L. Heald, and B. Ford, North African dust export and deposition: A satellite and model perspective, *J. Geophys. Res*., **117**, D02202, doi:10.1029/2011JD016794 (2012).

Ridley, D. A., C. L. Heald and J. M. Prospero, What controls the recent changes in African mineral dust aerosol across the Atlantic? *Atmos. Chem. Phys*., **14**, 5735-5747 (2014).

Rienecker, M.M., M.J. Suarez, R. Gelaro, R. Todling, J. Bacmeister, E. Liu, M.G. Bosilovich, S.D. Schubert, L. Takacs, G.-K. Kim, S. Bloom, J. Chen, D. Collins, A. Conaty, A. da Silva, W. Gu, J. Joiner, R. D. Koster, R. Lucchesi, A. Molod, T. Owens, S. Pawson, P. Pegion, C. R. Redder, R. Reichle, F. R. Robertson, A. G. Ruddick, M. Sienkiewicz and J. Woollen, MERRA: NASA's Modern-Era Retrospective Analysis for Research and Applications. *J. Clim*., **24**, 3624-3648, doi:10.1175/JCLI-D-11-00015.1 (2011).

Rodríguez, S., E. Cuevas, J. M. Prospero, A. Alastuey, X. Querol, J. López-Solano, M. I. García, and S. Alonso-Pérez, Modulation of Saharan dust export by the North African dipole, *Atmos. Chem. Phys*., **15**, 7471-7486, doi:10.5194/acp-15-7471-2015 (2015).

Rosenfeld, D., U. Lohmann, G. B. Raga, C. D. O'dowd, M. Kulmala, S. Fuzzi, A. Reissell, and M. O. Andreae, Flood or drought: How do aerosols affect precipitation? *Sci*. **321**, 5894, 1309-1313 Doi:10.1126/science.1160606 (2008).

Sarntheim, M., Sand deserts during glacial maximum and climate optimum, *Nature*, **272**, 43-46 (1978).

Savoie, D. L., and J. M. Prospero, Water-soluble potassium, calcium, and magnesium in the aerosols over the tropical North Atlantic, *J. Geophys. Res*., **85**(C1), 385–392, doi:10.1029/JC085iC01p00385 (1980).

Schepanski, K., I. Tegen, M. C. Todd, B. Heinold, G. Bonisch, B. Laurent and A. Macke, Meteorological processes forcing Saharan dust emission inferred from MSG-SEVIRI observations of subdaily dust source activation and numerical models. *J. Geophys. Res*., **114**, D10201 (2009).

Schepanski, K., I. Tegen, M. C. Todd, B. Heinold, G. Bonisch, B. Laurent, and A. Macke, Meteorological processes forcing Saharan dust emission inferred from MSG-SEVIRI observations of subdaily dust source activation and numerical models, *J. Geophys. Res*., **114**, D10201, doi:10.1029/2008JD010325 (2009).

Scheuvens, D., L. Schutz, K. Kandler, M. Ebert, S. Weinbruch, Bulk composition of northern African dust and its source sediments – A compilation, *Earth Sci. Rev*.. **116**, 170-194 (2013).

Skamarock, W. C., J. B. Klemp, J. Dudhia, D. O. Gill, D. M. Barker, M. G. Duda, X. Huang, W. Wang, and J. G. Powers, A description of the advanced research WRF version 3, NCAR Tech. Note, NCAR/TN-475+STR, 8 pp., Natl. Cent. for Atmos. Res., Boulder, Colo., available at: http://www.mmm.ucar.edu/wrf/users/docs/arw v3.pdf

(2008).

Skinner, C. B., M. Ashfaq, and N. S. Diffenbaugh, Influence of twenty-first-century atmospheric and sea surface temperature forcing on West African climate. *J. Clim*., **25**, 527-542, doi: http://dx.doi.org/10.1175/2011JCLI4183.1 (2012).
Sokolik, I. N., and O. B. Toon, Direct radiative forcing by anthropogenic airborne mineral aerosols, *Nature*, **381** (1996).

Stowe, L. L., A. M. Ignatov, and R. R. Singh, Development, validation, and potential enhancements to the second-generation operational aerosol product at the national environmental satellite, data, and information service of the national oceanic and atmospheric administration. *J. Geophys. Res*., **102**, 16923-16934 (1997).
Swap, R., M. Garstang, S. Greco, R. Talbot, and P. Kallberg, Saharan dust in the Amazon Basin. *Tellus B*, **44**, 133–149. doi: 10.1034/j.1600-0889.1992.t01-1-00005.x (1992).

Swap, R., S. Ulanski, M. Cobbett, and M. Garstang, Temporal and spatial characteristics of Saharan dust outbreaks, *J. Geophys. Res*., **101**(D2), 4205–4220, doi:10.1029/95JD03236 (1996).

Tegen, I. and I. Fung, Modeling of mineral dust in the atmosphere: Sources, transport, and optical thickness, *J. Geophys. Res*., **99** (1994).

Tegen, I. A. A. Lacis, and I. Fung, The influence on climate forcing of mineral aerosols from disturbed soils, *Nature*, **380** (1996).

Tegen, I., M. Werner, S. P. Harrison, and K. E. Kohfeld, Relative importance of climate and land use in determining present and future global soil dust emission, *Geophys. Res. Lett*., **31**, L05105, doi:10.1029/2003GL019216 (2004).

Tegen, I., K. Schepanski, and B. Heinold, Comparing two years of Saharan dust source activation obtained by regional modelling and satellite observations. *Atmos. Chem. Phys*. **13** (5), 2381–2390 (2013).

Thorncroft, C. D., and M. Blackbum, Maintenance of the African easterly jet. *Quart. J. Roy. Meteor. Soc.,* **125,** 763–786 (1999).

Torres, O., P. K. Bhartia, J. R. Herman, Z. Ahmad, and J. Gleason, Derivation of aerosol properties from satellite measurements of backscattered ultraviolet radiation: Theoretical basis, *J. Geophys. Res*., **103**(D14), 17099–17110, doi:10.1029/98JD00900 (1998).

Torres, O., P. K. Bhartia, J. R. Herman, A. Sinyuk, P. Ginoux, and B. Holben, A long-term record of aerosol optical depth from TOMS observations and comparison to AERONET measurements, *J. Atmos. Sci*., **59**, 398–413, doi:10.1175/1520-0469(2002)059<0398:ALTROA>2.0.CO;2 (2002).

Tegen, I., and I. Fung, Modeling of mineral dust in the atmosphere: Sources, transport, and optical thickness, *J. Geophys. Res*., **99**(D11), 22897–22914, doi:10.1029/94JD01928 (1994).

Tegen, I., S. Harrison, K. Kohfeld, I. Prentice, M. Coe, and M. Heimann

Impact of vegetation and preferential source areas on global dust aerosols: results from a model study, *J. Geophys. Res*., **107** (D21), 4576 (2002).

Torres, O., A. Tanskanen, B. Veihelmann, C. Ahn, R. Braak, P. K. Bhartia, P. Veefkind, and P. Levelt, Aerosols and surface UV products from Ozone Monitoring Instrument observations: An overview, J. *Geophys. Res*., **112**, D24S47, doi:10.1029/2007JD008809 (2007).

Vaughan, M., S. Young, D. Winker, K. Powell, A. Omar, Z. Liu, Y. Hu, and C. Hostetler, Fully automated analysis of space-based lidar data: an overview of the CALIPSO retrieval algorithms and data products, *Proc. of SPIE*, **5575**, 16-30 (2004).

Washington, R., M. Todd, N. J. Middleton, and A. S. Goudie, Dust-storm source areas determined by the Total Ozone Monitoring Spectrometer and surface observations, *Ann. Assoc. Am. Geogr*., **93**(2), 297-313 (2003).

Washington, R., M. C. Todd, G. Lizcano, I. Tegen, C. Flamant, I. Koren, P. Ginoux, S. Engelstaedter, C. S. Bristow, C. S. Zender, A. S. Goudie, A. Warren, and J. M. Prospero, Links between topography, wind, deflation, lakes and dust: The case of the Bodélé Depression, Chad, *Geophys. Res. Lett*., **33**, L09401, doi:10.1029/2006GL025827 (2006).

Washington, R., C. Flamant, D. Parker, J. Marsham, J. McQuaid, H. Brindley, M. C. Todd, E. J. Highwood, J.-P. Chaboureau, C. Kocha, A. Saci, M. Bechir, Fennec—The Saharan Climate System, *CLIVAR Exchanges*, **60**, 31–33 (2012).

Westphal, D. L., O. B. Toon and T. N. Carlson, A two-dimensional numerical investigation of the dynamics and microphysics of Saharan dust storms. *J. Geophys. Res*., **92** (1987).

Woodward, S., Modeling the atmospheric life-cycle and radiative impact of mineral dust in the Hadley Centre climate model, *J. Geophys. Res*., **106**, 18155–18166 (2001).

Wurzler, S., T. G. Reisin, and Z. Levin, Modification of mineral dust particles by cloud processing and subsequent effects on drop size distributions, *J. Geophys. Res*., **105**, 4501-4512, doi:10.1029/1999JD900980 (2000).

Yoshioka, M., Impact of desert dust radiative forcing on Sahel precipitation: Relative importance of dust compared to sea surface temperature variations, vegetation changes, and greenhouse gas warming. *J. Clim.*, **20** (2007).

Yu, G., and S. Harrison, An evaluation of the simulated water balance of Eurasia and northern Africa at 6000 yr B.P. using lake status data. *Clim. Dyn*., **12**, 723-735 (1996).

Zaveri, R. A. L. K. and Peters, A new lumped structure photochemical mechanism for large-scale applications, *J*. *Geophys*. *Res*., **104**, 30387–30415 (1999).

Zaveri, R. A., R. C. Easter, J. D. Fast, and L. K. Peters, Model for simulating aerosol interactions and chemistry (MOSAIC), *J*. *Geophys*. *Res*., **113**, D13204, doi:10.1029/2007JD008782 (2008).

Zender, C. S., R. L. L. Miller, and I. Tegen, Quantifying mineral dust mass budgets: Terminology, constraints, and current estimates, *Eos Trans*. AGU, **85**(48), 509–512, doi:10.1029/2004EO480002 (2004).

Zeng, N., Drought in the Sahel, *Sci*, **302**, 5647, 999-1000 (2003).

Zhao, C., X. Liu, L. R. Leung, B. Johnson, S. A. McFarlane, W. I. Gustafson Jr., J. D. Fast, and R. Easter, The spatial distribution of mineral dust and its shortwave radiative forcing over North Africa: modeling sensitivities to dust emissions and aerosol size treatments, *Atmos. Chem. Phys*., **10**, 8821–8838, doi:10.5194/acp-10-8821-2010, (2010).

Zhao, C., S. Chen, L.Y.R. Leung, Y. Qian, J. Kok, R.A. Zaveri, and J. Huang, Uncertainty in modeling dust mass balance and radiative forcing from size parameterization, *Atmos. Chem. Phys*., **13**, 10733–10753 (2013).